



universität
wien

MASTERARBEIT

Titel der Masterarbeit

„Effective Field Theory Approach to Heavy Flavor
Production in Deep Inelastic Scattering“

Verfasser

Daniel Samitz, BSc

angestrebter akademischer Grad

Master of Science (MSc)

Wien, 2014

Studienkennzahl lt. Studienblatt:

A 066 876

Studienrichtung lt. Studienblatt:

Masterstudium Physik UG2002

Betreuer:

Univ.-Prof. Dr. André H. Hoang

Abstract

In this thesis I describe a setup to treat effects of heavy flavors in deep inelastic scattering (DIS) using soft-collinear effective theory (SCET), both in the classical DIS region where $1 - x \sim \mathcal{O}(1)$ and the endpoint region $x \rightarrow 1$. The structure functions can be factorized into non-perturbative matrix elements of operators in the effective theory which correspond to the standard QCD parton distribution functions (PDFs) and Wilson coefficients encoding the hard interactions. In the classical region the renormalization of the effective theory operators leads to the usual DGLAP evolution for the PDFs. Two different schemes for including effects of a heavy flavor with mass $m \gg \Lambda_{\text{QCD}}$, a fixed flavor number (FFN) and a variable flavor number (VFN) scheme, are discussed. These are well-known in the QCD literature but are formulated here for DIS for the first time in an effective theory language. The FFN scheme is appropriate if the mass is larger or of the order of the hard scale (which is given by the momentum transfer Q^2 in the process), whereas in the VFN scheme the evolution of a new perturbatively generated PDF for the heavy flavor introduced at the mass scale resums logarithms of the ratio of the hard scale over the mass scale and therefore provides a setup that is applicable even if $m^2 \ll Q^2$. In the endpoint region a factorization theorem separating the physics at the hard scale, the jet scale, given by the invariant mass of the hadronic final state, and the scale Λ_{QCD} is derived in SCET, which allows for the resummation of logarithms of $1 - x$ that become large in that region. This was done for the first time for massive quark production in DIS. Finally a numerical analysis is performed to estimate the effects of the massive calculation compared to the massless one.

Zusammenfassung

In dieser Arbeit beschreibe ich eine Methode um die Effekte von schweren Quarks in tief-inelastischer Streuung (DIS) mithilfe von Soft-Collinear Effective Theory (SCET) zu behandeln, sowohl in der klassischen DIS Region $1 - x \sim \mathcal{O}(1)$ als auch in der Endpunktregion $x \rightarrow 1$. Die Strukturfunktionen können faktorisiert werden in nicht-perturbative Matrixelemente von Operatoren in der effektiven Theorie, welche den üblichen QCD Partonverteilungsfunktionen (PDFs) entsprechen, und Wilson Koeffizienten welche die harte Wechselwirkung beschreiben. In der klassischen Region ergibt die Renormierung der Operatoren in der effektiven Theorie die übliche DGLAP Evolution für die PDFs. Es werden zwei verschiedenen Schemen zur Einbindung von schweren Quarks mit Masse $m \gg \Lambda_{\text{QCD}}$ diskutiert, ein “fixed flavor number” (FFN) und ein “variable flavor number” (VFN) Schema. Diese sind in der QCD Literatur bekannt, werden hier jedoch zum ersten Mal für DIS mit Hilfe von effektiven Theorien formuliert. Das FFN Schema ist anwendbar wenn die Masse größer oder von der Ordnung der harten Skala ist (welche durch den Impulsübertrag Q^2 im Prozess gegeben ist), während im VFN Schema in der Evolution einer neuen, perturbativ an der Massenskala generierten PDF für das schwere Quark Logarithmen, die das Verhältnis der harten Skala und der Massenskala beinhalten, resummiert werden. Daher liefert das VFN Schema ein Setup welches auch für den Fall $m^2 \ll Q^2$ anwenbar ist. In der Endpunktregion wird ein Faktorisierungstheorem in SCET hergeleitet welches die Physik an der harten Skala, der Jetskala, gegeben durch die invariante Masse des hadronischen Endzustandes, und der Skala Λ_{QCD} trennt und das Resummieren von Logarithmen von $1 - x$ erlaubt, welche in dieser Region groß werden. Dies wurde zum ersten Mal für schwere Quark Produktion in DIS abgeleitet. In einer numerischen Analyse werden die Effekte der massiven Rechnung mit der masselosen verglichen.

Contents

1	Introduction	1
2	Soft-Collinear Effective Theory	3
2.1	Power Counting in SCET	3
2.2	SCET Fields and Lagrangian	4
2.3	SCET with Massive Quarks	8
2.4	Wilson Lines	8
2.4.1	Collinear Wilson Lines and Gauge Invariant Operators	8
2.4.2	Usoft Wilson Lines	10
3	DIS with Massless Quarks	12
3.1	Cross Section and Kinematics	12
3.2	DIS Factorization in SCET	15
3.2.1	Factorization of the Hadronic Tensor	15
3.2.2	The Quark PDF	17
3.2.3	The Gluon PDF	17
3.3	Hard Matching Coefficients	18
3.3.1	Quark Form Factor	19
3.3.2	Gluon Form Factor	22
3.4	Renormalization of the PDFs	24
3.4.1	Calculation of SCET Diagrams	24
3.4.2	Renormalization and Evolution	29
4	Heavy Flavor Production in DIS	31
4.1	Kinematics and Rescaling	31
4.2	Fixed Flavor Number Scheme	31
4.2.1	QCD Calculations	32
4.2.2	Matching	33
4.3	Variable Flavor Number Scheme	33
4.3.1	QCD Calculations	34
4.3.2	SCET Calculations	38
4.3.3	Matching at the Hard Scale	41
4.3.4	Matching at the Mass Scale	42
4.3.5	Massless Limit	43
5	DIS in the Endpoint Region	45
5.1	Factorization Theorem	45
5.1.1	PDF / Soft Function	48
5.1.2	Jet Function	50
5.1.3	Hard Function	54
5.2	Evolution Kernels	55
5.3	Consistency Relations	57
6	Numerical Analysis	59
7	Conclusions	65
A	Plus Distributions	66
B	Imaginary Parts	67
C	n-point Functions	67

1 Introduction

In the era of the search for new physics at hadron colliders high precision in our understanding of strong interaction is an import factor for success in currently running and future experiments. Therefore a lot of effort has been made to reduce theoretical uncertainties in the predictions of QCD and determination of its fundamental parameters. One essential ingredient for understanding processes with hadrons in the initial state are parton distribution functions (PDFs), which have to be fitted to experimental data.

The process that is mainly used for extracting PDFs from experiment is deep inelastic scattering (DIS) where one has to deal with only one hadron in the initial state. All common PDF sets like MSTW [1] or CTEQ10 [2] rely heavily on fits to DIS data.

For higher precision in the determination of PDFs and the analysis of processes at hadron colliders the effects of heavy quarks can not be neglected in the perturbative calculations. One challenge arising in these calculations is that if there is a large hierarchy between the mass and the hard scale Q^2 in the process, large logarithms of the ratio of these scales will weaken the convergence of the perturbative expansion when choosing an inappropriate scheme of including different numbers of active flavors. A scheme with n_f light active flavors not including the heavy quark in the RG evolution for PDFs and couplings is applicable in the regime where $m^2 \gtrsim Q^2$ because the massive flavor decouples in the limit $\frac{m^2}{Q^2} \rightarrow \infty$, but leads to large uncanceled logarithms of $\frac{m^2}{Q^2}$ in the case where $m^2 \ll Q^2$. On the other hand a scheme with n_f light plus one heavy active flavors provides the correct limit for $\frac{m^2}{Q^2} \rightarrow 0$ and is therefore suitable when $m^2 \lesssim Q^2$, but is inappropriate for $m^2 \gg Q^2$ because the heavy quark does not decouple properly.

In the early 1990s the so called ACOT scheme [3,4] was developed to systematically include heavy flavors with an arbitrary scaling of the mass relative to the hard scale by smoothly combining these two schemes. In this scheme a change from a description with PDFs for n_f light flavors to one with n_f light plus one heavy flavor is made at the mass scale by reshuffling terms containing mass singularities from nearly on-shell fluctuations from the hard Wilson coefficients into a new PDF for the heavy flavor. With the change between the two schemes at the mass scale the ACOT scheme provides a setup that is applicable for an arbitrary ratio of the mass and the hard scale (as long as both can still be treated perturbatively). Since then various similar schemes in the same spirit have been proposed for including effects of massive flavors, see for example Ref. [5] for a review.

From a more modern point of view these “variable flavor number schemes” can be associated to the use of different effective field theories in the different regimes, where the heavy particles are integrated out at their respective mass scale and do not contribute in the RG evolution below that scale. The appropriate effective field theory of QCD that is designed to deal with collimated hadronic objects, like we have for DIS in the initial state when using the Breit frame or also in the final state in the end-point region $x \rightarrow 1$, is soft-collinear effective theory (SCET) [6–9]. It allows for deriving factorization theorems for high energetic hadronic processes and for defining the PDFs as non-perturbative matrix elements of operators in the effective theory [10] analogous to the QCD operator definition of PDFs [11,12]. SCET can not only be used to factorize the structure functions into Wilson coefficients and PDFs and to provide a systematic way for including or integrating out massive flavors, but also to resum large logarithms that arise in the jet limit of the hadronic final state when its invariant mass reaches its minimum.

In Sec. 2 we start with a brief review of soft-collinear effective theory.

The effective field theory setup for DIS with massless quarks is described in Sec. 3. In Sec. 3.1 the kinematics of DIS with massless quarks, the cross section and the definition of the form factors are summarized. In Sec. 3.2 we will show how SCET can be used to separate non-perturbative and perturbative physics to factorize the form factors into matrix elements of SCET operators and hard Wilson coefficients and that these non-perturbative matrix elements correspond to the well known QCD parton distribution functions. In Sec. 3.3 this effective field theory setup is used to determine the matching coefficients at $\mathcal{O}(\alpha_s)$ by calculating the relevant 1-loop diagrams in QCD with massless quarks. Finally in Sec. 3.4 the renormalization of the PDFs leads to the standard DGLAP equations that allow for the evolution of the PDFs from one energy scale to another.

The effects of a massive quark are investigated in Sec. 4. In Sec. 4.1 the changes in the kinematics due to the mass of the initial state parton are discussed. In Sec. 4.2 a fixed flavor number scheme is used to include a heavy flavor with mass $m \gg \Lambda_{\text{QCD}}$. The relevant QCD 1-loop diagrams will be calculated with massive quarks on the internal lines and it will be shown that the matching coefficients that are obtained in that way do not lead to the correct massless limit because of uncanceled logarithms of $\frac{m^2}{Q^2}$. This problem can be solved by using a variable flavor number scheme where the number of active flavors

in the RG evolution is changed at the mass threshold to resum those logarithms in the evolution of a new PDF for the heavy flavor which directly leads to the ACOT scheme for DIS, as described in Sec. 4.3. The QCD and SCET diagrams with massive quarks are calculated to find the hard matching coefficients and the threshold corrections that arise in the change from a theory with n_f flavors to a theory with $n_f + 1$ flavors to $\mathcal{O}(\alpha_s)$ and to check that this new approach reproduces the known QCD results for the ACOT scheme. We show explicitly that the hard matching coefficients in the VFN scheme have the correct massless limit.

In Sec. 5 we will discuss DIS in the endpoint region $x \rightarrow 1$ where logarithms of $1 - x$ in the matching coefficients become large and can spoil the perturbative expansion. To avoid this the effective field theory setup can be extended by introducing a jet function at the scale $\mu_J = Q\sqrt{1 - x}$ and a factorization theorem that factorizes the form factor into a hard function, a jet function and the PDF is derived in Sec. 5.1 and the hard and the massive jet function are calculated to $\mathcal{O}(\alpha_s)$. In Sec. 5.2 and Sec. 5.3 the evolution kernels are calculated to LL approximation and consistency relations for the evolution kernels and anomalous dimensions are checked explicitly.

In Sec. 6 a numerical analysis is performed to compare the fixed order results with the results with NLL and NNLL resummation for large x , both in the massless and the massive case, with $Q = 30$ GeV and $Q = 5$ GeV and the masses of the bottom and the charm quark.

2 Soft-Collinear Effective Theory

Soft-Collinear Effective Theory (SCET) [6–10] is an effective field theory of QCD applicable for highly boosted quarks and gluons interacting among each other and with soft gluons and is therefore the right effective theory to describe jets, objects consisting of high energetic and narrowly collimated hadrons. It achieves a systematic separation of different energy scales involved in a process and allows for deriving factorization theorems that can be used to resum large logarithms of ratios of the different scales that could spoil the perturbative expansion. SCET has a wide range of use, from the decay of heavy to light particles to high energetic processes in particle colliders.

2.1 Power Counting in SCET

We start by introducing light-cone coordinates that will be useful for the separation of different modes in the effective theory. We define the lightlike vectors

$$n^\mu = (1, 0, 0, -1), \quad \bar{n}^\mu = (1, 0, 0, 1), \quad (2.1)$$

that fulfill the relations $n \cdot n = \bar{n} \cdot \bar{n} = 0$ and $n \cdot \bar{n} = 2$. Every four-vector can be decomposed into light-cone components p^+ and p^- and perpendicular components p_\perp

$$p^\mu = p^- \frac{n^\mu}{2} + p^+ \frac{\bar{n}^\mu}{2} + p_\perp^\mu, \quad p^2 = p^+ p^- - |p_\perp^2|, \quad (2.2)$$

where $p^+ = n \cdot p$ and $p^- = \bar{n} \cdot p$. In d dimensions the vector p_\perp^μ is $d - 2$ dimensional.¹ The same notation can also be used for gamma matrices and the metric tensor, so that

$$\gamma_\perp^\mu := \gamma^\mu - \not{n} \frac{n^\mu}{2} - \not{\bar{n}} \frac{\bar{n}^\mu}{2} \quad \gamma_\perp^\mu \gamma_\mu^\perp = d - 2 \quad (2.3)$$

$$g_\perp^{\mu\nu} := g^{\mu\nu} - \frac{\bar{n}^\mu n^\nu}{2} - \frac{n^\mu \bar{n}^\nu}{2} \quad g_\perp^{\mu\nu} g_{\mu\nu}^\perp = d - 2 \quad (2.4)$$

We can now distinguish different modes according to the scaling of their components with respect to the expansion parameter $\lambda \ll 1$ of the effective theory, Fig. 1:

$$\begin{array}{ll} \text{hard:} & (p_h^+, p_h^-, p_h^\perp) \sim Q(1, 1, 1) & p_h^2 \sim Q^2 \\ n\text{-coll.:} & (p_n^+, p_n^-, p_n^\perp) \sim Q(\lambda^2, 1, \lambda) & p_n^2 \sim Q^2 \lambda^2 \\ \bar{n}\text{-coll.:} & (p_{\bar{n}}^+, p_{\bar{n}}^-, p_{\bar{n}}^\perp) \sim Q(1, \lambda^2, \lambda) & p_{\bar{n}}^2 \sim Q^2 \lambda^2 \\ \text{usoft:} & (p_{us}^+, p_{us}^-, p_{us}^\perp) \sim Q(\lambda^2, \lambda^2, \lambda^2) & p_{us}^2 \sim Q^2 \lambda^4 \end{array} \quad (2.5)$$

The n - and \bar{n} -coll. modes describe 2 back to back jets, which is the situation that we will encounter for

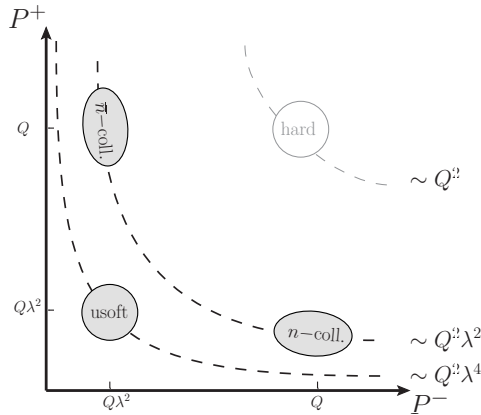


Figure 1: Modes in SCET_I in the $p^+ p^-$ plane. Hard modes with off-shellness $\sim Q^2$ are integrated out, the relevant modes in the effective theory are collinear and usoft with off-shellness $\sim Q^2 \lambda^2$ and $\sim Q^2 \lambda^4$ respectively.

¹Note that $|p_\perp^2|$ denotes the square of the three vector, i.e. $|p_\perp^2| = -p_\perp^\mu p_\mu^\perp > 0$.

DIS in the Breit frame for $x \rightarrow 1$. The Breit frame is the frame where no energy is transferred between the two scattering particles (the electron and the proton in the case of DIS). Here the initial state will be a n -coll. particle that scatters off the virtual photon with momentum Q to become an outgoing \bar{n} -coll. particle. So the hadronic initial and final state in DIS for $x \rightarrow 1$ in this particular frame can be described by two back to back jets, one incoming and one outgoing. For more jets in different directions one would have to introduce more lightlike vectors n_i but this is not necessary for DIS with one initial and one final state jet that are back to back. From the scaling of the momenta in (2.5) one can immediately see that the typical off-shellness p^2 is not conserved in an interaction between collinear particles along different light-cone directions or with hard modes, but it is conserved if a $n(\bar{n})$ -coll. particle interacts with another $n(\bar{n})$ -coll. particle or a ultra-soft (usoft) one. These interactions between collinear and usoft particles are the ones that will appear in the Lagrangian of the effective theory when hard modes with off-shellness $\sim Q^2$ are integrated out.

The above setup with collinear and usoft modes is called SCET_I, a different version of SCET with the usoft modes replaced by soft ones with the counting

$$\text{soft: } (p_s^+, p_s^-, p_s^\perp) \sim Q(\lambda, \lambda, \lambda), \quad p_s^2 \sim Q^2 \lambda^2, \quad (2.6)$$

is called SCET_{II}. In SCET_{II} there is no direct interaction between collinear and soft particles because $(p_n + p_s) \sim Q(\lambda, 1, \lambda)$ and therefore $(p_n + p_s)^2 \sim Q^2 \lambda \gg Q^2 \lambda^2$. Instead of matching SCET_{II} directly onto QCD it is easier to perform the matching in two steps, as shown in Ref. [13]: First SCET_I is matched onto QCD. The expansion parameter of SCET_I is λ_I and the relevant modes are usoft at the scale $Q\lambda_I^2$ and hard-collinear (hc) at the scale $Q\lambda_I$ with the usual SCET_I counting as in Eq. (2.5) and Fig. 1. Then in the second step SCET_{II} with the expansion parameter $\lambda_{II} = \lambda_I^2$ is matched onto SCET_I by integrating out the hc modes at the scale $Q\sqrt{\lambda_{II}}$ to be left with the low-energy degrees of freedom with soft (the usofts from SCET_I in the first step) and collinear modes, both at the scale $Q\lambda_{II}$, see Fig. 2.

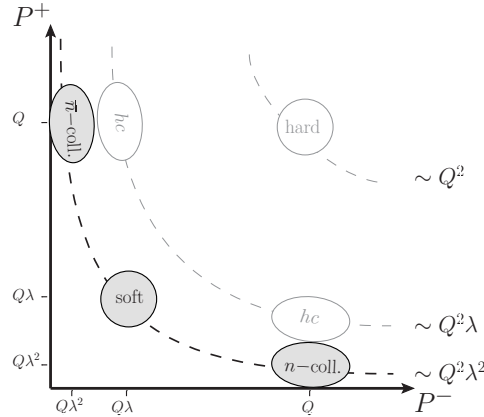


Figure 2: Modes in SCET_{II}. In the two step matching procedure hard modes are integrated out at Q^2 in the matching QCD \rightarrow SCET_I. In the second step hard collinear modes at $Q^2\lambda_{II}$ are integrated out in the matching SCET_I \rightarrow SCET_{II}. The remaining degrees of freedom are soft and collinear, both at the scale $Q^2\lambda_{II}^2$.

SCET_{II} is the appropriate effective field theory for DIS in the Breit frame because the incoming initial state jet is at the typical hadronic scale Λ_{QCD} which is also the scale of the soft fluctuations. In the endpoint region $x \rightarrow 1$ where also a final state jet is produced, this final state jet will be at a higher scale and has therefore to be described by hard collinear modes that will be integrated out in the matching SCET_I \rightarrow SCET_{II}, see Sec. 5.

2.2 SCET Fields and Lagrangian

Here we show the construction of the SCET Lagrangian for n -coll. fields, for particles along any other light-cone direction it can be obtained in exactly the same way. We start with a fermion field $\psi(x)$ that that can be decomposed as

$$\psi(x) = \psi^+(x) + \psi^-(x) \quad (2.7)$$

with

$$\psi^+(x) = \int \frac{d^4 p}{(2\pi)^3} \delta(p^2) \Theta(p^0) \sum_s u(p, s) a(p, s) e^{-ipx}, \quad (2.8)$$

$$\psi^-(x) = \int \frac{d^4 p}{(2\pi)^3} \delta(p^2) \Theta(p^0) \sum_s v(p, s) b^\dagger(p, s) e^{+ipx}. \quad (2.9)$$

u and v are particle and anti-particle spinors, a destroys a particle and b^\dagger creates an anti-particle. The short distance fluctuations can be removed by assigning a collinear scaling to the momentum $p \sim Q(\lambda^2, 1, \lambda)$ and split it into a large label $\tilde{p}^\mu = p^- \frac{n^\mu}{2} + p_\perp^\mu$ and small residual momentum $k^\mu \sim Q\lambda^2$, i.e. the full four-momentum is the sum of a large label momentum and a suppressed residual momentum $p^\mu = \tilde{p}^\mu + k^\mu$. With this separation the fields can be written as

$$\psi^+(x) = \sum_{\tilde{p} \neq 0} e^{-i\tilde{p}x} \psi_{n,\tilde{p}}^+(x), \quad (2.10)$$

$$\psi^-(x) = \sum_{\tilde{p} \neq 0} e^{+i\tilde{p}x} \psi_{n,\tilde{p}}^-(x), \quad (2.11)$$

where the residual fields $\psi_{n,\tilde{p}}^\pm(x)$ contain only long distance fluctuations, i.e. $\partial_\mu \psi_{n,\tilde{p}}^\pm(x) \sim \lambda^2$. They have the form

$$\psi_{n,\tilde{p}}^+(x) = \Theta(\tilde{p}^-) \int \frac{d^4 k}{(2\pi)^3} \delta(k^+ \tilde{p}^- - |\tilde{p}_\perp^2|) \sum_s u(k, s) a(k, s) e^{-ikx}, \quad (2.12)$$

$$\psi_{n,\tilde{p}}^-(x) = \Theta(\tilde{p}^-) \int \frac{d^4 k}{(2\pi)^3} \delta(k^+ \tilde{p}^- - |\tilde{p}_\perp^2|) \sum_s v(k, s) b^\dagger(k, s) e^{+ikx}. \quad (2.13)$$

So the field $\psi(x)$ can be written as

$$\psi(x) = \sum_{\tilde{p} \neq 0} e^{-i\tilde{p}x} \psi_{n,\tilde{p}}(x) \quad (2.14)$$

where the residual field $\psi_{n,\tilde{p}}(x)$ is defined as

$$\begin{aligned} \psi_{n,\tilde{p}}(x) &= \psi_{n,\tilde{p}}^+(x) + \psi_{n,-\tilde{p}}^-(x) \\ &= \Theta(\tilde{p}^-) \psi_{n,\tilde{p}}^+(x) + \Theta(-\tilde{p}^-) \psi_{n,-\tilde{p}}^-(x). \end{aligned} \quad (2.15)$$

The Theta functions in the second line are just the ones from Eqs. (2.12) and (2.13) written out explicitly once more to emphasize that fields with positive(negative) labels only contribute to particle(anti-particle) propagation. The zero-bin $\tilde{p}^\mu = 0$ is excluded in the sum to avoid double counting because if the label is zero it is no longer a collinear but a usoft particle. Technically this is achieved in loop calculations by zero-bin subtractions [14] where the same diagram with a usoft counting for the collinear gluon loop momentum is subtracted to cancel the zero-bin from the collinear diagrams. The projection operators

$$P_n = \frac{\not{n} \not{\bar{n}}}{4}, \quad P_{\bar{n}} = \frac{\not{\bar{n}} \not{n}}{4}, \quad (2.16)$$

can be used to project onto different components of the field $\psi_{n,\tilde{p}}$

$$\xi_{n,\tilde{p}} = P_n \psi_{n,\tilde{p}}, \quad \hat{\xi}_{n,\tilde{p}} = P_{\bar{n}} \psi_{n,\tilde{p}}. \quad (2.17)$$

Because $\not{n} \not{n} = n^2 = 0$ we find

$$\not{n} \xi_n = 0 \quad \bar{\xi}_n \not{n} = 0 \quad (2.18)$$

$$\not{\bar{n}} \hat{\xi}_n = 0 \quad \hat{\bar{\xi}}_n \not{\bar{n}} = 0 \quad (2.19)$$

We start from the massless fermion part of the QCD Lagrangian

$$\mathcal{L}_{q,\text{QCD}} = \bar{\psi} i \not{D} \psi, \quad (2.20)$$

with the covariant derivative in the form $iD_\mu = i\partial_\mu + gA_\mu$.² Using the above definitions when writing $\psi(x) = \sum_{\bar{p}} e^{-i\bar{p}x}(\xi_{n,\bar{p}}(x) + \hat{\xi}_{n,\bar{p}}(x))$ for the quark fields yields (here we drop the tilde on the label, and from here on a sum over all labels is implicit whenever there is a label on a field)

$$\begin{aligned} \mathcal{L}_q = e^{i(p'-p)x} & \left[\bar{\xi}_{n,p'} \frac{\not{p}}{2} iD^+ \xi_{n,p} + \bar{\xi}_{n,p'} \frac{\not{p}}{2} (p^- + iD^-) \hat{\xi}_{n,p} \right. \\ & \left. + \bar{\xi}_{n,p'} (\not{p}_\perp + i\not{D}_\perp) \hat{\xi}_{n,p} + \bar{\xi}_{n,p'} (\not{p}_\perp + i\not{D}_\perp) \xi_{n,p} \right]. \end{aligned} \quad (2.21)$$

The minus and perp. components of the label scale like λ^0 and λ^1 respectively, but the derivative in D acting on the collinear field scales like λ^2 (because these fields only contain residual momenta that are not in the label), so in the last three terms these derivatives are suppressed relative to the large label components and can be dropped. This implies that the field $\hat{\xi}_n$ is not dynamical and can be removed by applying the equation of motion for this field

$$\begin{aligned} \frac{\not{p}}{2} (p^- + iD^-) \hat{\xi}_{n,p} &= -(\not{p}_\perp + i\not{D}_\perp) \xi_{n,p} \\ \Rightarrow (p^- + iD^-) \hat{\xi}_{n,p} &= (\not{p}_\perp + i\not{D}_\perp) \frac{\not{p}}{2} \xi_{n,p}. \end{aligned} \quad (2.22)$$

This leads to the Lagrangian in the form

$$\mathcal{L}_q = e^{i(p'-p)x} \bar{\xi}_{n,p'} \left[iD^+ + (\not{p}_\perp + i\not{D}_\perp) (p^- + iD^-)^{-1} (\not{p}_\perp + i\not{D}_\perp) \right] \frac{\not{p}}{2} \xi_{n,p}. \quad (2.23)$$

Also the gluon fields can be split in a collinear part by pulling out the large labels explicitly and a usoft gluon field

$$A^\mu(x) = A_{us}^\mu(x) + e^{-iqx} A_{n,q}^\mu(x), \quad (2.24)$$

where again all derivatives acting on the fields are now suppressed as λ^2 . The usoft and the collinear gluon fields satisfy the same scaling as their respective momenta, i.e.

$$(A_{us}^+, A_{us}^-, A_{us}^\perp) \sim (\lambda^2, \lambda^2, \lambda^2), \quad (2.25)$$

$$(A_n^+, A_n^-, A_n^\perp) \sim (\lambda^2, 1, \lambda). \quad (2.26)$$

Using this in the Lagrangian above and neglecting all terms that are not leading in λ gives

$$\begin{aligned} \mathcal{L}_q = e^{i(p'-p)x} \bar{\xi}_{n,p'} & \left[i\partial^+ + gA_{us}^+ + ge^{-iqx} A_{n,q}^+ \right. \\ & \left. (\not{p}_\perp + i\not{\partial}_\perp + ge^{-iqx} A_{n,q}^\perp) (p^- + i\partial^- + ge^{-iqx} A_{n,q}^-)^{-1} (\not{p}_\perp + i\not{\partial}_\perp + ge^{-iqx} A_{n,q}^\perp) \right] \frac{\not{p}}{2} \xi_{n,p}. \end{aligned} \quad (2.27)$$

The term in the middle can be expanded

$$(p^- + i\partial^- + ge^{-iqx} A_{n,q}^-)^{-1} = \sum_{n=0}^{\infty} \left(\frac{-g}{p^- + i\partial^-} e^{-iqx} A_{n,q}^- \right)^n \frac{1}{p^- + i\partial^-}. \quad (2.28)$$

The derivatives acting on the collinear fields A_n^- are suppressed as λ^2 , but the derivatives acting on the exponential functions pick up a label momentum q^- that is of order λ^0 . So the sum gives an infinite number of terms that are not suppressed in the power counting and give rise to interaction terms between collinear quarks and an arbitrary number of gluons, each one order higher in the coupling g . In

²If there is no color index on a gluon field this means that the contraction with the SU(3) generators is implicit, i.e. $A_\mu := A_\mu^A T^A$

the derivation of the Feynman rules we will only keep terms up to $\mathcal{O}(g^2)$. Then the Lagrangian is

$$\begin{aligned}
 \mathcal{L}_q = & e^{i(p'-p)x} \bar{\xi}_{n,p'} \frac{\not{p}}{2} (i\partial^+ p^- - |p_\perp^2|) \frac{1}{p^-} \xi_{n,p} + e^{i(p'-p)x} \bar{\xi}_{n,p'} g A_{us}^+ \frac{\not{p}}{2} \xi_{n,p} \\
 & + e^{i(p'-p-q)x} \bar{\xi}_{n,p'} g \left[A_{n,q}^+ + \frac{A_{n,q}^\perp \not{p}_\perp}{p^-} + \frac{(\not{p}_\perp + \not{q}_\perp) A_{n,q}^\perp}{p^- + q^-} - \frac{(\not{p}_\perp + \not{q}_\perp) \not{p}_\perp}{(p^- + q^-) p^-} A_{n,q}^- \right] \frac{\not{p}}{2} \xi_{n,p} \\
 & + e^{i(p'-p-q-r)x} \bar{\xi}_{n,p'} \frac{g^2}{(p^- + r^-)} \left[A_{n,q}^\perp A_{n,r}^\perp - A_{n,q}^- \frac{(\not{p}_\perp + \not{q}_\perp + \not{r}_\perp) A_{n,r}^\perp}{p^- + q^- + r^-} - \frac{A_{n,q}^\perp \not{p}_\perp}{p^-} A_{n,r}^- \right. \\
 & \quad \left. + \frac{(\not{p}_\perp + \not{q}_\perp + \not{r}_\perp) \not{p}_\perp}{(p^- + q^- + r^-) p^-} A_{n,q}^- A_{n,r}^- \right] \frac{\not{p}}{2} \xi_{n,p} + \mathcal{O}(g^3). \quad (2.29)
 \end{aligned}$$

(Here and in the rest of this work all gluon momenta are incoming). The exponential function just states the conservation of label momentum so we can write

$$\begin{aligned}
 \mathcal{L}_q = & \bar{\xi}_{n,p} \frac{\not{p}}{2} (i\partial^+ p^- - |p_\perp^2|) \frac{1}{p^-} \xi_{n,p} + \bar{\xi}_{n,p} g A_{us}^+ \frac{\not{p}}{2} \xi_{n,p} \\
 & + \bar{\xi}_{n,p'} g \left[A_{n,p'-p}^+ + \frac{A_{n,p'-p}^\perp \not{p}_\perp}{p^-} + \frac{\not{p}'_\perp A_{n,p'-p}^\perp}{p'^-} - \frac{\not{p}'_\perp \not{p}_\perp}{p'^- p^-} A_{n,p'-p}^- \right] \frac{\not{p}}{2} \xi_{n,p} \\
 & + \bar{\xi}_{n,p'} \frac{g^2}{(p'^- - q^-)} \left[A_{n,q}^\perp A_{n,p'-p-q}^\perp - A_{n,q}^- \frac{\not{p}'_\perp A_{n,p'-p-q}^\perp}{p'^-} - \frac{A_{n,q}^\perp \not{p}_\perp}{p^-} A_{n,p'-p-q}^- \right. \\
 & \quad \left. + \frac{\not{p}'_\perp \not{p}_\perp}{p'^- p^-} A_{n,q}^- A_{n,p'-p-q}^- \right] \xi_{n,p} + \mathcal{O}(g^3). \quad (2.30)
 \end{aligned}$$

From this one can easily read off the Feynman rules, Fig. 3.

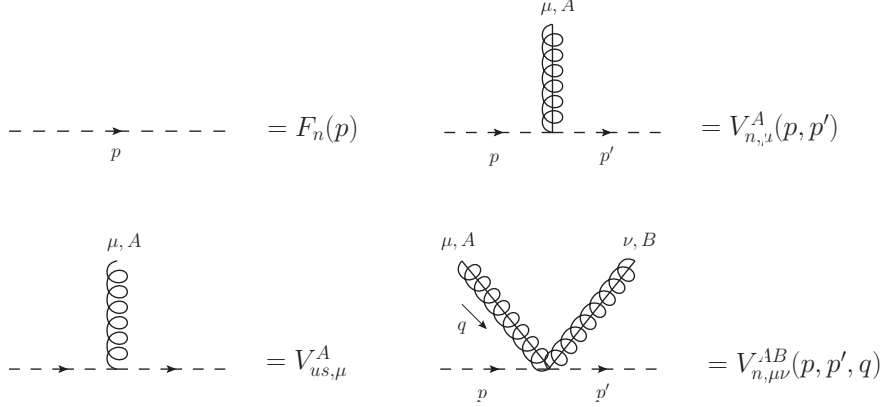


Figure 3: Feynman rules for SCET. The dashed line denotes a collinear quark, the gluon with a solid line in the middle a collinear gluons. Usft gluons are drawn as a standard gluon line.

$$F_n(p) = i \frac{\not{p}}{2} \frac{p^-}{p^2 + i0} \quad (2.31)$$

$$V_{us,\mu}^A = i g T^A n_\mu \frac{\not{p}}{2} \quad (2.32)$$

$$V_{n,\mu}^A(p, p') = i g T^A \left[n_\mu + \frac{\gamma_\mu^\perp \not{p}_\perp}{p^-} + \frac{\not{p}'_\perp \gamma_\mu^\perp}{p'^-} - \frac{\not{p}'_\perp \not{p}_\perp}{p'^- p^-} \bar{n}_\mu \right] \frac{\not{p}}{2} \quad (2.33)$$

$$\begin{aligned}
 V_{n,\mu\nu}^{AB}(p, p', q) = & \frac{i g^2 T^A T^B}{(p'^- - q^-)} \left[\gamma_\mu^\perp \gamma_\nu^\perp - \frac{\gamma_\mu^\perp \not{p}_\perp}{p^-} \bar{n}_\nu - \frac{\not{p}'_\perp \gamma_\nu^\perp}{p'^-} \bar{n}_\mu + \frac{\not{p}'_\perp \not{p}_\perp}{p'^- p^-} \bar{n}_\mu \bar{n}_\nu \right] \frac{\not{p}}{2} \\
 & + \frac{i g^2 T^B T^A}{(p^- + q^-)} \left[\gamma_\nu^\perp \gamma_\mu^\perp - \frac{\gamma_\nu^\perp \not{p}_\perp}{p^-} \bar{n}_\mu - \frac{\not{p}'_\perp \gamma_\mu^\perp}{p'^-} \bar{n}_\nu + \frac{\not{p}'_\perp \not{p}_\perp}{p'^- p^-} \bar{n}_\mu \bar{n}_\nu \right] \frac{\not{p}}{2} \quad (2.34)
 \end{aligned}$$

2.3 SCET with Massive Quarks

To include massive collinear quarks in SCET we start from the massive QCD Lagrangian

$$\mathcal{L}_{q,\text{QCD}} = \bar{\psi}(i\not{D} - m)\psi \quad (2.35)$$

and assign the scaling $m \sim Q\lambda$ to the mass, such that $p^2 \sim m^2 \sim Q^2\lambda^2$, see Ref. [15]. Following the same steps as in the previous section changes the Lagrangian from Eq. (2.21) to

$$\begin{aligned} \mathcal{L}_q = e^{i(p'-p)x} & \left[\bar{\xi}_{n,p'} \frac{\not{n}}{2} iD^+ \xi_{n,p} + \bar{\xi}_{n,p'} \frac{\not{n}}{2} (p^- + iD^-) \hat{\xi}_{n,p} \right. \\ & \left. + \bar{\xi}_{n,p'} (\not{p}_\perp - m + i\not{D}_\perp) \hat{\xi}_{n,p} + \bar{\xi}_{n,p'} (\not{p}_\perp - m + i\not{D}_\perp) \xi_{n,p} \right] \end{aligned} \quad (2.36)$$

and the equation of motion for the field $\hat{\xi}$ is

$$(p^- + iD^-) \hat{\xi}_{n,p} = (\not{p}_\perp + m + i\not{D}_\perp) \frac{\not{n}}{2} \xi_{n,p}. \quad (2.37)$$

The Lagrangian after removing the field $\hat{\xi}$ reads

$$\mathcal{L}_q = e^{i(p'-p)x} \bar{\xi}_{n,p'} \left[iD^+ + (\not{p}_\perp - m + i\not{D}_\perp) (p^- + iD^-)^{-1} (\not{p}_\perp + m + i\not{D}_\perp) \right] \frac{\not{n}}{2} \xi_{n,p}. \quad (2.38)$$

From this we see that all the changes relative to the massless case are just $\not{p}_\perp \rightarrow \not{p}_\perp - m$ in the left and $\not{p}_\perp \rightarrow \not{p}_\perp + m$ in the right term. So the Feynman rules for the vertices can be derived from the massless ones with the replacement $\not{p}_\perp \rightarrow \not{p}_\perp + m$ and $\not{p}'_\perp \rightarrow \not{p}'_\perp - m$, the one for the propagator with $p^2 \rightarrow p^2 - m^2$:

$$F_n(p, m) = i \frac{\not{n}}{2} \frac{p^-}{p^2 - m^2 + i0} \quad (2.39)$$

$$\begin{aligned} V_{n,\mu}^A(p, p', m) = igT^A & \left[n_\mu + \frac{\gamma_\mu^\perp \not{p}_\perp}{p^-} + \frac{\not{p}'_\perp \gamma_\mu^\perp}{p'^-} - \frac{\not{p}'_\perp \not{p}_\perp}{p^- p'^-} \bar{n}_\mu \right. \\ & \left. + \frac{m}{p^- p'^-} \left(\gamma_\mu^\perp (p'^- - p^-) + \bar{n}_\mu (\not{p}_\perp - \not{p}'_\perp + m) \right) \right] \frac{\not{n}}{2} \end{aligned} \quad (2.40)$$

$$\begin{aligned} V_{n,\mu\nu}^{AB}(p, p', q, m) = \frac{ig^2 T^A T^B}{(p'^- - q^-)} & \left[\gamma_\mu^\perp \gamma_\nu^\perp - \frac{\gamma_\mu^\perp \not{p}_\perp}{p^-} \bar{n}_\nu - \frac{\not{p}'_\perp \gamma_\nu^\perp}{p'^-} \bar{n}_\mu + \frac{\not{p}'_\perp \not{p}_\perp}{p'^- p^-} \bar{n}_\mu \bar{n}_\nu \right. \\ & \left. + \frac{m}{p'^- p^-} \left(p^- \gamma_\nu^\perp \bar{n}_\mu - p'^- \gamma_\mu^\perp \bar{n}_\nu + \bar{n}_\mu \bar{n}_\nu (\not{p}'_\perp - \not{p}_\perp - m) \right) \right] \frac{\not{n}}{2} \\ & + \frac{ig^2 T^B T^A}{(p^- + q^-)} \left[\gamma_\nu^\perp \gamma_\mu^\perp - \frac{\gamma_\nu^\perp \not{p}_\perp}{p^-} \bar{n}_\mu - \frac{\not{p}'_\perp \gamma_\mu^\perp}{p'^-} \bar{n}_\nu + \frac{\not{p}'_\perp \not{p}_\perp}{p'^- p^-} \bar{n}_\mu \bar{n}_\nu \right. \\ & \left. + \frac{m}{p'^- p^-} \left(p^- \gamma_\mu^\perp \bar{n}_\nu - p'^- \gamma_\nu^\perp \bar{n}_\mu + \bar{n}_\mu \bar{n}_\nu (\not{p}'_\perp - \not{p}_\perp - m) \right) \right] \frac{\not{n}}{2} \end{aligned} \quad (2.41)$$

The usoft gluon vertex is left unchanged.

2.4 Wilson Lines

2.4.1 Collinear Wilson Lines and Gauge Invariant Operators

In full QCD, a n -coll. quark can emit \bar{n} -coll. gluons before going into the hard interaction. Since the quark gets pushed far off-shell by this, these propagations of off-shell quarks are integrated out and do not appear in the effective theory, so there is no interaction between the n - and the \bar{n} -coll. sector in the SCET Lagrangian. These \bar{n} -coll. gluons reappear in the matching between the full theory and the effective theory current as collinear Wilson lines, Fig. 4. To find the correct \bar{n} -collinear Wilson line, containing the \bar{n} -coll. gluons emitted from an n -coll. incoming quark, we write down the full QCD

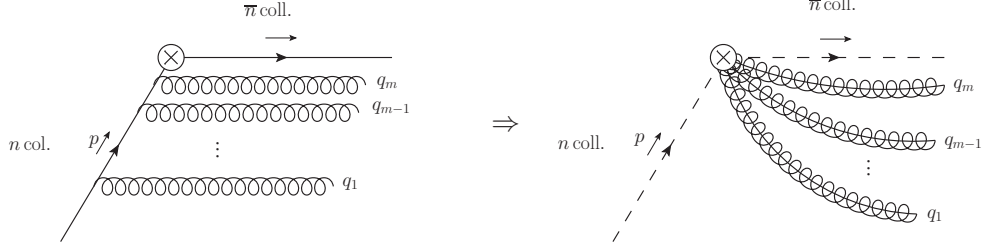


Figure 4: Collinear Wilson line. The contributions from \bar{n} -coll. gluons emitted from a n -coll. incoming quark are summed in a \bar{n} -coll. Wilson line. These collinear Wilson lines appear in external currents in the matching QCD \rightarrow SCET, where there is no interaction between \bar{n} - and n -coll. particles.

expression for the left diagram in Fig. 4 and then change to collinear external fields ξ and expand in λ , using the SCET power counting for collinear fields (again all gluon momenta are incoming)

$$\begin{aligned} & \bar{\xi}_{\bar{n}} \Gamma \frac{i(\not{p} + \sum_{i=1}^m \not{q}_i)}{(p + \sum_{i=1}^m q_i)^2 + i0} (ig\gamma^{\mu_m} A_{\mu_m}) \frac{i(\not{p} + \sum_{i=1}^{m-1} \not{q}_i)}{(p + \sum_{i=1}^{m-1} q_i)^2 + i0} (ig\gamma^{\mu_{m-1}} A_{\mu_{m-1}}) \\ & \times \dots \times \frac{i(\not{p} + \not{q}_1)}{(p + q_1)^2 + i0} (ig\gamma^{\mu_1} A_{\mu_1}) \xi_n. \end{aligned} \quad (2.42)$$

The momentum p^μ has a n -coll. scaling $p^\mu \sim Q(\lambda^2, 1, \lambda)$, for the gluon momenta q_i and for the gluon fields themselves we use a \bar{n} -coll. power counting $\sim Q(1, \lambda^2, \lambda)$. With that counting the leading order in λ of the expression above is

$$\bar{\xi}_{\bar{n}} \Gamma \frac{(-g)^m n^{\mu_m} \dots n^{\mu_1}}{(q_1^+ + i0) \dots (\sum_{i=1}^m q_i^+ + i0)} A_{\mu_m} \dots A_{\mu_1} \xi_n. \quad (2.43)$$

To get all contributions from the \bar{n} -coll. gluons coming from the n -coll. quark one also has to include the sum over the number of final state gluons m as well as the sum over all permutations of the gluons. Then we can write the SCET current as $\bar{\chi}_{\bar{n}} \Gamma \xi_n$ with the \bar{n} -coll. jet field $\chi_{\bar{n}} = W_{\bar{n}}^\dagger \xi_{\bar{n}}$ where the \bar{n} -coll. Wilson line is

$$W_{\bar{n}} = \sum_m \sum_{\text{perm.}} \frac{(-g)^m n_{\mu_1} \dots n_{\mu_m}}{(q_1^+ + i0) \dots (\sum_{j=1}^m q_j^+ + i0)} A_{\bar{n}}^{\mu_m}(q_m) \dots A_{\bar{n}}^{\mu_1}(q_1). \quad (2.44)$$

In position space the Wilson line has the form

$$W_{\bar{n}}(x) = \text{P exp} \left[ig \int_{-\infty}^x ds \, n \cdot A_{\bar{n}}(sn) \right], \quad (2.45)$$

where P denotes the path-ordering operator, i.e. all fields at spacetime points that are run through earlier in the integration are further to the right. The same can be done for an outgoing \bar{n} -coll. quark emitting n -coll. gluons, which leads to a n -coll. Wilson line

$$W_n = \sum_m \sum_{\text{perm.}} \frac{(-g)^m \bar{n}_{\mu_1} \dots \bar{n}_{\mu_m}}{(q_1^- - i0) \dots (\sum_{j=1}^m q_j^- - i0)} A_n^{\mu_m}(q_m) \dots A_n^{\mu_1}(q_1), \quad (2.46)$$

$$W_n(x) = \bar{\text{P exp}} \left[-ig \int_x^\infty ds \, \bar{n} \cdot A_n(s\bar{n}) \right]. \quad (2.47)$$

such that the full SCET current has the form $\bar{\chi}_{\bar{n}} \Gamma \chi_n$ with

$$\chi_n = W_n^\dagger \xi_n, \quad \chi_{\bar{n}} = W_{\bar{n}}^\dagger \xi_{\bar{n}}. \quad (2.48)$$

To pull out the large label components from the jet field one has to make sure that the label of the jet field is the sum of the label of the collinear quark and all gluons. To assure this it is convenient to define the label operator \mathcal{P}^μ that picks up the labels of the fields it is acting on, i.e. $\mathcal{P}^\mu \prod_i \xi_{n,p_i} = (\sum_i p_i^\mu) \prod_i \xi_{n,p_i}$. Then the decomposition in large label components and a residual jet field reads

$$\chi_n(x) = e^{-i\mathcal{P}^- x} (W_n^\dagger \xi_{n,p})(x) = \int d\omega e^{-i\omega x} \delta(\omega - \mathcal{P}^-) (W_n^\dagger \xi_{n,p})(x) \quad (2.49)$$

The collinear Wilson lines are necessary to construct the jet fields χ in such a way they are invariant under collinear gauge transformations $U(x) = e^{i\alpha^A(x)T^A}$. Collinear gauge transformation means that $\partial_\mu \alpha^A(x)$ scales like a collinear momentum [7, 8]. The physical interpretation of this is that a collinear gauge transformation leaves a particle within the same jet, i.e. a $n(\bar{n})$ -coll. particle is always transformed into another $n(\bar{n})$ -coll. particle under a $n(\bar{n})$ -coll. gauge transformation. In the same way the gluonic operator $\mathcal{G}^{\mu\nu}$ invariant under collinear gauge transformations can be constructed from collinear Wilson lines and the field strength tensor $G^{\mu\nu}$

$$\mathcal{G}_n^{\mu\nu} = W_n^\dagger G_n^{\mu\nu} W_n. \quad (2.50)$$

When we write the field strength tensor as $G_n^{\mu\nu} = -\frac{i}{g} [iD_n^\mu, iD_n^\nu]$ and use a n -coll. covariant derivative D_n^μ , i.e.

$$\begin{aligned} iD_n^\mu &= \mathcal{P}^\mu + gA_n^\mu \\ &= (\mathcal{P}^- + gA_n^-) \frac{n^\mu}{2} + \left(\mathcal{P}_\perp^\mu + gA_{n,\perp}^\mu \right) + \mathcal{O}(\lambda^2) \end{aligned} \quad (2.51)$$

and use the fact that, by definition, the covariant derivative along the light-cone acting on a n -coll. Wilson line is zero, i.e.

$$iD^- W_n = W_n \mathcal{P}^-, \quad W_n^\dagger iD^- = \mathcal{P}^- W_n^\dagger, \quad (2.52)$$

$\mathcal{G}_n^{\mu\nu}$ can be written in the form

$$\mathcal{G}_n^{\mu\nu} = -\frac{i}{g} \left([\mathcal{P}^-, W_n^\dagger iD_\perp^\nu W_n] \frac{n^\mu}{2} - [\mathcal{P}^-, W_n^\dagger iD_\perp^\mu W_n] \frac{n^\nu}{2} \right) + \mathcal{O}(\lambda^2). \quad (2.53)$$

In Sec. 3.2 we will use the gauge invariant quark and gluon jet fields as basic building blocks for constructing the relevant EFT operators. For n -coll. quarks the leading order operator is $\bar{\chi}_n \frac{\not{n}}{2} \chi_n$ (note that $\bar{\chi}_n \chi_n$ is zero because of the relations in Eq. (2.18)), for a collinear gluon it has to be some contraction of $\mathcal{G}_n^{\mu\nu}$. $\mathcal{G}_n^{\mu\nu} \mathcal{G}_{n,\mu\nu}$ is $\mathcal{O}(\lambda^4)$, but $\mathcal{G}_n^{\mu\alpha} \mathcal{G}_{n,\mu}^\beta \bar{n}_\alpha \bar{n}_\beta$ is $\mathcal{O}(\lambda^2)$, so the gluon jet field is defined as

$$B_n^\mu = \mathcal{G}_n^{\mu\nu} \bar{n}_\nu = \frac{i}{g} [\mathcal{P}^-, W_n^\dagger iD_\perp^\mu W_n] \quad (2.54)$$

and the leading order gauge invariant n -coll. gluon operator is

$$B_n^\mu B_{n,\mu} \sim \mathcal{O}(\lambda^2). \quad (2.55)$$

2.4.2 Usoft Wilson Lines

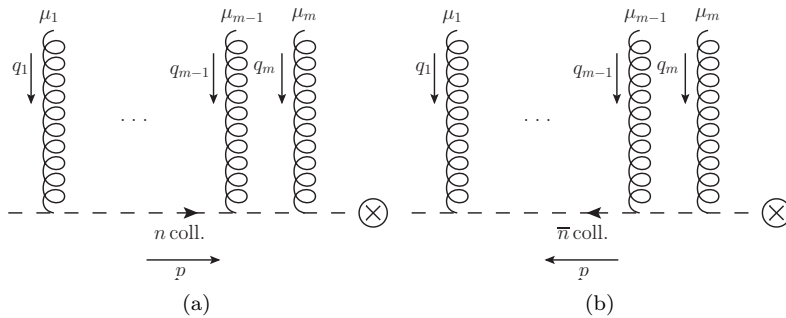


Figure 5: Usoft Wilson lines for DIS. The contributions from usoft gluons coupling to collinear quarks can be summed in usoft Wilson lines. For DIS in the Breit frame we have to consider an n -coll. incoming quark (a) and an \bar{n} -coll. outgoing quark (b).

The interactions between collinear and usoft particles can be removed from the Lagrangian with the field redefinitions [9]

$$\begin{aligned} \xi_n &\rightarrow Y_n \xi_n^{(0)} & \xi_{\bar{n}} &\rightarrow Y_{\bar{n}} \xi_{\bar{n}}^{(0)} \\ A_n &\rightarrow Y_n A_n^{(0)} Y_n^\dagger & A_{\bar{n}} &\rightarrow Y_{\bar{n}} A_{\bar{n}}^{(0)} Y_{\bar{n}}^\dagger \end{aligned} \quad (2.56)$$

With this redefinitions the Lagrangian in terms of these new fields contains no longer interaction terms between usoft fields and the new collinear fields with the superscript (0). All effects of usoft particles are encoded in usoft Wilson lines $Y_n, Y_{\bar{n}}$ that appear in external currents. The correct Wilson lines for DIS in the Breit frame with one incoming n -coll. and one outgoing \bar{n} -coll. (anti-) quark in the current can be found from the diagrams in Fig. 5 (plus all permutations).

$$Y_n = \sum_{\text{perm.}} \sum_m \frac{(-g)^m n_{\mu_1} \dots n_{\mu_m}}{(q_1^+ + i0) \dots (\sum_{j=1}^m q_j^+ + i0)} A_{us}^{\mu_m}(q_m) \dots A_{us}^{\mu_1}(q_1) \quad (2.57)$$

$$Y_n(x) = \text{P exp} \left[ig \int_{-\infty}^x ds n \cdot A_{us}(sn) \right] \quad (2.58)$$

$$Y_{\bar{n}} = \sum_{\text{perm.}} \sum_m \frac{(-g)^m \bar{n}_{\mu_1} \dots \bar{n}_{\mu_m}}{(q_1^- - i0) \dots (\sum_{j=1}^m q_j^- - i0)} A_{us}^{\mu_m}(q_m) \dots A_{us}^{\mu_1}(q_1) \quad (2.59)$$

$$Y_{\bar{n}}(x) = \bar{\text{P exp}} \left[-ig \int_x^\infty ds \bar{n} \cdot A_{us}(s\bar{n}) \right] \quad (2.60)$$

3 Deep Inelastic Scattering with Massless Quarks

The process of “deep inelastic scattering” (DIS) is the scattering of a lepton on a hadron. The term “inelastic” implies that the kinetic energy of the incoming lepton is not conserved whereas “deep” refers to the high momentum transfer Q^2 in the process. Deep inelastic scattering can be studied with various kinds of leptons and hadrons, but the standard process is the scattering of a high energetic electron on a proton. In the following we will only concentrate on unpolarized DIS of a charged lepton on a hadron and set the lepton and the hadron mass to zero. As a further simplification we will only consider neutral current DIS with a photon exchange. The process will be studied at leading order in QED and with one-loop QCD corrections to the hadronic tensor, i.e. at order $\mathcal{O}(\alpha)\mathcal{O}(\alpha_s)$.

3.1 Cross Section and Kinematics

The general cross section for a process $1 + 2 \rightarrow 3 + \dots$ is

$$\sigma = \frac{S}{2\lambda^{\frac{1}{2}}(s, m_1^2, m_2^2)} \int \prod_j \frac{d^3\mathbf{k}_j}{(2\pi)^3} \frac{1}{2\sqrt{\mathbf{k}_j^2 + m_j^2}} (2\pi)^4 \delta^{(4)}(p_1 + p_2 - \sum_i k_i) |\mathcal{M}|^2, \quad (3.1)$$

with the symmetry factor S for identical particles, the total center of mass energy s and the function $\lambda(x, y, z) = x^2 + y^2 + z^2 - 2xy - 2xz - 2yz$. Here we consider the process $e + P \rightarrow e + X$ and set the electron and proton mass to zero, see Fig. 6.

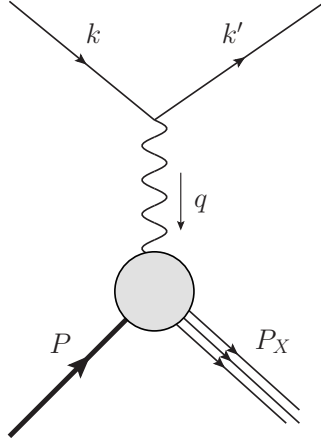


Figure 6: Deep inelastic scattering. An incoming electron with momentum k scatters off a hadron with momentum P via the exchange of a virtual photon.

$$d\sigma = \frac{1}{2s} \frac{d^3\mathbf{k}'}{(2\pi)^3} \frac{1}{2|\mathbf{k}'|} \sum_X d\Pi_X (2\pi)^4 \delta^{(4)}(P + \underbrace{k - k'}_q - P_X) |\mathcal{M}|^2 \quad (3.2)$$

\sum_X denotes the sum over all possible hadronic final states and $d\Pi_X$ the integration over the whole phase space. We want to change to proper variables to get the differential cross section with respect to Lorentz-invariants, so we use

$$Q^2 = -q^2 \quad (3.3)$$

$$x = \frac{-q^2}{2P \cdot q} \quad (3.4)$$

$$y = \frac{P \cdot q}{P \cdot k} = \frac{Q^2}{sx} \quad (3.5)$$

$$\frac{d^3\mathbf{k}'}{(2\pi)^3} \frac{1}{2|\mathbf{k}'|} = \frac{d|\mathbf{k}'| d\cos\theta |\mathbf{k}'|}{(2\pi)^2} \frac{1}{2} = \frac{dx dQ^2 y}{(4\pi)^2 x} \quad (3.6)$$

With this substitution the cross section reads

$$d\sigma = \frac{dx dQ^2 y}{(4\pi)^2 Q^2} \sum_X d\Pi_X (2\pi)^4 \delta^{(4)}(P + q - P_X) |\mathcal{M}|^2. \quad (3.7)$$

The amplitude \mathcal{M} for the process at leading order in QED is

$$\mathcal{M}(eP \rightarrow eX) = \bar{u}(k')(-ie\gamma_\mu)u(k)\frac{-i}{q^2}(ie)\langle X|J^\mu(0)|P\rangle \quad (3.8)$$

and the spin-averaged square (from here on all matrix elements should be understood as spin-averaged) is

$$|\mathcal{M}|^2 = \frac{2(4\pi)^2\alpha^2}{Q^4}L_{\mu\nu}\langle P|J^\mu(0)|X\rangle\langle X|J^\nu(0)|P\rangle, \quad (3.9)$$

where the leptonic tensor is defined as

$$L_{\mu\nu} = k_\mu k'_\nu + k_\nu k'_\mu - k \cdot k' g_{\mu\nu}. \quad (3.10)$$

The electromagnetic current for quark fields with flavor i is

$$J^\mu = \sum_i Q_i \bar{q}_i \gamma^\mu q_i. \quad (3.11)$$

With the definition of the hadronic tensor $W^{\mu\nu}$

$$\begin{aligned} W^{\mu\nu} &= \frac{1}{4\pi} \sum_X d\Pi_X (2\pi)^4 \delta^{(4)}(q + P - P_X) \langle P|J^\mu(0)|X\rangle \langle X|J^\nu(0)|P\rangle \\ &= \frac{1}{4\pi} \sum_X d\Pi_X \int d^4x e^{i(q+P-P_X)x} \langle P|J^\mu(0)|X\rangle \langle X|J^\nu(0)|P\rangle \\ &= \frac{1}{4\pi} \sum_X d\Pi_X \int d^4x e^{iqx} \langle P|J^\mu(x)|X\rangle \langle X|J^\nu(0)|P\rangle \\ &= \frac{1}{4\pi} \int d^4x e^{iqx} \langle P|J^\mu(x)J^\nu(0)|P\rangle \end{aligned} \quad (3.12)$$

we get the double differential cross section in the form

$$\frac{d^2\sigma}{dx dQ^2} = \frac{4\pi\alpha^2 y^2}{Q^6} L_{\mu\nu} W^{\mu\nu}. \quad (3.13)$$

Using the fact of current conservation $q_\mu W^{\mu\nu} = q_\nu W^{\mu\nu} = 0$ one can write down the most general ansatz for the hadronic tensor³:

$$W^{\mu\nu} = \left(-g^{\mu\nu} - \frac{q^\mu q^\nu}{Q^2}\right) W_1(x, Q^2) + \left(P^\mu + \frac{q^\mu}{2x}\right) \left(P^\nu + \frac{q^\nu}{2x}\right) W_2(x, Q^2). \quad (3.14)$$

From the expression above we can find the projectors onto W_1 and W_2 :

$$\begin{aligned} A &:= \frac{Q^2}{4x^2}, \\ P_1^{\mu\nu} &= \frac{1}{(d-2)A} (P^\mu P^\nu - A g^{\mu\nu}), \end{aligned} \quad P_1^{\mu\nu} W_{\mu\nu} = W_1, \quad (3.15)$$

$$P_2^{\mu\nu} = \frac{1}{(d-2)A^2} ((d-1)P^\mu P^\nu - A g^{\mu\nu}), \quad P_2^{\mu\nu} W_{\mu\nu} = W_2, \quad (3.16)$$

with d the number of spacetime dimensions. One often defines a longitudinal form factor

$$W_L = A W_2 - W_1, \quad (3.17)$$

$$P_L^{\mu\nu} = \frac{1}{A} P^\mu P^\nu, \quad P_L^{\mu\nu} W_{\mu\nu} = W_L. \quad (3.18)$$

With the standard definitions for the form factors

$$F_1(x, Q^2) = W_1(x, Q^2), \quad (3.19)$$

$$F_2(x, Q^2) = \frac{Q^2}{2x} W_2(x, Q^2), \quad (3.20)$$

$$F_L(x, Q^2) = F_2(x, Q^2) - 2x F_1(x, Q^2), \quad (3.21)$$

³Also an additional term $\sim \epsilon^{\mu\nu\alpha\beta} P_\alpha q_\beta$ would be consistent with current conservation, but since the leptonic tensor $L_{\mu\nu}$ is symmetric in μ and ν if we consider only vector coupling, this term does not contribute.

the differential cross section for a massless hadron reads

$$\frac{d^2\sigma}{dx dQ^2} = \frac{4\pi\alpha^2}{Q^4} \left(((1-y)^2 + 1)F_1(x, Q^2) + \frac{1-y}{x}F_L(x, Q^2) \right). \quad (3.22)$$

The definition of the Bjorken variable x in Eq. (3.4) gives a relation between x and the invariant mass of the hadronic final state $P_X^2 = (P + q)^2$

$$x := \frac{-q^2}{2 P \cdot q} = \frac{1}{1 + \frac{P_X^2}{Q^2}}. \quad (3.23)$$

In the case where all particles in the final state are collimated in one narrow jet the invariant mass reaches its minimum and therefore x its maximum. If all particles are massless the limit is $P_X^2 \rightarrow 0$ and $x \rightarrow 1$. If we assume that at least one quark antiquark pair of a heavy flavor with mass m is produced we have the restraints $P_X^2 \geq 4m^2$ and $x \leq \frac{1}{1 + 4\frac{m^2}{Q^2}}$, see Sec. 4.1.

DIS in the Parton Model

An incoming hadron with four-momentum P^μ scatters off a virtual photon with momentum q^μ . Here we assume the hadron to be massless, and choose the Breit-frame, in which the incoming photon transmits just the momentum Q and no energy. Then the four-momenta of the particles can be decomposed into light-cone components as following:

$$P^\mu = \frac{Q}{x} \frac{n^\mu}{2}, \quad (3.24)$$

$$q^\mu = -Q \frac{n^\mu}{2} + Q \frac{\bar{n}^\mu}{2}, \quad (3.25)$$

where x is the Bjorken scaling variable as defined in Eq. (3.4). In the parton model we can interpret the interaction in Fig. 6 as a free parton inside the hadron that got struck by the photon, see Fig. 7. If

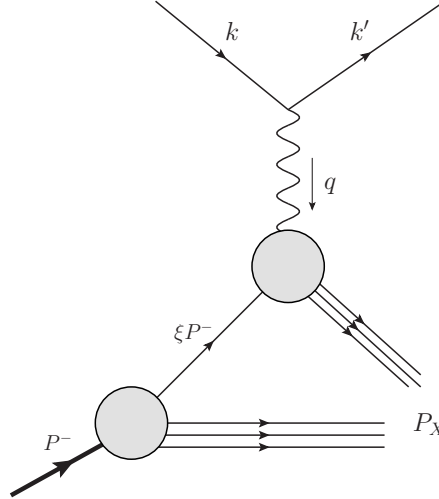


Figure 7: Deep inelastic scattering in the parton model. An incoming electron with momentum k scatters off a parton with fraction ξ of the hadron's longitudinal momentum. The total final state consists of beam remnants and hadrons created in the hard interaction.

the parton has the fraction ξ of the longitudinal momentum of the hadron and is also considered to be massless we find

$$\hat{P}^\mu = \frac{\xi Q}{x} \frac{n^\mu}{2} = \frac{Q}{\hat{x}} \frac{n^\mu}{2} \quad (3.26)$$

for the parton momentum \hat{P} with the partonic Bjorken variable

$$\hat{x} = \frac{x}{\xi}, \quad (3.27)$$

i.e. the Bjorken- x for the incoming parton. At tree-level the amplitude for the hard scattering of a free incoming parton with \hat{x} is $\sim \delta(1 - \hat{x})$, so $x = \xi$. So the measurable quantity x tells us (at tree-level) which momentum fraction of the hadron the struck parton was carrying. Even though this is no longer exactly true beyond tree-level, the requirement that $(\hat{P} + q)^2 \geq 0$ assures that $\xi \geq x$. So in the case where $x \rightarrow 1$ we also have $\xi \rightarrow 1$, i.e. the parton going into the hard interaction was carrying almost all of the hadron's momentum and all the beam remnants are soft.

3.2 DIS Factorization in SCET

3.2.1 Factorization of the Hadronic Tensor

The hadronic tensor in Eq. (3.14) can be factorized into non-perturbative matrix elements and Wilson coefficients describing the hard interaction by using SCET, as shown in Ref. [10]. With the definition

$$W_L = \frac{Q^2}{4x^2} W_2 - W_1 \quad (3.28)$$

the hadronic tensor can be written in the form

$$W^{\mu\nu} = -g_{\perp}^{\mu\nu} W_1 + \frac{1}{4} (n^\mu + \bar{n}^\mu) (n^\nu + \bar{n}^\nu) W_L. \quad (3.29)$$

To project onto W_1 and W_L one can use the projectors in Eqs. (3.15) and (3.18). This can be matched onto SCET operators. Since we constrain ourselves to the classical OPE region where the invariant mass of the hadronic final state scales like $Q^2(1-x)/x \sim Q^2$ (unlike the situation in the endpoint region where we have $Q^2(1-x) \ll Q^2$, see Sec. 5) the final state is integrated out and we are left with the n -coll. modes with an invariant mass of order $\sim \Lambda_{\text{QCD}}^2$ in the initial state, which can be described by a n -coll. jet field while all the hard interaction goes into a Wilson coefficient. The appropriate SCET operators for an incoming quark with flavor i or a gluon are

$$\bar{\chi}_{n,p}^{(i)}(0) \frac{\not{n}}{2} \chi_{n,p'}^{(i)}(0), \quad (3.30)$$

$$-\text{Tr} [B_{n,p}^\mu(0) B_{n,p'\mu}(0)]. \quad (3.31)$$

Note that if the soft-collinear decoupling is made explicit with the field redefinitions shown in Sec. 2.4.2, the usoft Wilson lines cancel to all orders because $Y_n^\dagger Y_n = \mathbf{1}$ and therefore only purely n -coll. objects remain. Following the arguments in Refs. [16] and [17] this also implies that all soft-bin subtractions vanish and we are not sensitive to any soft physics. The hard interaction is encoded in a Wilson coefficient and so the matching condition reads

$$W_j = \frac{1}{Q} \left(\sum_i \mathcal{O}_j^{(i)} + \frac{\mathcal{O}_j^{(g)}}{Q} \right), \quad (3.32)$$

$$\mathcal{O}_j^{(i,g)} = \langle P | \hat{\mathcal{O}}_j^{(i,g)} | P \rangle, \quad (3.33)$$

where $j = \{1, L\}$ and the sum runs over all active quark flavors and

$$\hat{\mathcal{O}}_j^{(i)} = \bar{\chi}_{n,p}^{(i)}(0) \frac{\not{n}}{2} C_j^{(i)}(\mathcal{P}^{\dagger-}, \mathcal{P}^-) \chi_{n,p'}^{(i)}(0), \quad (3.34)$$

$$\hat{\mathcal{O}}_j^{(g)} = -\text{Tr} [B_{n,p}^\mu(0) C_j^{(g)}(\mathcal{P}^{\dagger-}, \mathcal{P}^-) B_{n,p'\mu}(0)]. \quad (3.35)$$

Since all operators are local we neglect the argument from now on, i.e. $\chi_{n,p} := \chi_{n,p}(0)$. $C_j^{(q,g)}$ are the Wilson coefficients that have to be determined from the matching. First we work out the factorized form for the matrix elements of the quark operator:

$$\begin{aligned} \mathcal{O}_j^{(i)} &= \langle P | \left[\bar{\chi}_{n,p}^{(i)} \frac{\not{n}}{2} C_j^{(i)}(\mathcal{P}^{\dagger-}, \mathcal{P}^-) \chi_{n,p'}^{(i)} \right] | P \rangle \\ &= \int d\omega d\omega' C_j^{(i)}(\omega, \omega') \langle P | \left[\bar{\chi}_{n,p}^{(i)} \delta(\omega - \mathcal{P}^{\dagger-}) \frac{\not{n}}{2} \delta(\omega' - \mathcal{P}^-) \chi_{n,p'}^{(i)} \right] | P \rangle. \end{aligned} \quad (3.36)$$

The label operator \mathcal{P} acts only to the right, its conjugate \mathcal{P}^\dagger only to the left, both only inside the brackets. Momentum conservation tells us that $\mathcal{P}^- = \mathcal{P}^{\dagger-}$ between the states and we can rewrite $\delta(\omega - \mathcal{P}^{\dagger-})\delta(\omega' - \mathcal{P}^-) = \delta(\omega' - \omega)\delta(\omega' - \mathcal{P}^-)$. So with $C_j^{(i)}(\omega) := C_j^{(i)}(\omega, \omega)$ and

$$f_{i/P}(\xi) = \langle P | \bar{\chi}_{n,p}^{(i)} \frac{\not{P}}{2} [\delta(P^- \xi - \mathcal{P}^-) \chi_{n,p'}^{(i)}] | P \rangle, \quad (3.37)$$

$$\bar{f}_{i/P}(\xi) := -f_{i/P}(-\xi) \quad (3.38)$$

one gets

$$\begin{aligned} \mathcal{O}_j^{(i)} &= \int d\omega C_j^{(i)}(\omega) f_{i/P}\left(\frac{\omega}{P^-}\right) \\ &= \int d\omega \left(\Theta(\omega) C_j^{(i)}(\omega) f_{i/P}\left(\frac{\omega}{P^-}\right) + \Theta(-\omega) C_j^{(i)}(\omega) f_{i/P}\left(\frac{\omega}{P^-}\right) \right) \\ &= \int d\omega \Theta(\omega) \left(C_j^{(i)}(\omega) f_{i/P}\left(\frac{\omega}{P^-}\right) + C_j^{(i)}(-\omega) f_{i/P}\left(\frac{-\omega}{P^-}\right) \right) \\ &= \int d\omega \Theta(\omega) \left(C_j^{(i)}(\omega) f_{i/P}\left(\frac{\omega}{P^-}\right) - C_j^{(i)}(-\omega) \bar{f}_{i/P}\left(\frac{\omega}{P^-}\right) \right). \end{aligned} \quad (3.39)$$

The splitting into a part $\sim \Theta(\omega)$ with positive labels and a part $\sim \Theta(-\omega)$ with negative labels already suggests that one term will depend on the quark and one on the anti-quark content in the hadron (compare with the splitting of the fermion field into residual quark and anti-quark fields with positive and negative labels respectively in Eq. (2.15)). It will be shown in Sec. 3.2.2 that $f_{i/P}(\xi)$ and $\bar{f}_{i/P}(\xi)$ are the quark and anti-quark PDFs in terms of SCET fields. Because of charge conjugation symmetry $C_j^{(i)}(\omega) = -C_j^{(i)}(-\omega)$ and with the redefinition of the hard coefficient $C_j^{(i)}(\omega) = \frac{Q}{\omega} H_j^{(i)}\left(\frac{Q}{\omega}\right)$ and the substitution $\omega = P^- \xi$ the final expression for the matrix elements reads

$$\mathcal{O}_j^{(i)} = Q \int \frac{d\xi}{\xi} \Theta(\xi) H_j^{(i)}\left(\frac{x}{\xi}\right) (f_{i/P}(\xi) + \bar{f}_{i/P}(-\xi)). \quad (3.40)$$

Next we will do the same for the gluon operator

$$\begin{aligned} \mathcal{O}_j^{(g)} &= -\langle P | \text{Tr} \left[B_{n,p}^\mu C_j^{(g)}(\mathcal{P}^{\dagger-}, \mathcal{P}^-) B_{n,p'\mu} \right] | P \rangle \\ &= -\int d\omega d\omega' C_j^{(g)}(\omega, \omega') \langle P | \text{Tr} \left[B_{n,p}^\mu \delta(\omega - \mathcal{P}^{\dagger-}) \delta(\omega' - \mathcal{P}^-) B_{n,p'\mu} \right] | P \rangle. \end{aligned} \quad (3.41)$$

Similar steps as for the quark case, including the same argument from momentum conservation to rewrite the delta distributions and the substitution $\omega = P^- \xi$ lead to

$$\mathcal{O}_j^{(g)} = T_f (P^-)^2 \int d\xi \xi C_j^{(g)}(P^- \xi) \left(-\frac{1}{T_f P^- \xi} \langle P | \text{Tr} \left[B_{n,p}^\mu [\delta(P^- \xi - \mathcal{P}^-) B_{n,p'\mu}] \right] | P \rangle \right). \quad (3.42)$$

Since the gluon is its own anti-particle there is no need to split the whole expression into terms with positive and negative labels and with the substitution $C_j^{(g)}(\omega) = \frac{1}{T_f} \frac{Q^2}{\omega^2} H_j^{(g)}\left(\frac{Q}{\omega}\right)$ and

$$f_{g/P}(\xi) = -\frac{1}{T_f P^- \xi} \langle P | \text{Tr} \left[B_{n,p}^\mu [\delta(P^- \xi - \mathcal{P}^-) B_{n,p'\mu}] \right] | P \rangle, \quad (3.43)$$

where $f_{g/P}(\xi)$ is the gluon PDF in SCET (see Sec. 3.2.3), we finally get the factorized form of the matrix elements for the gluon operator:

$$\mathcal{O}_j^{(g)} = Q^2 \int \frac{d\xi}{\xi} \Theta(\xi) H_j^{(g)}\left(\frac{x}{\xi}\right) f_{g/P}(\xi). \quad (3.44)$$

Eventually the factorized form of the full hadronic tensor is ($j = (1, L)$):

$$W_j^{(P)}(x, \mu^2) = \sum_i \left(H_j^{(i)} \otimes (f_{i/P} + \bar{f}_{i/P}) \right)(x, \mu^2) + \left(H_j^{(g)} \otimes f_{g/P} \right)(x, \mu^2), \quad (3.45)$$

with the convolution defined as

$$(g \otimes h)(x, \mu^2) = \int \frac{d\xi}{\xi} g\left(\frac{x}{\xi}, \mu^2\right) h(\xi, \mu^2). \quad (3.46)$$

3.2.2 The Quark PDF

We check that the definition of the PDF in SCET in Eq. (3.37) agrees with the common QCD definition. The standard QCD definition of the quark PDF is given in Ref. [11] as

$$f_{i/P}(\xi) = \frac{1}{2\pi} \int dt e^{-i\xi P^- t} \langle P | \bar{\psi}^{(i)}(t\bar{n}) \frac{\not{n}}{2} U^\dagger(t\bar{n}, 0) \psi^{(i)}(0) | P \rangle, \quad (3.47)$$

with the Wilson line

$$U^\dagger(t\bar{n}, 0) = \text{P exp} \left[ig \int_0^t ds \bar{n} \cdot A(s\bar{n}) \right]. \quad (3.48)$$

To write this in SCET we switch to n-coll. fields

$$\psi^{(i)}(x) \rightarrow \xi_n^{(i)}(x), \quad (3.49)$$

$$A^\mu(x) \rightarrow A_n^\mu(x). \quad (3.50)$$

Then the Wilson line $U^\dagger(t\bar{n}, 0)$ in Eq. (3.47) becomes a collinear Wilson line $W_n^\dagger(t\bar{n}, 0)$ that can be decomposed into two Wilson lines going to ∞ like in Eq. (2.47)

$$U^\dagger(t\bar{n}, 0) \rightarrow W_n^\dagger(t\bar{n}, 0) = W_n(t\bar{n}) W_n^\dagger(0). \quad (3.51)$$

Therefore we find the usual SCET jet fields $\chi_n = W_n^\dagger \xi_n$ and the PDF becomes

$$f_{i/P}(\xi) = \frac{1}{2\pi} \int dt e^{-i\xi P^- t} \langle P | \bar{\chi}_n^{(i)}(t\bar{n}) \frac{\not{n}}{2} \chi_n^{(i)}(0) | P \rangle. \quad (3.52)$$

Pulling out the large label components by writing

$$\chi_n(x) = \int d\omega e^{-i\omega x} \delta(\omega - \mathcal{P}^-) \chi_{n,p}(x) \quad (3.53)$$

and using the argument from momentum conservation as in the previous section we find

$$f_{i/P}(\xi) = \frac{1}{2\pi} \int d\omega dt e^{-i(\xi P^- - \omega)t} \langle P | \bar{\chi}_{n,p}^{(i)}(t\bar{n}) \frac{\not{n}}{2} \left[\delta(\omega - \mathcal{P}^-) \chi_{n,p'}^{(i)}(0) \right] | P \rangle. \quad (3.54)$$

Note that the field $\bar{\chi}_{n,p}(x)$ only depends on residual momenta, i.e. long distance fluctuations, so we can shift it by applying a residual momentum operator K : $\bar{\chi}_{n,p}(x) = e^{-iKx} \bar{\chi}_{n,p}(0) e^{iKx}$. Since $K \sim \lambda^2$ while the other terms in the exponential function, ξP^- and ω , are all large label components, the residual momentum can be dropped. This yields

$$\begin{aligned} f_{i/P}(\xi) &= \frac{1}{2\pi} \int d\omega dt e^{-i(\xi P^- - \omega)t} \langle P | \bar{\chi}_{n,p}^{(i)}(0) \frac{\not{n}}{2} \left[\delta(\omega - \mathcal{P}^-) \chi_{n,p'}^{(i)}(0) \right] | P \rangle \\ &= \langle P | \bar{\chi}_{n,p}^{(i)}(0) \frac{\not{n}}{2} \left[\delta(P^- \xi - \mathcal{P}^-) \chi_{n,p'}^{(i)}(0) \right] | P \rangle, \end{aligned} \quad (3.55)$$

which is precisely the term we encountered in Eq. (3.37). The anti-quark PDF is defined as

$$\begin{aligned} \bar{f}_{i/P}(\xi) &= \frac{1}{2\pi} \int dt e^{-i\xi P^- t} \langle P | \text{Tr} \left[\frac{\not{n}}{2} \psi^{(i)}(t\bar{n}) U^T(t\bar{n}, 0) \bar{\psi}^{(i)}(0) \right] | P \rangle \\ &= -\frac{1}{2\pi} \int dt e^{-i\xi P^- t} \langle P | \left(\bar{\psi}^{(i)}(t\bar{n}) \frac{\not{n}}{2} U^\dagger(t\bar{n}, 0) \psi^{(i)}(0) \right)^* | P \rangle \\ &= -\left(f_{i/P}(-\xi) \right)^* \\ &= -f_{i/P}(-\xi). \end{aligned} \quad (3.56)$$

3.2.3 The Gluon PDF

To see that Eq. (3.43) is indeed the SCET version of the gluon PDF we go back to the Collins-Soper definition of the gluon PDF (Ref. [11]), which is

$$f_{g/P}(\xi) = \frac{1}{2\pi\xi P^-} \int dt e^{-i\xi P^- t} \langle P | G^{\alpha\mu,A}(t\bar{n}) \mathcal{U}_{AB}^\dagger(t\bar{n}, 0) G_{\mu\beta}^B(0) | P \rangle \bar{n}_\alpha \bar{n}^\beta, \quad (3.57)$$

with the gluon field strength tensor $G_{\mu\nu}^A = \partial_\mu A_\nu^A - \partial_\nu A_\mu^A + g f^{ABC} A_\mu^B A_\nu^C$ and the Wilson line in the adjoint representation

$$\mathcal{U}_{AB}^\dagger(t\bar{n}, 0) = \text{P exp} \left[ig \int_0^t ds \bar{n} \cdot A^C(s\bar{n}) \mathcal{T}^C \right]_{AB}. \quad (3.58)$$

\mathcal{T}^C denotes the generator of SU(3) in the adjoint, and T^C in the fundamental representation. When we change to SCET fields $A^\mu \rightarrow A_n^\mu$ we get a collinear Wilson line in the adjoint representation $\mathcal{U}_{AB}^\dagger(t\bar{n}, 0) \rightarrow \mathcal{W}_{AB}^\dagger(t\bar{n}, 0) = \mathcal{W}_{AC}(t\bar{n}) \mathcal{W}_{CB}^\dagger(0)$. By using the trace relation for the generators in the fundamental representation $\text{Tr} [T^A T^B] = T_f \delta^{AB}$ and $\mathcal{W}_{AB} T^B = T^B \mathcal{W}_{BA}^\dagger = W_n^\dagger T^A W_n$ (see Ref. [9]) we can write

$$\begin{aligned} \mathcal{W}_{AC}(t\bar{n}) \delta^{CD} \mathcal{W}_{DB}^\dagger(0) &= \frac{1}{T_f} \text{Tr} [T^C T^D] \mathcal{W}_{AC}(t\bar{n}) \mathcal{W}_{DB}^\dagger(0) \\ &= \frac{1}{T_f} \text{Tr} [\mathcal{W}_{AC}(t\bar{n}) T^C T^D \mathcal{W}_{DB}^\dagger(0)] \\ &= \frac{1}{T_f} \text{Tr} [(W_n^\dagger T^A W_n)(t\bar{n}) (W_n^\dagger T^B W_n)(0)]. \end{aligned} \quad (3.59)$$

So with the definition of the gluon jet field as in Eq. (2.54)

$$B_n^\mu = W_n^\dagger G_n^{\mu\nu, A} T^A W_n \bar{n}_\nu \quad (3.60)$$

we get

$$\begin{aligned} \bar{n}_\alpha \bar{n}^\beta G_n^{\alpha\mu, A}(t\bar{n}) \mathcal{W}_{AB}^\dagger(t\bar{n}, 0) G_{n\mu\beta}^B &= -\frac{1}{T_f} \text{Tr} [B_n^\mu(t\bar{n}) B_{n\mu}(0)] \\ &= -\frac{1}{T_f} \int d\omega e^{i\omega t} \text{Tr} [B_{n,p}^\mu(0) [\delta(\omega - \mathcal{P}^-) B_{n\mu,p'}(0)]] \end{aligned} \quad (3.61)$$

which leads to the SCET gluon PDF in Eq. (3.43). The covariant derivative in the gluon jet field can also be split into a perpendicular label operator and a gluon field

$$iD_\perp^\mu = \mathcal{P}_\perp^\mu + gA_\perp^\mu \quad (3.62)$$

and when using this in B_n^μ in the gluon PDF Eq. (3.43) and using the fact of momentum conservation, i.e.

$$\langle P | [\dots \mathcal{P}] | P \rangle = 0 = \langle P | [\mathcal{P} \dots] | P \rangle, \quad (3.63)$$

the SCET gluon PDF can be written in terms of collinear Wilson lines, gluon fields and label operators as

$$f_{g/P}(\xi) = -\frac{P^- \xi}{T_f g^2} \langle P | \text{Tr} [W_n^\dagger [(\mathcal{P}_\perp^\mu + gA_{n\perp}^\mu) W_n] [\delta(P^- \xi - \mathcal{P}^-) W_n^\dagger [(\mathcal{P}_\mu^\perp + gA_{n\mu}^\perp) W_n]] | P \rangle. \quad (3.64)$$

3.3 Hard Matching Coefficients

To find the hard coefficients $H_j(x, \mu^2)$ in Eq. (3.45) one has to perform the matching between full QCD and the SCET operators for different partonic initial states $|\hat{P}\rangle$. Since the hard coefficients encode the physics above the matching scale and are not sensitive to any physics at lower scales, one can use partons instead of hadrons as initial states to do the matching calculation and identify the hard coefficients. In the massless case this is most conveniently done in pure dimensional regularization without any additional IR regulator because then all effective theory diagrams beyond tree level are scaleless and therefore vanish in dimensional regularization. This implies that the matching coefficient is just the finite piece of the full QCD result⁴, while the UV divergences of the SCET operators are the same as the IR divergences of the

⁴Because the matching is between renormalized operators the UV divergences do not enter the matching anyway. Since the full theory and effective theory must have the same IR divergences (because the effective theory has to reproduce the full theory at low energies), the IR divergences will cancel in the matching. So only the finite parts contribute to the matching coefficient.

full theory with a different sign⁵. We will also check this result by doing the SCET calculations with an off-shellness as an IR regulator to see the UV divergences explicitly in Sec. 3.4. The partonic tensor $\hat{W}^{\mu\nu}$ can be calculated by taking the imaginary part of the time-ordered product of the currents

$$\hat{T}^{\mu\nu} = i \int d^4x e^{iqx} \langle \hat{P} | T \{ J^\mu(x) J^\nu(0) \} | \hat{P} \rangle, \quad (3.65)$$

$$\hat{W}^{\mu\nu} = \frac{1}{2\pi} \text{Im} \hat{T}^{\mu\nu}. \quad (3.66)$$

This has the advantage that the time-order matrix elements $\hat{T}^{\mu\nu}$ can be calculated with usual Feynman diagrams.

3.3.1 Quark Form Factor

The relevant diagrams to order α_s with quarks in the initial state are shown in Fig. 8, the matrix elements are averaged over the spin of the incoming quark. The imaginary part was taken with the relations in

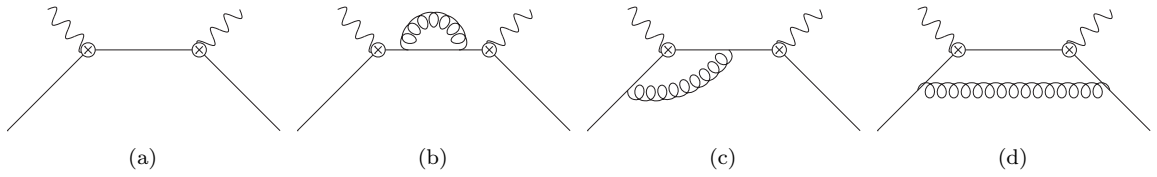


Figure 8: QCD Diagrams for DIS with Initial Quarks

appendix B. Here only the calculations for the form factor \hat{W}_1 are shown explicitly, the result for \hat{W}_L will be given at the end of the section.

Diagram Fig. 8a:

The tree level diagram is

$$\begin{aligned} \hat{T}^{\mu\nu (q),(a)}(x) &= i \frac{1}{2} \sum_s \bar{u}(p, s) \gamma^\nu \frac{i(\not{p} + \not{q})}{(p+q)^2 + i0} \gamma^\mu u(p, s) \\ &= -\frac{x}{2Q^2} \frac{1}{(1-x+i0)} \text{Tr} [\not{p} \gamma^\nu (\not{p} + \not{q}) \gamma^\mu] \\ &= -\frac{2x}{Q^2} \frac{1}{(1-x+i0)} \left(2p^\mu p^\nu + p^\mu q^\nu + q^\mu p^\nu - \frac{Q^2}{2x} g^{\mu\nu} \right). \end{aligned} \quad (3.67)$$

The projection onto $\hat{T}_1^{(q),(a)}$ with the projector in Eq. (3.15) yields

$$\hat{T}_1^{(q),(a)}(x) = P_1^{\mu\nu} \hat{T}_{\mu\nu}^{(q),(a)}(x) = \frac{-1}{1-x+i0} \quad (3.68)$$

and taking the imaginary part gives

$$\text{Im} \left[\hat{T}_1^{(q),(a)}(x) \right] = \pi \delta(1-x). \quad (3.69)$$

Diagram Fig. 8b:

Diagram 8b contains the self energy diagram

$$= i \not{k} \Sigma(k^2)$$

⁵The scaleless integrals are zero in dimensional regularization because they take the form $\sim \left(\frac{1}{\epsilon_{UV}} - \frac{1}{\epsilon_{IR}} \right)$, i.e. the UV and IR divergences are the same just with a different sign. Since we know that the full theory and the effective theory have the same IR divergences, we therefore also know the UV divergences of the effective theory.

$$\Sigma(k^2) := \frac{\alpha_s(\mu)C_F}{4\pi} \left(\frac{1}{\epsilon} + \text{Log} \frac{\mu^2}{-k^2 - i0} + 1 \right). \quad (3.70)$$

So the full diagram is proportional to the tree level result $\hat{T}^{\mu\nu (q),(a)}$

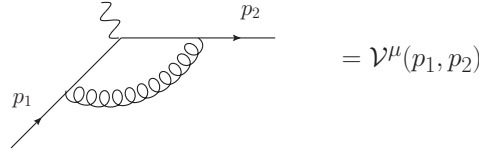
$$\begin{aligned} \hat{T}^{\mu\nu (q),(b)}(x) &= i \frac{1}{2} \sum_s \bar{u}(p, s) \gamma^\nu \frac{i(\not{p} + \not{q})}{(p+q)^2 + i0} i(\not{p} + \not{q}) \Sigma((p+q)^2) \frac{i(\not{p} + \not{q})}{(p+q)^2 + i0} \gamma^\mu u(p, s) \\ &= -\hat{T}^{\mu\nu (q),(a)}(x) \times \Sigma \left(\frac{Q^2(1-x)}{x} \right). \end{aligned} \quad (3.71)$$

After projecting onto $\hat{T}_1^{(q),(b)}$ and taking the imaginary part we find

$$\text{Im} \left[T_1^{(q),(b)}(x) \right] = \frac{\alpha_s(\mu)C_F}{4} \Theta(1-x) \left[-\delta(1-x) \left(\frac{1}{\epsilon} + \text{Log} \frac{\mu^2}{Q^2} + 1 \right) + \frac{1}{(1-x)_+} \right]. \quad (3.72)$$

Diagram Fig. 8c:

The diagram in Fig. 8c contains the vertex correction of the form



$$\mathcal{V}^\mu(p_1, p_2) = -4i\pi\alpha_s(\mu)C_F\tilde{\mu}^{2\epsilon} \int \frac{d^d k}{(2\pi)^d} \frac{\gamma^\alpha(\not{p}_2 - \not{k})\gamma^\mu(\not{p}_1 - \not{k})\gamma_\alpha}{((k-p_1)^2 + i0)((k-p_2)^2 + i0)(k^2 + i0)}. \quad (3.73)$$

By introducing Feynman parameters this can be written as

$$\mathcal{V}^\mu(p_1, p_2) = -8i\pi\alpha_s(\mu)C_F\tilde{\mu}^{2\epsilon} \int_0^1 dz \int_0^{1-z} dy \int \frac{d^d k}{(2\pi)^d} \frac{\gamma^\alpha(\not{p}_2 - \not{k})\gamma^\mu(\not{p}_1 - \not{k})\gamma_\alpha}{(k^2 - A)^3}, \quad (3.74)$$

$$c_1^\mu = (1-y)p_1^\mu - zp_2^\mu, \quad (3.75)$$

$$c_2^\mu = -yp_1^\mu + (1-z)p_2^\mu, \quad (3.76)$$

$$A = 2zyp_1 \cdot p_2 - y(1-y)p_1^2 - z(1-z)p_2^2. \quad (3.77)$$

With this the full diagram takes the form

$$\begin{aligned} \hat{T}^{\mu\nu (q),(c)}(x) &= i \frac{1}{2} \sum_s \bar{u}(p, s) \gamma^\nu \frac{i(\not{p} + \not{q})}{(p+q)^2 + i0} \mathcal{V}^\mu(p, p+q) u(p, s) \\ &= -\frac{x}{2Q^2} \frac{1}{1-x+i0} \text{Tr} [\not{p} \gamma^\nu (\not{p} + \not{q}) \mathcal{V}^\mu(p, p+q)]. \end{aligned} \quad (3.78)$$

The trace projected onto \hat{T}_1 , dropping any terms linear in k because they are antisymmetric and vanish when integrated over, can be reduced to

$$\begin{aligned} P_1^{\mu\nu} \text{Tr} [\not{p} \gamma^\nu (\not{p} + \not{q}) \mathcal{V}^\mu(p, p+q)] &= \int_0^1 dz \int_0^{1-z} dy \int \frac{d^d k}{(2\pi)^d} 4 \left\{ 4k^\alpha k^\beta \left(p_\alpha(p_\beta + q_\beta) - \epsilon \frac{Q^2}{4x} g_{\alpha\beta} \right) \right. \\ &\quad \left. + \frac{Q^4}{x^2} [(z-1)((x-1)(\epsilon-2)z-1) + y(z(1-\epsilon)-1)] \right\}. \end{aligned} \quad (3.79)$$

This reduces the momentum integration to standard integrals

$$\int \frac{d^d k}{(2\pi)^d} \frac{1}{(k^2 - A)^3} = C \frac{x}{Q^2} \Gamma(1+\epsilon)(\tilde{A} - i0)^{-1-\epsilon} \quad (3.80)$$

$$\int \frac{d^d k}{(2\pi)^d} \frac{k^\alpha k^\beta}{(k^2 - A)^3} = -\frac{C}{2} \Gamma(\epsilon)(\tilde{A} - i0)^{-\epsilon} g^{\alpha\beta} \quad (3.81)$$

$$C = -\frac{i}{32\pi^2} \left(\frac{4\pi x}{Q^2} \right)^\epsilon \quad (3.82)$$

$$\tilde{A} = z(y - (1-x)(1-z)) \quad (3.83)$$

With

$$g^{\alpha\beta} \left(p_\alpha(p_\beta + q_\beta) - \epsilon \frac{Q^2}{4x} g_{\alpha\beta} \right) = \frac{Q^2}{2x} (1 - 2\epsilon + \epsilon^2) \quad (3.84)$$

the remaining integrals give

$$\begin{aligned} \hat{T}_1^{(q),(c)}(x) &= \frac{\alpha_s(\mu)C_F}{2\pi} \frac{1}{(1-x+i0)} \int_0^1 dz \int_0^{1-z} dy \left[-(1-2\epsilon+\epsilon^2)\Gamma(\epsilon)(\tilde{A}-i0)^{-\epsilon} \right. \\ &\quad \left. + \Gamma(1+\epsilon)[(z-1)((x-1)(\epsilon-2)z-1) + y(z(1-\epsilon-1))](\tilde{A}-i0)^{-1-\epsilon} \right] \\ &= \frac{\alpha_s(\mu)C_F}{4\pi} \frac{1}{(1-x+i0)} \left[\frac{1}{\epsilon} (1+2x\ell) - x\ell^2 + 2x\ell \left(1 + \text{Log} \frac{\mu^2}{Q^2} \right) + \text{Log} \frac{\mu^2}{Q^2} + 4 \right], \end{aligned} \quad (3.85)$$

with $\ell := \text{Log} \frac{-(1-x)-i0}{x}$. Taking the imaginary part yields

$$\begin{aligned} \text{Im} \left[\hat{T}_1^{(q),(c)}(x) \right] &= \frac{\alpha_s(\mu)C_F}{4} \Theta(1-x) \left[-\frac{1}{\epsilon} \left(\delta(1-x) + 2 \frac{1}{(1-x)_+} - 2 \right) + 2 \left(\frac{\text{Log}(1-x)}{1-x} \right)_+ \right. \\ &\quad \left. - 2 \left(1 + \text{Log} \frac{\mu^2}{Q^2} \right) \frac{1}{(1-x)_+} - \delta(1-x) \left(4 + \frac{\pi^2}{3} + \text{Log} \frac{\mu^2}{Q^2} \right) \right. \\ &\quad \left. - 2 \text{Log}(1-x) - \frac{2x \text{Log} x}{1-x} + 2 \text{Log} \frac{\mu^2}{Q^2} + 2 \right]. \end{aligned} \quad (3.86)$$

Diagram Fig. 8d:

Diagram 8d was calculated by taking the imaginary part before the integration, i.e. applying the Cutkosky rules and cutting through the internal quark and gluon lines by replacing the denominator of the propagators of the cut lines $\frac{1}{k^2+i0} \rightarrow -2\pi i \delta(k^2)$

$$\begin{aligned} 2 \text{Im} \left[\hat{T}^{\mu\nu (q),(d)} \right] &= i \int \frac{d^d k}{(2\pi)^d} \frac{1}{2} \sum_s \left[\bar{u}(p,s) (ig\tilde{\mu}^\epsilon T^A \gamma^\alpha) \frac{i\cancel{k}}{(k^2+i0)} \gamma^\nu i(\cancel{k} + \cancel{q}) \gamma^\mu \frac{i\cancel{k}}{(k^2+i0)} \right. \\ &\quad \left. \times (ig\tilde{\mu}^\epsilon T^A \gamma_\alpha) u(p,s) \right] (-2\pi) \delta((k+q)^2) 2\pi \delta((k-p)^2) \\ &= (2\pi)^3 \alpha_s(\mu) C_F \tilde{\mu}^{2\epsilon} \int \frac{d^d k}{(2\pi)^d} \delta((k+q)^2) \delta((k-p)^2) \frac{1}{(k^2+i0)^2} \\ &\quad \times \text{Tr} \left[\cancel{p} \gamma^\alpha \cancel{k} \gamma^\nu (\cancel{k} + \cancel{q}) \gamma^\mu \cancel{k} \gamma_\alpha \right]. \end{aligned} \quad (3.87)$$

We change to light-cone variables with $k^\mu = k^- \frac{n^\mu}{2} + k^+ \frac{\bar{n}^\mu}{2} + k_\perp^\mu$ and

$$\int \frac{d^d k}{(2\pi)^d} \rightarrow \frac{(4\pi)^\epsilon}{32\pi^3 \Gamma(1-\epsilon)} \int dk^+ dk^- d|k_\perp^2| \Theta(|k_\perp^2|) |k_\perp^2|^{-\epsilon}. \quad (3.88)$$

With the further substitution $k^- = \frac{k^2 + |k_\perp^2|}{k^+}$ the delta functions can be rewritten as

$$\delta((k+q)^2) \delta((k-p)^2) = \frac{x^2 k^2}{Q^3} \delta \left(k^+ - \frac{x}{Q^2} k^2 \right) \delta \left(|k_\perp^2| + (1-x)k^2 \left(1 + \frac{x}{Q^2} k^2 \right) \right), \quad (3.89)$$

so that the k^+ and $|k_\perp^2|$ integrations become trivial. With these replacements for k^+ and $|k_\perp^2|$ the trace projected onto \hat{T}_1 is

$$P_1^{\mu\nu} \text{Tr} \left[\cancel{p} \gamma^\alpha \cancel{k} \gamma_\nu (\cancel{k} + \cancel{q}) \gamma_\mu \cancel{k} \gamma_\alpha \right] = 4k^2 \left(\frac{Q^2(1-x)(1-\epsilon)}{x} + 2k^2(1 - (1-x)\epsilon) + \frac{2x^2}{Q^2} (k^2)^2 \right). \quad (3.90)$$

Then the remaining k^2 integral reads

$$\int_{-\frac{Q^2}{x}}^0 dk^2 \frac{\left[k^2 \left(1 + \frac{xk^2}{Q^2}\right)\right]^{-\epsilon}}{k^2} \left(\frac{Q^2(1-x)(1-\epsilon)}{x} + 2k^2(1-(1-x)\epsilon) + \frac{2x^2}{Q^2}(k^2)^2 \right). \quad (3.91)$$

With the substitution $k^2 = -\frac{Q^2}{x}y$ this can be written as a sum of three Beta functions $B(a, b) = \int_0^1 dy (1-y)^{a-1} y^{b-1} = \frac{\Gamma(a)\Gamma(b)}{\Gamma(a+b)}$

$$\begin{aligned} & \left(\frac{Q^2}{x}\right)^{1-\epsilon} \int_0^1 dy (1-y)^{-\epsilon} [(1-x)(1-\epsilon) - 2(1-(1-x)\epsilon)y + 2xy^2] \\ &= \left(\frac{Q^2}{x}\right)^{1-\epsilon} ((1-x)(1-\epsilon)B(1-\epsilon, -\epsilon) - 2(1-(1-x)\epsilon)B(1-\epsilon, 1-\epsilon) + 2xB(1-\epsilon, 2-\epsilon)). \end{aligned} \quad (3.92)$$

Putting everything together and expanding in ϵ yields the result for the imaginary part of $\hat{T}_1^{(q),(d)}$

$$\text{Im} \left[\hat{T}_1^{(q),(d)}(x) \right] = \frac{\alpha_s(\mu)C_F}{2} \Theta(1-x) \left[-(1-x) \left(\frac{1}{\epsilon} + \text{Log} \frac{\mu^2}{Q^2} + \text{Log} x - \text{Log}(1-x) \right) + 1 \right]. \quad (3.93)$$

Final Result:

For each external leg one has to add $\frac{1}{2}$ times the on-shell wave function counter term which is 0 in dimensional regularization for a massless on-shell particle, so the full result for the partonic form factor for an incoming quark of flavor i is

$$\begin{aligned} \hat{W}_1^{(i)}(x, Q^2, \mu^2) &= \frac{Q_i^2}{2\pi} \text{Im} \left[T_1^{(q),(a)} + T_1^{(q),(b)} + 2T_1^{(q),(c)} + T_1^{(q),(d)} \right] (x, Q^2, \mu^2) \\ &= \left[\frac{1}{2} \delta(1-x) + \frac{\alpha_s(\mu)}{4\pi} \Theta(1-x) \left(-\frac{1}{\epsilon} P_{qq}(x) + C_{qq}(x, Q^2, \mu^2) \right) \right] Q_i^2. \end{aligned} \quad (3.94)$$

Here P_{qq} is the quark-quark splitting function

$$P_{qq}(x) = C_F \left(\frac{3}{2} \delta(1-x) + \frac{1+x^2}{(1-x)_+} \right) \quad (3.95)$$

and the finite parts are

$$\begin{aligned} C_{qq}(x, Q^2, \mu^2) &= C_F \left(-\frac{P_{qq}(x)}{C_F} \text{Log} \frac{\mu^2}{Q^2} + 2 \left(\frac{\text{Log}(1-x)}{1-x} \right)_+ - \frac{3}{2} \frac{1}{(1-x)_+} - \delta(1-x) \left(\frac{9}{2} + \frac{\pi^2}{3} \right) \right. \\ &\quad \left. - (1+x) \text{Log}(1-x) - \frac{1+x^2}{1-x} \text{Log} x + 3 \right). \end{aligned} \quad (3.96)$$

Similar calculations with the projector $P_L^{\mu\nu}$ instead of $P_1^{\mu\nu}$ give the longitudinal form factor \hat{W}_L

$$\hat{W}_L^{(i)}(x, Q^2, \mu^2) = \frac{\alpha_s(\mu)C_F}{2\pi} \Theta(1-x) x Q_i^2. \quad (3.97)$$

3.3.2 Gluon Form Factor

The relevant diagrams for the partonic tensor with gluons in the initial state are shown in Fig. 9. Here the average over polarization⁶ and color of the initial state gluon is implicit. Again the Cutkosky rules were used to take the imaginary part before the integration.

Diagram Fig. 9a:

$$\begin{aligned} 2 \text{Im} \left[T^{\mu\nu (g),(a)}(x) \right] &= (-i) \frac{1}{2(1-\epsilon)} \sum_{\text{pol.}} \frac{1}{8} \sum_{\text{col.}} \int \frac{d^d k}{(2\pi)^d} (2\pi)^2 \delta((k+q)^2) \delta((k-p)^2) \\ &\quad \times \epsilon_\alpha^A(p) \epsilon_\beta^B(p) \text{Tr} [T^A T^B] (ig\tilde{\mu}^\epsilon)^2 \left(\frac{i}{k^2 + i0} \right)^2 \\ &\quad \times \text{Tr} [\not{k} \gamma^\alpha (\not{k} - \not{p}) \gamma^\beta \not{k} \gamma^\nu (\not{k} + \not{q}) \gamma^\mu]. \end{aligned} \quad (3.98)$$

⁶Note that a massless vector boson in d dimensions has not just 2 but $(d-2)$ degrees of freedom.

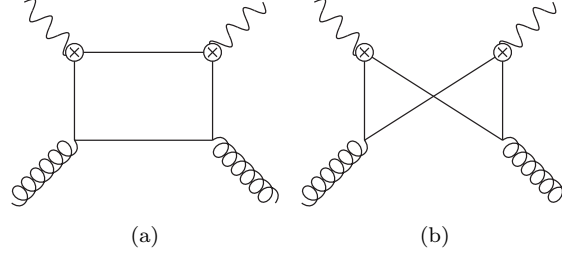


Figure 9: QCD Diagrams for DIS with Initial Gluons

The sums and color trace can be solved with $\sum_{\text{pol.}} \epsilon_\alpha^A(p) \epsilon_\beta^B(p) = -g_{\alpha\beta} \delta^{AB}$ and $\frac{1}{8} \sum_A \text{Tr} [T^A T^A] = T_f$, the rest of the calculation is analogous to the one for the box diagram with quarks in the initial state $\hat{T}^{\mu\nu (q),(d)}$. The delta functions are the same and the spin trace reduces to

$$P_1^{\mu\nu} \text{Tr} [k \gamma^\alpha (k - \not{p}) \gamma_\alpha k \gamma_\nu (k + \not{q}) \gamma_\mu] = \frac{-4(1-\epsilon)Q^2}{x} k^2 \left(1 + \frac{k^2 x}{Q^2}\right). \quad (3.99)$$

With the substitution $k^2 = -\frac{Q^2}{x} y$ the remaining integral is

$$\begin{aligned} & \frac{\alpha_s(\mu) T_f}{\Gamma(1-\epsilon)} \left(\frac{\mu^2 e^{\gamma_E} x}{Q^2(1-x)} \right)^\epsilon \Theta(1-x) \int_0^1 dy y^{-1-\epsilon} (1-y)^{1-\epsilon} \\ &= \alpha_s(\mu) T_f \left(\frac{\mu^2 e^{\gamma_E} x}{Q^2(1-x)} \right)^\epsilon \Theta(1-x) \frac{\Gamma(-\epsilon) \Gamma(2-\epsilon)}{\Gamma(1-\epsilon) \Gamma(2-2\epsilon)}. \end{aligned} \quad (3.100)$$

The final result for the imaginary part of $\hat{T}_1^{(g),(a)}$ is

$$\text{Im} [T_1^{(g),(a)}(x)] = \frac{\alpha_s(\mu) T_f}{2} \Theta(1-x) \left[-\frac{1}{\epsilon} - \text{Log} \frac{\mu^2}{Q^2} - \text{Log} x + \text{Log}(1-x) - 1 \right]. \quad (3.101)$$

Diagram Fig. 9b:

$$\begin{aligned} 2 \text{Im} [T^{\mu\nu (g),(b)}(x)] &= (-i) \frac{1}{2(1-\epsilon)} \sum_{\text{pol.}} \frac{1}{8} \sum_{\text{col.}} \int \frac{d^d k}{(2\pi)^d} (2\pi)^2 \delta((k+q)^2) \delta((k-p)^2) \\ &\times \epsilon_\alpha^A(p) \epsilon_\beta^B(p) \text{Tr} [T^A T^B] (ig\tilde{\mu}^\epsilon)^2 \frac{i}{(k^2+i0)} \frac{i}{((k+q-p)^2+i0)} \\ &\times \text{Tr} [k \gamma^\alpha (k - \not{p}) \gamma^\nu (k + \not{q} - \not{p}) \gamma^\beta (k + \not{q}) \gamma^\mu]. \end{aligned} \quad (3.102)$$

Again we have the same delta functions and with the change to the variables $k^+, |k_\perp^2|$ and $y = -\frac{xk^2}{Q^2}$ the spin trace becomes

$$P_1^{\mu\nu} \text{Tr} [k \gamma^\alpha (k - \not{p}) \gamma_\nu (k + \not{q} - \not{p}) \gamma_\alpha (k + \not{q}) \gamma_\mu] = \frac{-4Q^4(1-x)}{x} \left[1 + \left(\frac{\epsilon}{x(1-x)} - \frac{2}{1-\epsilon} \right) y(1-y) \right]. \quad (3.103)$$

The second propagator is $\frac{1}{(k+q-p)^2} = -\frac{x}{Q^2} \frac{1}{(1-y)}$ and so the last integral is

$$\begin{aligned} & \int_0^1 dy \left[y^{-1-\epsilon} (1-y)^{-1-\epsilon} + \left(\frac{\epsilon}{x(1-x)} - \frac{2}{1-\epsilon} \right) y^{-\epsilon} (1-y)^{-\epsilon} \right] \\ &= B(-\epsilon, -\epsilon) + \left(\frac{\epsilon}{x(1-x)} - \frac{2}{1-\epsilon} \right) B(1-\epsilon, 1-\epsilon). \end{aligned} \quad (3.104)$$

The full result for $\text{Im} [T_1^{(g),(b)}]$ expanded in ϵ is

$$\text{Im} [T_1^{(g),(b)}(x)] = \alpha_s(\mu) T_f \Theta(1-x) x(1-x) \left[\frac{1}{\epsilon} + \text{Log} \frac{\mu^2}{Q^2} + \text{Log} x - \text{Log}(1-x) + 2 \right]. \quad (3.105)$$

Final Result:

The full partonic form factor \hat{W}_1 for the gluon is the sum of both diagrams:

$$\hat{W}_1^{(g)}(x, Q^2, \mu^2) = \frac{\alpha_s(\mu)}{4\pi} \Theta(1-x) \left(-\frac{1}{\epsilon} P_{qg}(x) + C_{qg}(x, Q^2, \mu^2) \right) \sum_i Q_i^2, \quad (3.106)$$

$$\hat{W}_L^{(g)}(x, Q^2, \mu^2) = \frac{\alpha_s(\mu) T_f x(1-x)}{\pi} \Theta(1-x) \sum_i Q_i^2, \quad (3.107)$$

with the splitting function P_{qg} and finite parts C_{qg}

$$P_{qg}(x) = T_f (x^2 + (1-x)^2), \quad (3.108)$$

$$C_{qg}(x, Q^2, \mu^2) = T_f \left(-\frac{P_{qg}(x)}{T_f} \left(\text{Log} \frac{\mu^2}{Q^2} + \text{Log} x - \text{Log}(1-x) \right) - (1-2x)^2 \right). \quad (3.109)$$

Hard Matching Coefficients

The hard matching coefficients $H_j^{(i,g)}$ in Eq. (3.45) are the finite parts of the partonic form factors \hat{W} :

$$H_1^{(i)}(x, Q^2, \mu^2) = \left(\frac{1}{2} \delta(1-x) + \frac{\alpha_s(\mu)}{4\pi} \Theta(1-x) C_{qq}(x, Q^2, \mu^2) \right) Q_i^2, \quad (3.110)$$

$$H_L^{(i)}(x, Q^2, \mu^2) = \frac{\alpha_s(\mu) C_F}{2\pi} \Theta(1-x) x Q_i^2, \quad (3.111)$$

$$H_1^{(g)}(x, Q^2, \mu^2) = \frac{\alpha_s(\mu)}{4\pi} \Theta(1-x) C_{qg}(x, Q^2, \mu^2) \sum_i Q_i^2, \quad (3.112)$$

$$H_L^{(g)}(x, Q^2, \mu^2) = \frac{\alpha_s(\mu) T_f}{\pi} \Theta(1-x) x(1-x) \sum_i Q_i^2. \quad (3.113)$$

The functions C_{qq} and C_{qg} are defined in Eqs. (3.96) and (3.109). The calculations analogous to the quark case with anti-quarks in the initial state yield exactly the same matching coefficients. Since the electromagnetic current is conserved under QCD corrections it does not lead to any uncanceled UV divergences, so all $\frac{1}{\epsilon}$ terms in the results for the partonic form factors \hat{W}_1 have to be IR divergences. This implies that these $\frac{1}{\epsilon}$ terms are just the UV divergences of the EFT operators with opposite sign, as will be shown explicitly in the next section.

3.4 Renormalization of the PDFs

The EFT operators need to be renormalized when performing calculations beyond tree level. The corresponding UV divergences can be obtained in a purely partonic computation since the high energy physics is not sensitive to the structure of the IR physics. So we have to identify the UV divergences of the matrix elements $f_{i/j} = \langle j | f_i | j \rangle$, where the index j can stand for a quark or anti-quark of any active flavor or a gluon. The bare PDFs $f_i^0(x)$ have to be rewritten in terms of the renormalized PDFs $f_j(x, \mu^2)$ and the counter terms $Z_{ij}(x, \mu^2)$. The matrix $Z(x, \mu^2)$ will not be diagonal beyond leading order, so there will be a mixing between the PDFs

$$f_i^0(x) = \sum_j (Z_{ij} \otimes f_j)(x). \quad (3.114)$$

3.4.1 Calculation of SCET Diagrams

First we calculate $f_{i/i}^0(x, \mu^2)$, the bare partonic quark PDF with the same flavor in the initial state. From Eq. (3.55) we find the expression for $f_{i/i}$ with an incoming quark with momentum p

$$f_{i/i}^0(\xi) = \langle i(p) | \bar{\chi}_{n,p}^{(i)} \frac{\not{p}}{2} \left[\delta(p^- \xi - \mathcal{P}^-) \chi_{n,p'}^{(i)} \right] | i(p) \rangle. \quad (3.115)$$

The relevant diagrams to order α_s are shown in Fig. 10.

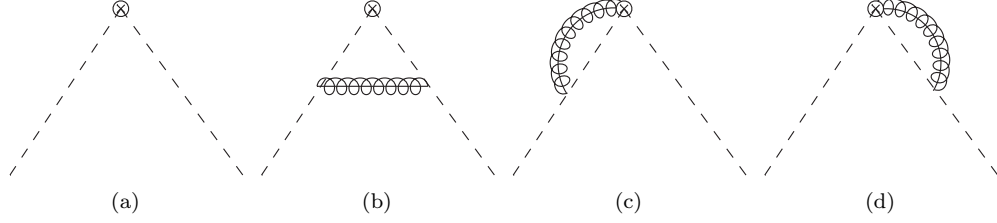
Figure 10: SCET Diagrams for $f_{i/i}$

Diagram Fig. 10a:
At tree level we have

$$\begin{aligned}
 f_{i/i}^{(a)}(\xi) &= \delta(p^- \xi - p^-) \frac{1}{2} \sum_s \bar{u}_n(p, s) \frac{\not{p}}{2} u_n(p, s) \\
 &= \frac{1}{4p^-} \delta(1 - \xi) \text{Tr}[\not{p} \not{p}] \\
 &= \delta(1 - \xi).
 \end{aligned} \tag{3.116}$$

Diagram Fig. 10b:

$$f_{i/i}^{(b)} = \int \frac{d^d k}{(2\pi)^d} \delta(p^- \xi - k^-) \frac{-i}{(p-k)^2 + i0} \frac{1}{2} \sum_s \bar{u}_n(p, s) V_{n,\mu}^{\mu,A}(p, k) F_n(k) \frac{\not{p}}{2} F_n(k) V_{n,\mu}^A(k, p) u_n(p, s), \tag{3.117}$$

where $F_n(k)$ and $V_{n,\mu}^A(p, k)$ are the fermion propagator and the collinear-collinear vertex in SCET respectively (see Eqs. (2.31)(2.33)). Since we choose the light-cone axis n along the incoming quark, $p_\perp^\mu = 0$. For a massless on-shell quark with $p^+ p^- = p^2 = 0$ this would give a scaleless integral which is zero in dimensional regularization, but to see the UV divergences explicitly we use an off-shellness $p^2 > 0$ as an IR regulator. After carrying out all the spin traces we get

$$f_{i/i}^{(b)}(\xi) = 8i\pi\alpha_s(\mu)C_F(1-\epsilon)\tilde{\mu}^2 p^- \int \frac{d^d k}{(2\pi)^d} \delta(p^- \xi - k^-) \frac{|k_\perp^2|}{(k^2 + i0)^2((p-k)^2 + i0)} \tag{3.118}$$

and using Eq. (3.88), performing the k^- integration with the delta distribution and substituting $k^+ = zp^+$ yields

$$\frac{i\alpha_s(\mu)C_F(\mu^2 e^{\gamma_E})^\epsilon(1-\epsilon)}{4\pi^2\Gamma(1-\epsilon)(p^2)^2} \int_0^\infty d|k_\perp^2| |k_\perp^2|^{1-\epsilon} \int_{-\infty}^\infty dz \frac{1}{\left(z\xi - \frac{|k_\perp^2|}{p^2} + i0\right)^2 \left((z-1)(\xi-1) - \frac{|k_\perp^2|}{p^2} + i0\right)}. \tag{3.119}$$

If $\xi > 1$ or $\xi < 0$ all three poles lie below or above the real axis and the integral is zero. Only if $0 < \xi < 1$ we have a double pole below and a single pole above the real axis and can close the contour in either the positive or the negative imaginary half-plane to get

$$\int_{-\infty}^\infty dz \frac{1}{\left(z\xi - \frac{|k_\perp^2|}{p^2} + i0\right)^2 \left((z-1)(\xi-1) - \frac{|k_\perp^2|}{p^2} + i0\right)} = -\Theta(\xi)\Theta(1-\xi) \frac{2i\pi(p^2)^2}{(|k_\perp^2| - p^2\xi(1-\xi))^2}. \tag{3.120}$$

The remaining $|k_\perp^2|$ integral gives

$$\int_0^\infty d|k_\perp^2| \frac{|k_\perp^2|^{1-\epsilon}}{(|k_\perp^2| - p^2\xi(1-\xi))^2} = (1-\epsilon)\Gamma(1-\epsilon)\Gamma(\epsilon)(-p^2\xi(1-\xi))^{-\epsilon} \tag{3.121}$$

and so the final result for the diagram is

$$\begin{aligned}
 f_{i/i}^{(b)}(\xi) &= \frac{\alpha_s(\mu)C_F}{2\pi} \Theta(\xi)\Theta(1-\xi)(1-\xi)(1-\epsilon)^2\Gamma(\epsilon) \left(\frac{\mu^2 e^{\gamma_E}}{-p^2\xi(1-\xi)} \right)^\epsilon \\
 &= \frac{\alpha_s(\mu)C_F}{2\pi} \Theta(\xi)\Theta(1-\xi)(1-\xi) \left(\frac{1}{\epsilon} + \text{Log} \frac{\mu^2}{-p^2} - \text{Log} \xi - \text{Log}(1-\xi) - 2 \right).
 \end{aligned} \tag{3.122}$$

Diagram Fig. 10c:

For this diagram we have to distinguish two cases because we can connect the gluon either to the left Wilson line W_n or the right Wilson line W_n^\dagger , Fig. 11. This gives a different sign because of the complex conjugation in the Wilson line, but also the label operator in Eq. (3.115), acting only on the right jet field, picks up different momenta.

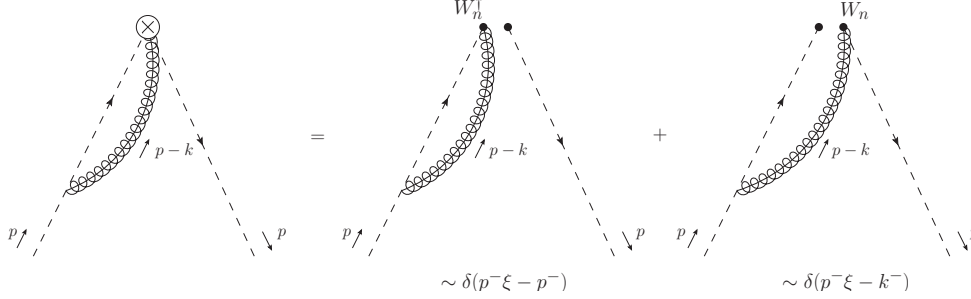


Figure 11: Different Wilson lines for diagram 10c. The label operator in the delta distribution picks out different momenta depending on to which Wilson line the gluon is attached.

$$f_{i/i}^{(c)}(\xi) = \int \frac{d^d k}{(2\pi)^d} (\delta(p^- \xi - p^-) - \delta(p^- \xi - k^-)) \frac{-i}{((p-k)^2 + i0)} \frac{gT^A \tilde{\mu}^\epsilon \tilde{n}^\mu}{(p^- - k^- - i0)} \times \frac{1}{2} \sum_s \bar{u}_n(p, s) F_n(k) V_{n,\mu}^A(p, k) u_n(p, s). \quad (3.123)$$

The k^+ and the $|k_\perp^2|$ integrations are equivalent to the integrals in the previous diagram, the k^- integration can be done with the delta distribution $\delta(p^- \xi - k^-)$ for the one term and with a reduction to a Beta function: $B(x, y) = \int_0^1 dt t^{x-1} (1-t)^{y-1} = \frac{\Gamma(x)\Gamma(y)}{\Gamma(x+y)}$ for the other one

$$f_{i/i}^{(c)}(\xi) = \frac{\alpha_s(\mu) C_F}{2\pi} \Gamma(\epsilon) \left(\frac{\mu^2 e^{\gamma_E}}{-p^2 \xi} \right)^\epsilon \Theta(\xi) \Theta(1-\xi) \left(\xi(1-\xi)^{-1-\epsilon} - \frac{\Gamma(2-\epsilon)\Gamma(-\epsilon)}{\Gamma(2-2\epsilon)} \delta(1-\xi) \right). \quad (3.124)$$

To expand the term $\xi(1-\xi)^{-1-\epsilon}$ one can use Eq. (A.3) to get

$$f_{i/i}^{(c)}(\xi) = \frac{\alpha_s(\mu) C_F}{2\pi} \Theta(\xi) \Theta(1-\xi) \left(\left(\frac{1}{\epsilon} + \text{Log} \frac{\mu^2}{-p^2 \xi} \right) \left(\delta(1-\xi) + \frac{1}{(1-\xi)_+} - 1 \right) + \delta(1-\xi) \left(2 - \frac{\pi^2}{6} \right) - \left(\frac{\text{Log}(1-\xi)}{1-\xi} \right)_+ + \text{Log}(1-\xi) \right). \quad (3.125)$$

The diagram in Fig. 10d gives the same result as the one in Fig. 10c. For each external leg we have to add $\frac{1}{2}$ times the wave function counter term times the tree level diagram. The counter term is the same as for full QCD, but here it is not zero as in the last section because of the IR regulator $p^2 \neq 0$, but has the form

$$- \frac{\alpha_s(\mu) C_F}{4\pi} \left(\frac{1}{\epsilon} + \text{Log} \frac{\mu^2}{-p^2} + 1 \right) \quad (3.126)$$

and so the bare quark-quark PDF to order α_s is

$$f_{q/q}^0(\xi, \mu^2) = \delta(1-\xi) + \frac{\alpha_s(\mu) C_F}{2\pi} \left(\left(\frac{1}{\epsilon} + \text{Log} \frac{\mu^2}{-p^2 \xi} \right) \frac{P_{qq}(\xi)}{C_F} + \delta(1-\xi) \left(\frac{7}{2} - \frac{\pi^2}{3} \right) - 2 \left(\frac{\text{Log}(1-\xi)}{1-\xi} \right)_+ + (1+\xi) \text{Log}(1-\xi) - 2(1-\xi) \right). \quad (3.127)$$

From this result we find the UV divergence to be

$$\frac{\alpha_s(\mu)}{2\pi} \frac{P_{qq}(\xi)}{\epsilon}, \quad (3.128)$$

which is indeed just the IR divergence of the full theory result with a different sign (the factor $\frac{1}{2}$ just results from a different normalization of the SCET operators).

Diagram Fig. 12:

The order α_s diagram for the quark PDF with a gluon in the initial state $f_{i/g}$ is shown in Fig. 12. It

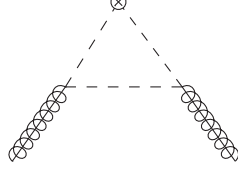


Figure 12: SCET Diagram for $f_{i/g}$

gives the expression

$$f_{i/g}(\xi) = \int \frac{d^d k}{(2\pi)^d} \delta(p^- \xi - k^-) \frac{1}{2(1-\epsilon)} \sum_{\text{pol.}} \frac{1}{8} \sum_{\text{col.}} \epsilon_\mu^A(p) \epsilon_\nu^{*B}(p) \times (-1) \text{Tr} \left[V_n^{\mu,A}(k, k-p) F_n(k) \frac{\not{k}}{2} F_n(k) V_n^{\nu,B}(k-p, p) F(k-p) \right], \quad (3.129)$$

with the trace over color and spin. After performing all traces and sums we get

$$f_{i/g}(\xi) = -8i\pi\alpha_s(\mu) T_f \tilde{\mu}^2 \int \frac{d^d k}{(2\pi)^d} \delta(p^- \xi - k^-) \frac{|k_\perp^2|}{(k^2 + i0)^2 ((k-p)^2 + i0)} \left(\frac{(p^-)^2}{k^- - p^-} + \frac{4k^-}{2(1-\epsilon)} \right). \quad (3.130)$$

Again the k^- integral and the k^+ and $|k_\perp^2|$ integrals are analogous to diagram Fig. 10b, and so we find for the bare quark-gluon PDF

$$f_{q/g}^0(\xi, \mu^2) = \frac{\alpha_s T_f}{2\pi} \Theta(\xi) \Theta(1-\xi) \Gamma(\epsilon) \left(\frac{\mu^2 e^{\gamma_E}}{-p^2 \xi (1-\xi)} \right)^\epsilon (1-\epsilon - 2\xi(1-\xi)) \\ = \frac{\alpha_s(\mu) T_f}{2\pi} \left(\left(\frac{1}{\epsilon} + \text{Log} \frac{\mu^2}{-p^2} - \text{Log}(1-\xi) - \text{Log} \xi \right) \frac{P_{qg}(\xi)}{T_f} - 1 \right). \quad (3.131)$$

Again the UV divergence

$$\frac{\alpha_s(\mu)}{2\pi} \frac{P_{qg}(\xi)}{\epsilon} \quad (3.132)$$

is the same as the IR divergence in the full theory calculation up to a minus sign. The results for $f_{q/q}$ and $f_{q/g}$ agree with Ref. [16].

gluon PDF tree level:

For the gluon PDF with an incoming gluon with momentum p we have to evaluate

$$f_{g/g}(\xi) = -\frac{p^- \xi}{T_f g^2} \langle g(p) | \text{Tr} [W_n^\dagger [(\mathcal{P}_\perp^\mu + g A_{n\perp}^\mu) W_n] [\delta(p^- \xi - \mathcal{P}^-) W_n^\dagger [(\mathcal{P}_\mu^\perp + g A_{n\mu}^\perp) W_n]] | g(p) \rangle. \quad (3.133)$$

Since we choose the light-cone axis along the incoming momentum p^μ we have $p_\perp^\mu = 0$ and therefore the perp. momentum operator \mathcal{P}_\perp^μ will always give zero at tree level. So the tree level expression is just

$$-\frac{p^- \xi}{T_f} \langle g(p) | \text{Tr} [A_n^\mu [\delta(p^- \xi - \mathcal{P}^-) A_n^\nu]] | g(p) \rangle g_{\mu\nu}^\perp. \quad (3.134)$$

Again the matrix element is averaged over polarization and color so we get

$$f_{g/g}^{(0)}(\xi) = -\frac{1}{T_f} \delta(1-\xi) \frac{1}{2(1-\epsilon)} \sum_{\text{pol.}} \frac{1}{8} \sum_{\text{col.}} \epsilon_\mu^A(p) \epsilon_\nu^{*B}(p) g_{\perp}^{\mu\nu} \text{Tr} [T^A T^B] \\ = \delta(1-\xi). \quad (3.135)$$

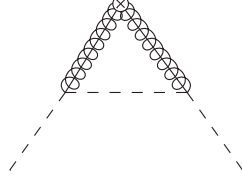
Figure 13: SCET Diagram for $f_{g/i}$

Diagram Fig. 13:

For the gluon-quark PDF $f_{g/i}$ at order α_s we have to consider four different terms

$$\begin{aligned}
 f_{g/i}(\xi) = & -\frac{p^- \xi}{T_f g^2} \left(\langle i(p) | \text{Tr} [g A_{n\perp}^\mu [\delta(p^- \xi - \mathcal{P}^-) g A_{n\mu}^\perp]] | i(p) \rangle \right. & (I) \\
 & \langle i(p) | \text{Tr} [[\mathcal{P}_\perp^\mu W_n] [\delta(p^- \xi - \mathcal{P}^-) \mathcal{P}_\mu^\perp W_n]] | i(p) \rangle & (II) \\
 & \langle i(p) | \text{Tr} [[\mathcal{P}_\perp^\mu W_n] [\delta(p^- \xi - \mathcal{P}^-) g A_{n\mu}^\perp]] | i(p) \rangle & (III) \\
 & \left. \langle i(p) | \text{Tr} [g A_{n\perp}^\mu [\delta(p^- \xi - \mathcal{P}^-) \mathcal{P}_\mu^\perp W_n]] | i(p) \rangle \right). & (IV)
 \end{aligned} \tag{3.136}$$

The first gives term gives

$$\begin{aligned}
 f_{g/i}^{(I)}(\xi) = & -\frac{p^- \xi}{T_f} \int \frac{d^d k}{(2\pi)^d} \delta(p^- \xi - k^-) \frac{1}{2} \sum_s \bar{u}_n(p, s) V_{n,\mu}^A(p-k, p) F_n(p-k) V_{n,\nu}^B(p, p-k) u_n(p, s) g_{\perp}^{\mu\nu} \\
 & \times \left(\frac{-i}{k^2 + i0} \right)^2 \text{Tr} [T^A T^B] \\
 = & \frac{(1-\epsilon)\xi}{1-\xi} A,
 \end{aligned} \tag{3.137}$$

where A is the integral

$$\begin{aligned}
 A := & 8i\pi\alpha_s(\mu) C_F \tilde{\mu}^2 p^- \int \frac{d^d k}{(2\pi)^d} \delta(p^- \xi - k^-) \frac{|k_\perp^2|}{(k^2 + i0)^2 ((p-k)^2 + i0)} \\
 = & \frac{\alpha_s(\mu) C_F}{2\pi} \Theta(\xi) \Theta(1-\xi) (1-\xi) \left(\frac{1}{\epsilon} + \text{Log} \frac{\mu^2}{-p^2 \xi} - \text{Log}(1-\xi) - 1 \right).
 \end{aligned} \tag{3.138}$$

The second term contains the same integral

$$\begin{aligned}
 f_{g/i}^{(II)}(\xi) = & -\frac{p^- \xi}{T_f g^2} \int \frac{d^d k}{(2\pi)^d} \delta(p^- \xi - k^-) \frac{1}{2} \sum_s \bar{u}_n(p, s) V_{n,\mu}^A(p-k, p) F_n(p-k) V_{n,\nu}^B(p, p-k) u_n(p, s) \\
 & \times \left(\frac{-i}{k^2 + i0} \right)^2 \frac{-g \bar{n}^\mu}{(-k^- - i0)} \frac{-g \bar{n}^\nu}{(k^- - i0)} k_\perp^\rho (-k_\rho^\perp) \text{Tr} [T^A T^B] \\
 = & \frac{2(1-\xi)}{\xi} A,
 \end{aligned} \tag{3.139}$$

as well as the third term

$$\begin{aligned}
 f_{g/i}^{(III)}(\xi) = & -\frac{p^- \xi}{T_f g} \int \frac{d^d k}{(2\pi)^d} \delta(p^- \xi - k^-) \frac{1}{2} \sum_s \bar{u}_n(p, s) V_{n,\mu}^A(p-k, p) F_n(p-k) V_{n,\nu}^B u_n(p, s) \\
 & \times \left(\frac{-i}{k^2 + i0} \right)^2 k_\perp^\mu \frac{-g \bar{n}^\nu}{(k^- - i0)} \text{Tr} [T^A T^B] \\
 = & A.
 \end{aligned} \tag{3.140}$$

Because the $i0$ prescription in the Wilson lines does not matter in these integrals, $f_{g/i}^{(IV)} = f_{g/i}^{(III)}$. Putting all four terms together gives the bare gluon-quark PDF at order α_s

$$f_{g/q}^0(\xi, \mu^2) = \frac{\alpha_s(\mu) C_F}{2\pi} \Theta(\xi) \Theta(1-\xi) \left(\left(\frac{1}{\epsilon} + \text{Log} \frac{\mu^2}{-p^2 \xi} - \text{Log}(1-\xi) \right) \frac{P_{gq}(\xi)}{C_F} - \frac{2(\xi(1-\xi) - 1)}{\xi} \right). \tag{3.141}$$

The splitting function P_{gq} is

$$P_{gq}(\xi) = C_F \frac{1 + (1 - \xi)^2}{\xi}. \quad (3.142)$$

So far we have calculated three of the four splitting functions as the coefficients of the UV divergences of SCET operators to order α_s . To get the remaining one P_{gg} in the same way one would have to calculate the UV divergences of the gluon PDF with gluons in the initial state. We have not done this calculation, it can be found for example in Ref. [18]. The leading order gluon-gluon splitting function is

$$P_{gg}(\xi) = 2C_A \left(\frac{1}{(1 - \xi)_+} + \frac{1 - \xi}{\xi} + \xi(1 - \xi) - 1 \right) + \delta(1 - \xi) \frac{11C_A - 4n_f T_f}{6}. \quad (3.143)$$

3.4.2 Renormalization and Evolution

As shown above, in dimensional regularization the matrix elements for the bare PDF operators up to order α_s have the form

$$f_{i/j}^0(x) = \delta_{ij} \delta(1 - x) + \frac{\alpha_s(\mu)}{2\pi} \Theta(1 - x) \left(\frac{P_{ij}^{(0)}(x)}{\epsilon} + c_{ij}^{(0)}(x, \mu^2) \right) + \mathcal{O}(\alpha_s^2). \quad (3.144)$$

Here the $\frac{1}{\epsilon}$ are only UV divergences, i.e. any IR divergences have already been regularized by the off-shellness $p^2 \neq 0$. With this the counter terms and the running of the PDFs can be determined from Eq. (3.114). In the $\overline{\text{MS}}$ -scheme only the $\frac{1}{\epsilon}$ terms are absorbed into the counter terms, which yields

$$Z_{ij}(x, \mu^2) = \delta_{ij} \delta(1 - x) + \frac{\alpha_s(\mu)}{2\pi} \Theta(1 - x) \frac{P_{ij}^{(0)}(x)}{\epsilon} + \mathcal{O}(\alpha_s^2). \quad (3.145)$$

Solving the equation

$$0 = \frac{d}{d \text{Log} \mu^2} f_i^0(x) = \sum_j \frac{d}{d \text{Log} \mu^2} (Z_{ij} \otimes f_j)(x, \mu^2) \quad (3.146)$$

for the derivative of $f_i(x, \mu^2)$ gives the usual DGLAP equations

$$\frac{d}{d \text{Log} \mu^2} f_i(x, \mu^2) = \frac{\alpha_s(\mu)}{2\pi} \sum_j (P_{ij} \otimes f_j)(x, \mu^2). \quad (3.147)$$

This implies that the PDFs are evolved from a scale μ_0^2 to μ^2 in a convolution with an evolution kernel $U(x, \mu^2, \mu_0^2)$ that mixes the different PDFs

$$f_i(x, \mu^2) = \sum_j (U_{ij}(\mu^2) \otimes f_j)(x, \mu_0^2) = \sum_j \int \frac{d\xi}{\xi} U_{ij} \left(\frac{x}{\xi}, \mu^2, \mu_0^2 \right) f_j(\xi, \mu_0^2). \quad (3.148)$$

The DGLAP equations can in general not be solved analytically but only with numerical methods, either in x -space or in Mellin space where the convolution is disentangled to become a multiplication of two functions. The splitting functions $P_{ij}(x) = \sum_n \left(\frac{\alpha_s(\mu)}{2\pi} \right)^n P_{ij}^{(n)}(x)$ can be calculated perturbatively order by order in α_s .

It is important to notice that the results of the calculations in Sec. 3.4 would not change if we replaced a quark by its corresponding anti-quark. Also the flavor of the quark does not play a role because a gluon does not distinguish different quark flavors. This implies that some of the splitting functions in Eq. (3.147) are actually the same:

$$\begin{aligned} P_{qq'} &= P_{\bar{q}\bar{q}'} & P_{qg} &= P_{\bar{q}g} \\ P_{q\bar{q}'} &= P_{\bar{q}q'} & P_{gq} &= P_{g\bar{q}} \end{aligned} \quad (3.149)$$

This fact can be used to find suitable linear combinations of the quark PDFs such that the mixing is reduced to a 2×2 matrix. We define the non-singlet PDFs (i, j for any quark flavor)

$$f_{\text{NS}, ij}^\pm = (f_i \pm \bar{f}_i) - (f_j \pm \bar{f}_j) \quad (3.150)$$

$$f_{\text{NS}}^V = \sum_i^{n_f} (f_i - \bar{f}_i) \quad (3.151)$$

and the singlet PDF

$$\Sigma = \sum_i^{nf} (f_i + \bar{f}_i), \quad (3.152)$$

such that all non-singlet PDFs evolve without any mixing

$$\frac{d}{d \text{Log} \mu^2} f_{\text{NS},ij}^{\pm}(x, \mu^2) = \frac{\alpha_s(\mu)}{2\pi} \left(P_{\text{NS}}^{\pm} \otimes f_{\text{NS},ij}^{\pm} \right) (x, \mu^2) \quad (3.153)$$

$$\frac{d}{d \text{Log} \mu^2} f_{\text{NS}}^V(x, \mu^2) = \frac{\alpha_s(\mu)}{2\pi} \left(P_{\text{NS}}^V \otimes f_{\text{NS}}^V \right) (x, \mu^2) \quad (3.154)$$

while the singlet PDF mixes with the gluon PDF. The evolution of the singlet and non-singlet PDFs are discussed in great detail in Refs. [19, 20]. At $\mathcal{O}(\alpha_s)$ this simplifies even more since we do not see any flavor changing, which implies that

$$P_{\text{NS}}^{\pm} = P_{\text{NS}}^V = P_{qq}^{(0)}. \quad (3.155)$$

The evolution of the singlet and the gluon PDF takes the form

$$\left[\frac{d}{d \text{Log} \mu^2} \begin{pmatrix} \Sigma \\ f_g \end{pmatrix} \right] (x, \mu^2) = \left[\begin{pmatrix} P_{qq}^{(0)} & 2n_f P_{qg}^{(0)} \\ 2n_f P_{gq}^{(0)} & P_{gg}^{(0)} \end{pmatrix} \otimes \begin{pmatrix} \Sigma \\ f_g \end{pmatrix} \right] (x, \mu^2). \quad (3.156)$$

The leading order splitting functions $P_{ab}^{(0)}$ are given in Eqs. (3.95),(3.108),(3.142),(3.143).

4 Heavy Flavor Production in Deep Inelastic Scattering

We will now add an additional quark flavor with mass m and work out the corrections we get compared to the massless case. This can be done in different schemes, namely a fixed flavor number (FFN) scheme and a variable flavor number (VFN) scheme. Here it is assumed that the mass m is above the scale Λ_{QCD} and can be treated perturbatively. The FFN scheme will give a good description in the case where Q^2 is of the order of the mass threshold or smaller and gives the decoupling limit for $m^2 \gg Q^2$, but suffers from large logarithms $\text{Log } \frac{m^2}{Q^2}$ in the case where $m^2 \ll Q^2$. These logs can be resummed in a VFN scheme in the evolution of a new PDF for the heavy quark that is introduced at a scale $\mu_m^2 \sim m^2$. The VFN scheme agrees with the FFN scheme for $m^2 \gtrsim Q^2$, but because of the log resummation it is also able to deal with the case where the scale Q^2 is much greater than m^2 and it provides the correct massless limit for $\frac{m^2}{Q^2} \rightarrow 0$ due to the cancellation of IR sensitive contributions in the matching.

4.1 Kinematics and Rescaling

In the VFN scheme a new PDF for a heavy quark is introduced, so we need to perform the matching on the parton level with a massive initial state (see Sec. 4.3). In the case where the parton going into the hard interaction has a mass m the kinematics change a little bit compared to the massless case discussed in Sec. 3.1. To fulfill the on-shell relation $\hat{P}^2 = m^2$ and maintain the definition of the (partonic) Bjorken variable $\hat{P} \cdot q = \frac{Q^2}{2\hat{x}}$ the parton momentum has to be

$$\hat{P}^\mu = \frac{Q}{\eta} \frac{n^\mu}{2} + \frac{m^2 \eta}{Q} \frac{\bar{n}^\mu}{2}, \quad \eta = \frac{2\hat{x}}{1 + \sqrt{1 + \frac{4m^2 \hat{x}^2}{Q^2}}}. \quad (4.1)$$

If ξ is again the longitudinal momentum fraction, i.e. $\hat{P}^- = \xi P^-$, we find at tree level, where $\hat{x} = 1$, the relation between the Bjorken variable and the momentum fraction to be $x = \frac{2}{1 + \sqrt{1 + 4\frac{m^2}{Q^2}}} \xi$. So in the case of a massive parton the tree-level relation is no longer just $x = \xi$ but is rescaled by a factor depending on the parton mass. The restriction $(\hat{P} + q)^2 \geq m^2$ leads to $\xi \geq \frac{1 + \sqrt{1 + 4\frac{m^2}{Q^2}}}{2} x$, so again for $x \rightarrow 1$ we also have $\xi \rightarrow 1$. The mass of the initial state also changes the form of the convolution in the matching condition Eq. (3.45). The convolution for an arbitrary mass of the initial state with momentum \hat{P} was of the form

$$\int \frac{d\xi}{\xi} H\left(\frac{Q}{\xi \hat{P}^-}\right) f(\xi). \quad (4.2)$$

For a massless parton we had $\hat{P}^- = \frac{Q}{x}$ which lead to the matching condition in Eq. (3.45). For a massive quark in the initial state we have to use Eq. (4.1), i.e. $\hat{P}^- = \frac{Q}{\eta}$, so the matching condition becomes

$$\hat{W}_j^{(p)}(\hat{x}, m^2, \mu^2) = \sum_i \left(H_j^{(i)} \otimes (f_{i/p} + \bar{f}_{i/p}) \right) (\eta, \mu^2) + \left(H_j^{(g)} \otimes f_{g/p} \right) (\eta, \mu^2), \quad (4.3)$$

where the argument of the convolution is now the variable η instead of \hat{x} . This rescaling only depends on the mass of the initial state, so the matching for massless partons or the convolution with the PDFs for the (massless) hadron are not changed. Note that the rescaling only affects the convolution in the matching (because here the light-cone component \hat{P}^- explicitly enters the argument of the convolution) but has no effect on the renormalization of the PDFs. Also the projectors in Eqs. (3.15)(3.16)(3.18) have to be changed for the partonic tensor with a massive quark. The factor A is shifted to $A \rightarrow m^2 + \frac{Q^2}{4x^2}$ because of the mass of the initial state. Since we still consider the hadron to be massless the definition of the hadronic form factors in Eqs. (3.19)-(3.21) and the form of the cross section Eq. (3.22) as well as the convolution in the factorized form of the full hadronic tensor is not changed.

4.2 Fixed Flavor Number Scheme

In a FFN scheme it is straight forward to include the effects of an additional heavy flavor. We just stick to the same effective theory setup with PDFs for n_f light flavors like before, but add one additional heavy quark flavor in the full theory calculations. At $\mathcal{O}(\alpha_s)$ this only gives two new diagrams of the type of Fig. 9 with massive quarks for the internal lines. On the side of the effective theory operators nothing changes at all, because modes with $p^2 \sim m^2 \sim Q^2$ would be considered as hard in the SCET power counting and are therefore integrated out. So all effects of the new heavy quark go into the hard coefficients.

4.2.1 QCD Calculations

The diagrams in Fig. 9 with massive quarks were calculated by using the Mathematica package FeynCalc [21] that does the Passarino-Veltman reduction to standard scalar integrals automatically. The result in terms of these integrals is

$$\begin{aligned} \hat{T}_{1,m}^{(g)}(x, Q^2, m^2, \mu^2) = & \frac{-\alpha_s(\mu)T_f}{\pi} \left[\left(-\frac{m^2}{Q^2}x - \frac{2}{3} \right) b_2 + \left(\frac{m^2}{Q^2}(1-2x)x - 2x^2 - \frac{5}{6} \right) b_3 \right. \\ & + \left((x-1)x - \frac{1}{2} \right) b_4 + x \left(\frac{m^2}{Q^2}2x + x + 1 \right) b_5 \\ & - m^2 c_2 + \frac{Q^2}{3} \left(\frac{m^2}{Q^2}(3x-2) + 1 \right) c_3 + Q^2 \left(\frac{m^2}{Q^2}(3-2x) + \frac{1-4x}{2x} \right) c_4 \\ & \left. + Q^4 \left(2\frac{m^4}{Q^4} - \frac{m^2}{Q^2} \right) d_2 + Q^4 \left(\frac{4x\frac{m^4}{Q^4} + \frac{m^2}{Q^2} - x - 1}{2x} \right) d_3 \right] Q_m^2, \quad (4.4) \end{aligned}$$

$$\begin{aligned} \hat{T}_{L,m}^{(g)}(x, Q^2, m^2, \mu^2) = & \frac{-\alpha_s(\mu)T_f}{\pi} \left[\left(-2x\frac{m^2}{Q^2} - \frac{1}{3} \right) b_2 + \left(2x(1-2x)\frac{m^2}{Q^2} - 4x^2 + \frac{1}{3} \right) b_3 \right. \\ & - 2x(1-x)b_4 + 2x \left(2x\frac{m^2}{Q^2} + x + 1 \right) b_5 \\ & \left. + \frac{Q^2}{3} \left((6x+2)\frac{m^2}{Q^2} - 1 \right) c_3 - 4xm^2 c_4 \right] Q_m^2. \quad (4.5) \end{aligned}$$

The n-point functions $\{b, c, d\}_i$ are given in appendix C. Only b_4 , c_4 , d_2 and d_3 have a non-vanishing imaginary part (see appendix B)

$$\begin{aligned} \text{Im}[b_4] &= \pi\Theta\left(\frac{1}{w^2} - x\right)s, \\ \text{Im}[c_4] &= \pi\Theta\left(\frac{1}{w^2} - x\right)\frac{x}{Q^2}\text{Log}\left(\frac{1-s}{1+s}\right), \\ \text{Im}[d_2] &= \pi\Theta\left(\frac{1}{w^2} - x\right)\frac{sx(1-x)}{m^2Q^2}, \\ \text{Im}[d_3] &= \pi\Theta\left(\frac{1}{w^2} - x\right)\frac{-2x^2}{Q^4}\text{Log}\left(\frac{1-s}{1+s}\right), \end{aligned} \quad (4.6)$$

where w and s are

$$w := \sqrt{1 + \frac{4m^2}{Q^2}}, \quad s := \sqrt{1 - \frac{4m^2x}{Q^2(1-x)}}. \quad (4.7)$$

This gives the final result for the massive part of the gluon form factor

$$\begin{aligned} \hat{W}_{1,m}^{(g)}(x, Q^2, m^2, \mu^2) &= \frac{1}{2\pi} \text{Im} \left[T_{1,m}^{(g)} \right] \\ &= \frac{\alpha_s(\mu)T_f}{4\pi} \Theta\left(\frac{1}{w^2} - x\right) \left[\text{Log}\left(\frac{1+s}{1-s}\right) \left(\frac{P_{qg}(x)}{T_f} + 4x\rho(1-2x\rho-x) \right) \right. \\ &\quad \left. + 4sx(1-x)(1-\rho) - s \right] Q_m^2, \end{aligned} \quad (4.8)$$

$$\begin{aligned} \hat{W}_{L,m}^{(g)}(x, Q^2, m^2, \mu^2) &= \frac{1}{2\pi} \text{Im} \left[T_{L,m}^{(g)} \right] \\ &= \frac{\alpha_s(\mu)T_f}{\pi} \Theta\left(\frac{1}{w^2} - x\right) x \left[-2x\frac{m^2}{Q^2}\text{Log}\left(\frac{1+s}{1-s}\right) + s(1-x) \right] Q_m^2. \end{aligned} \quad (4.9)$$

The splitting function P_{qg} was defined in Eq. (3.108).

4.2.2 Matching

To find the corrections $H_{j,m}$ to the hard coefficients we have to do the matching at the scale μ^2 . All contributions from massless quarks are the same as in the previous section, so we just write the new terms we get from the heavy quark

$$\hat{W}_{j,m}^{(a)}(x, Q^2, m^2, \mu^2) = \sum_i \left(H_{j,m,F}^{(i)} \otimes f_{i/a} \right)(x, \mu^2) + \left(H_{j,m,F}^{(g)} \otimes f_{g/a} \right)(x, \mu^2). \quad (4.10)$$

Again j denotes the form factor, $j = \{1, L\}$, a can stand for any initial state parton, so a light (anti-) quark or a gluon, and the sum i runs over all light (anti-) quark flavors. The subscript m should remind us that these are just the contributions from the massive quark, the subscript F that these are the matching coefficients in the FFN scheme. If we insert the leading order results for the partonic PDFs

$$\begin{aligned} f_{i/j}^{(0)}(x) &= \delta_{ij} \delta(1-x), \\ f_{g/g}^{(0)}(x) &= \delta(1-x), \\ f_{i/g}^{(0)}(x) &= 0, \\ f_{g/i}^{(0)}(x) &= 0 \end{aligned} \quad (4.11)$$

and use that $\hat{W}_{j,m}^{(a),(0)} = 0$ and $\hat{W}_{j,m}^{(i),(1)} = 0$ we find that the only non zero contribution is from the gluon coefficient at $\mathcal{O}(\alpha_s)$. This is because at $\mathcal{O}(\alpha_s)$ we do not see any flavor changing so there is no mixing between the contributions from different quark flavors. So on a hadronic target P the fixed flavor number result for W_j with one massive quark reads

$$W_j^{(P)}(x, \mu^2) = W_{j,m=0}^{(P)}(x, \mu^2) + \left(H_{j,m,F}^{(g)} \otimes f_{g/P} \right)(x, \mu^2) + \mathcal{O}(\alpha_s^2), \quad (4.12)$$

where $H_{j,m,F}^{(g)} = \hat{W}_{j,m}^{(g)}$ from Eqs. (4.8)(4.9) and $W_{j,m=0}^{(P)}$ is just the massless result without the heavy quark. In the limit $\frac{m^2}{Q^2} \rightarrow 0$ the longitudinal coefficient $H_{L,m,F}^{(g)}$ reduces to the massless coefficient Eq. (3.107), but one important thing to notice is that for the coefficient $H_{1,m,F}^{(g)}$ the limit $\frac{m^2}{Q^2} \rightarrow 0$ contains logarithmic singularities of the form $\text{Log } \frac{m^2}{Q^2}$

$$H_{1,m,F}^{(g)}(x, Q^2, m^2, \mu^2) \xrightarrow{m^2 \rightarrow 0} -\frac{\alpha_s(\mu) T_f}{4\pi} \Theta(1-x) \left[\frac{P_{qg}(x)}{T_f} \left(\text{Log } \frac{m^2}{Q^2} - \text{Log } \left(\frac{1-x}{x} \right) \right) + (1-2x)^2 \right]. \quad (4.13)$$

This tells us that we get a large logarithm if $m^2 \ll Q^2$ and the FFN scheme is not a good choice in that case. This is resolved by the use of a VFN scheme, as will be shown in the next section.

4.3 Variable Flavor Number Scheme

Another way to include the effects of a heavy flavor with mass m is to use a variable flavor number scheme, as was first proposed for DIS by Aivazis et al. [3, 4]. Here two different effective theories are used, one with n_f light flavors for $\mu^2 \lesssim m^2$, and one with n_f light plus 1 heavy flavor for $\mu^2 \gtrsim m^2$. At the scale $\mu_m^2 \sim m^2$ the two theories have to be matched which will give a PDF for the heavy quark in the $n_f + 1$ theory. So for $\mu^2 \gtrsim m^2$ one has to run the PDFs (and also α_s) with $n_f + 1$ instead of n_f flavors, see Fig. 14a. In the case where the mass is above the hard scale the threshold is not crossed at all and so the VFN scheme simply reduces to the FFN scheme, see Fig. 14b.

In the VFN scheme (scenario I) the form factor W is written as

$$W = \sum_{l,k=\binom{(-)}{q}, \binom{(-)}{Q}, \binom{(-)}{g}} \sum_{i,j=\binom{(-)}{q}, \binom{(-)}{g}} H_V^{(l)}(\mu_H) \otimes U_{lk}^{n_f+1}(\mu_H, \mu_m) \otimes A_{kj}(\mu_m) \otimes U_{ji}^{n_f}(\mu_m, \mu_f) \otimes f_i(\mu_f). \quad (4.14)$$

Here H_V are the hard matching coefficients in the VFN scheme (whereas the matching coefficients in the FFN scheme were denoted as H_F) that will be determined in Sec. 4.3.3. The indices i, j run over light (anti-) quark flavors and the gluon, k, l also include the heavy (anti-) quark. The matching coefficients in $A(\mu_m)$ relate the PDFs in the two theories to each other (see Sec. 4.3.4), the evolution kernels $U(\mu, \mu_0)$ run the PDFs from the scale μ_0 to μ . The evolution of the new heavy quark PDF from the scale $\mu_m \rightarrow \mu_H$

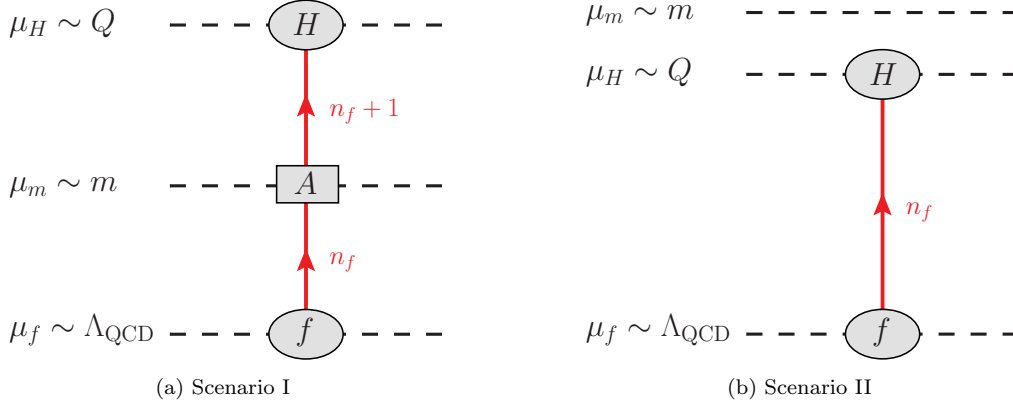


Figure 14: Variable flavor number scheme. In scenario I (left), where the mass is between Λ_{QCD} and the hard scale, the PDFs are run from their natural scale Λ_{QCD} to the matching scale μ_m where they are matched onto a theory with $n_f + 1$ flavors. The threshold corrections in A relate the PDFs in the two theories with each other. From μ_m to the hard scale the PDFs are run with $n_f + 1$ flavors. In scenario II (right) the mass is above the hard scale. Here the threshold is never crossed in the evolution and the PDFs are run from Λ_{QCD} to the hard scale with n_f flavors. All effects of the massive flavor are in the hard coefficients.

will eventually resum the logarithms $\text{Log } \frac{m^2}{Q^2}$ that appeared in Eq. (4.13). To find the hard coefficients in the VFN scheme H_V we have to perform the matching between SCET and QCD again, this time also allowing for a heavy quark in the initial state in the $n_f + 1$ theory. All diagrams with light quarks and the contributions from the heavy quark to the one loop diagrams with gluons in the initial state have already been computed in the last sections, to get all necessary matching coefficients in the $n_f + 1$ theory also the partonic QCD form factor for a heavy quark $W_j^{(Q)}$ (capital Q for a heavy quark) and the partonic PDFs $f_{Q/Q}$ and $f_{Q/g}$ need to be calculated (at $\mathcal{O}(\alpha_s)$ there is no flavor changing between heavy and light quarks).

4.3.1 QCD Calculations

The diagrams in Fig. 8 plus one additional with a mass counter term on the internal line have to be calculated again, this time with a massive quark in the initial state. Again this was done by using the Mathematica package FeynCalc to perform the tensor reduction for the integrals. The relevant n-point function can be found in appendix C. The wave function counter term for the external legs in the on-shell scheme and the mass counter term in the $\overline{\text{MS}}$ scheme are

$$\delta Z_\psi^{\text{OS}} = -\frac{\alpha_s(\mu)C_F}{4\pi} \left(\frac{3}{\epsilon} + 3 \text{Log } \frac{\mu^2}{m^2} + 4 \right), \quad (4.15)$$

$$\delta Z_m^{\overline{\text{MS}}} = -\frac{3\alpha_s(\mu)C_F}{4\pi\epsilon}. \quad (4.16)$$

For a shorter notation we use the abbreviations

$$w := \sqrt{1 + \frac{4m^2}{Q^2}}, \quad r := \sqrt{1 + \frac{4m^2x^2}{Q^2}}, \quad u := \frac{w-1}{w+1}. \quad (4.17)$$

Diagram Fig. 8a:

The tree-level result is

$$\hat{T}_1^{(Q),(a)}(x) = -\frac{1}{(1-x+i0)} \left(\frac{2\frac{m^2}{Q^2}x(x(2\epsilon-3)+1)+\epsilon-1}{(1-\epsilon)r^2} \right). \quad (4.18)$$

The imaginary part is independent of the mass and just leads to the massless result

$$\text{Im} \left[\hat{T}_1^{(Q),(a)}(x) \right] = \pi\delta(1-x). \quad (4.19)$$

Mass Counter Term:

The diagram with the mass counter term on the internal quark line yields

$$\hat{T}_1^{(Q),(ac)}(x) = 2 \frac{m^2}{Q^2} \delta Z_m^{\overline{\text{MS}}} \left(\frac{1}{(1-x+i0)^2} + \frac{2\epsilon-3}{1-\epsilon} \left(\frac{1}{(1-x+i0)} - \frac{1}{2} \right) + \frac{1}{2(1-\epsilon)r^2} \right). \quad (4.20)$$

The imaginary part is

$$\text{Im} \left[\hat{T}_1^{(Q),(ac)}(x) \right] = -2\pi \frac{m^2}{Q^2} \delta Z_m^{\overline{\text{MS}}} ((3+\epsilon)\delta(1-x) + \delta'(1-x)). \quad (4.21)$$

Diagram Fig. 8b:

The diagram in terms of the scalar integrals in appendix C reads

$$\begin{aligned} \hat{T}_1^{(Q),(b)}(x) = & \frac{\alpha_s(\mu) C_F e^{\epsilon\gamma_E}}{4\pi \left(1-x+\frac{m^2}{Q^2}x\right) r^2 \Gamma(2-\epsilon)} \\ & \times \left[\frac{1-\epsilon}{Q^2} \left(\frac{2\frac{m^2}{Q^2}w^2(1-\epsilon)}{(1-x+i0)^2} + \frac{8\frac{m^4}{Q^4}(5\epsilon-6) + 2\frac{m^2}{Q^2}(\epsilon-2) - \epsilon + 1}{1-x+i0} \right. \right. \\ & + \frac{m^2}{Q^2} [x^2(4\epsilon-6) + 2x\epsilon + \epsilon + 1] \\ & + \frac{m^4}{Q^4} [x^3(12-8\epsilon) + x^2(24-16\epsilon) + x(32-24\epsilon) + 40-32\epsilon] \Big) a_1 \\ & + \left(4\frac{m^2}{Q^2} \left(\frac{\frac{m^2}{Q^2}w^2(1-\epsilon)}{(1-x+i0)^2} - \frac{4\frac{m^4}{Q^4}(6-5\epsilon) + \frac{m^2}{Q^2}\epsilon + \epsilon - 1}{(1-x+i0)} \right) \right. \\ & + \frac{m^6}{Q^6} [x^3(24-16\epsilon) + x^2(48-32\epsilon) + x(64-48\epsilon) + 80-64\epsilon] \\ & + \frac{m^4}{Q^4} [x^3(-8\epsilon^2 + 36\epsilon - 36) + x^2(16\epsilon - 24) + x(12\epsilon - 8) + 8\epsilon - 4] \\ & \left. \left. + \frac{m^2}{Q^2} [x^2(-4\epsilon^2 + 10\epsilon - 6) + x(-2\epsilon^2 + 8\epsilon - 10) + 4\epsilon - 4] - (1-\epsilon)^2 \right) b_6 \right]. \quad (4.22) \end{aligned}$$

The imaginary part can be found with the relations in appendix B. The result expanded in ϵ is

$$\begin{aligned} \text{Im} \left[\hat{T}_1^{(Q),(b)}(x) \right] = & \frac{\alpha_s(\mu) C_F}{2} \Theta(1-x) \left\{ - \frac{\left(9\frac{m^2}{Q^2} + \frac{1}{2}\right) \delta(1-x) + 3\frac{m^2}{Q^2} \delta'(1-x)}{\epsilon} \right. \\ & - 2 \frac{1}{(1-x)_+} - \frac{m^2}{Q^2} \left[3 \text{Log} \frac{\mu^2}{m^2} + 4 \right] \delta'(1-x) \\ & - \left[\left(9\frac{m^2}{Q^2} + \frac{1}{2}\right) \text{Log} \frac{\mu^2}{m^2} - 2 \text{Log} \frac{m^2}{Q^2} + 15 \frac{m^2}{Q^2} \right] \delta(1-x) \\ & \left. + \frac{8\frac{m^6}{Q^6}(3x+1)x^3 + 4\frac{m^4}{Q^4}(x(11-9x)+4)x^2 + 2\frac{m^2}{Q^2}(x(6-11x)+7)x - 5(x-1)}{2 \left(1-x+\frac{m^2}{Q^2}x\right)^2 r^2} \right\}. \quad (4.23) \end{aligned}$$

Diagram Fig. 8c:

$$\begin{aligned}
\hat{T}_1^{(Q),(c)}(x) &= \frac{\alpha_s(\mu) C_F e^{\epsilon\gamma_E}}{2\pi r^2 \Gamma(2-\epsilon)} \\
&\times \left[-\frac{(1-\epsilon)x\left(\frac{m^2}{Q^2}x(2x+1)+1\right)}{Q^2\left(1-x+\frac{m^2}{Q^2}x\right)}a_1 + \frac{r^2\left(1-\frac{m^2}{Q^2}x-\epsilon\right)}{(1-x+i0)}b_1 \right. \\
&+ \frac{4\frac{m^2}{Q^2}x(2x^2(\epsilon^2-1)+x(\epsilon-2)+1)-(1-\epsilon)(2x(1+\epsilon)+1)}{2(1-x+i0)}b_3 \\
&+ \left(\frac{w^2(1+\frac{m^2}{Q^2}-\epsilon)}{(1-x+i0)} \right. \\
&+ \frac{-4\frac{m^6}{Q^6}x(x^2+x+1)+\frac{m^4}{Q^4}[x^3(4\epsilon^2-2\epsilon+2)+x^2(4\epsilon-6)+x(4\epsilon-5)-4]}{1-x+\frac{m^2}{Q^2}x} \\
&+ \left. \frac{\frac{m^2}{Q^2}[x^3(4-4\epsilon^2)+x^2(4\epsilon^2-5\epsilon+3)+x(\epsilon^2-2)+4\epsilon-5]-(1-x)(1-\epsilon^2)}{1-x+\frac{m^2}{Q^2}x} \right)b_6 \\
&+ Q^2 \frac{-r^2\epsilon(2\frac{m^2}{Q^2}x+1)+\frac{m^2}{Q^2}(1+x)\left[4x\left(\frac{m^2}{Q^2}(2x-1)+1\right)-1\right]+1}{(1-x+i0)}c_5 \Big]. \quad (4.24)
\end{aligned}$$

Except for the term with c_5 it is again straight forward to get the imaginary parts with the relations given in appendix B. The term proportional to $\frac{c_5}{1-x+i0}$ can be split in a singular and a non-singular part

$$\frac{c_5}{1-x+i0} = \frac{c_{5,x \rightarrow 1}}{1-x+i0} + \frac{c_5 - c_{5,x \rightarrow 1}}{1-x}, \quad (4.25)$$

so that the imaginary part is

$$\text{Im} \left[\frac{c_5}{1-x+i0} \right] = \text{Im} \left[\frac{c_{5,x \rightarrow 1}}{1-x+i0} \right] + \frac{\text{Im}[c_5] - \text{Im}[c_{5,x \rightarrow 1}]}{1-x}. \quad (4.26)$$

Only one of the dilogarithms in c_5 has a non-zero imaginary part and so we have

$$\text{Im}[c_5] = -\frac{x\pi}{Q^2 r} \text{Log} \left(\frac{(r+1)(r+2x-1)}{(r-1)(r-2x+1)} \right), \quad (4.27)$$

$$\text{Im}[c_{5,x \rightarrow 1}] = \left[\text{Im}[c_5] \right]_{x \rightarrow 1} = \frac{2\pi}{Q^2 w} \text{Log } u. \quad (4.28)$$

c_5 in the limit $x \rightarrow 1$ is

$$\begin{aligned}
c_{5,x \rightarrow 1} &= \frac{1}{Q^2 w} \left[-2 \text{Log } u \text{Log}(-(1-x)-i0) - \frac{\pi^2}{6} - \text{Li}_2 \left(\frac{w-1}{2w} \right) + \text{Li}_2 \left(\frac{w+1}{2w} \right) \right. \\
&\quad \left. + \text{Li}_2(u^2) + \text{Log } u \left(\frac{1}{2} \text{Log } u + \text{Log} \left(\frac{2w^3}{w+1} \right) \right) \right]. \quad (4.29)
\end{aligned}$$

From this we find the imaginary part of the full term in question to be

$$\begin{aligned}
\text{Im} \left[\frac{c_5}{1-x+i0} \right] &= \frac{\pi}{Q^2 w} \left[2 \text{Log } u \frac{1}{(1-x)_+} + \left(\text{Li}_2 \left(\frac{w-1}{2w} \right) - \text{Li}_2 \left(\frac{w+1}{2w} \right) - \text{Li}_2(u^2) \right. \right. \\
&\quad \left. \left. - \text{Log } u \left(\frac{1}{2} \text{Log } u + \text{Log} \left(\frac{2w^3}{w+1} \right) \right) + \frac{\pi^2}{6} \right) \delta(1-x) \right. \\
&\quad \left. - \frac{\frac{xw}{r} \text{Log} \left(\frac{(r+1)(r+2x-1)}{(r-1)(r-2x+1)} \right) + 2 \text{Log } u}{1-x} \right]. \quad (4.30)
\end{aligned}$$

Then the imaginary part for the full diagram is

$$\begin{aligned}
\text{Im} \left[\hat{T}_1^{(Q),(c)}(x) \right] = & \frac{\alpha_s(\mu)C_F}{4} \Theta(1-x) \left\{ \frac{1}{\epsilon} \delta(1-x) \right. \\
& + \left\{ \text{Log} \frac{\mu^2}{m^2} - 3w \text{Log} u - \frac{1+w^2}{w} \left[\text{Li}_2 \left(\frac{w-1}{2w} \right) - \text{Li}_2(u^2) - \text{Li}_2 \left(\frac{w+1}{2w} \right) \right. \right. \\
& + \left. \left. \text{Log} u \left(-\text{Log} u + \frac{1}{2} \text{Log} \frac{m^2}{Q^2} - \text{Log}(w^3) \right) + \frac{\pi^2}{6} \right] \right\} \delta(1-x) \\
& - \frac{2(1+w^2) \text{Log} u}{w} \frac{1}{(1-x)_+} + \frac{2(1+w^2) \text{Log} u + \frac{wx}{r} \text{Log} \left(\frac{(r+1)(r+2x-1)}{(r-1)(r-2x+1)} \right)}{w(1-x)} \\
& + \frac{(1-r^2)(r^2(2x+1)+x-1) \text{Log} \left(\frac{(r+1)(r+2x-1)}{(r-1)(r-2x+1)} \right)}{2r^3x^2} \\
& + \left. \frac{2x \left(-4\frac{m^6}{Q^6}x^3 + \frac{m^4}{Q^4}(2(x-4)x+1)x + \frac{m^2}{Q^2}((4x-5)(x+1)x+1) + x-1 \right)}{\left(1-x + \frac{m^2}{Q^2}x \right)^2 r^2} \right\}.
\end{aligned} \tag{4.31}$$

Diagram Fig. 8d:

$$\begin{aligned}
\hat{T}_1^{(Q),(d)}(x) = & \frac{\alpha_s(\mu)C_F e^{\epsilon\gamma_E}}{2\pi r^2 \Gamma(2-\epsilon)} \\
& \times \left[\frac{x^2(1-\epsilon)(2\frac{m^2}{Q^2}x+1)}{Q^2(1-x+\frac{m^2}{Q^2}x)} a_1 + (1-\epsilon) \left(2\frac{m^2}{Q^2}x^2(2\epsilon-1) + \epsilon-1 \right) b_1 \right. \\
& + \left(-\frac{2r^2(1-\epsilon)^3}{2\epsilon-3} + 2\frac{m^2}{Q^2}x \right) b_2 + \left(x(1-2\frac{m^2}{Q^2}-\epsilon) + 1 + \frac{2-\epsilon}{2\epsilon-3}r^2 \right) b_3 \\
& + x(\epsilon-1) \left(\frac{2x^2-3x+1}{1-x+\frac{m^2}{Q^2}x} + 2x + \frac{4\frac{m^2}{Q^2}x\epsilon}{\epsilon-1} \right) b_6 + m^2 \left(r^2(1-2\epsilon) + 1 \right) c_1 \\
& + 2Q^2 \left(\frac{(\epsilon-1)^2(\epsilon-1+2\frac{m^2}{Q^2})r^2}{2\epsilon-3} - \frac{m^2}{Q^2}x \left(1 + 4\frac{m^2}{Q^2}x \right) \right) c_3 \\
& + \frac{Q^2}{x} \left(2\frac{m^2}{Q^2}x \left(r^2 + (1-x) \left(x(\epsilon-1)(2\epsilon-1) - 2 \right) \right) + (1-x)(1-\epsilon)^2 \right) c_5 \\
& + \left. 2m^2Q^2 \left(2\frac{m^2}{Q^2} \left(-1 + 2x + x^2(1-2\epsilon) \right) - \epsilon + 1 \right) d_1 \right].
\end{aligned} \tag{4.32}$$

The imaginary part of this is

$$\begin{aligned}
\text{Im} \left[\hat{T}_1^{(Q),(d)}(x) \right] = & \frac{\alpha_s(\mu)C_F}{2} \Theta(1-x) \left\{ \frac{1}{\epsilon} \delta(1-x) - 2 \frac{1}{(1-x)_+} \right. \\
& + \left[\text{Log} \frac{\mu^2}{m^2} + 2 \text{Log} \frac{m^2}{Q^2} - \frac{1+w^2}{w} \text{Log} u \right] \delta(1-x) \\
& + \frac{(r^4 - r^2((x-3)x+3) - x^2 - x + 2) \text{Log} \left(\frac{(r+1)(r+2x-1)}{(r-1)(r-2x+1)} \right)}{2r^3x} \\
& + \left. \frac{4\frac{m^6}{Q^6}(x+1)x^3 + 2\frac{m^4}{Q^4}x^2(5-4x^2) + 2\frac{m^2}{Q^2}(x-2)(x-1)(x+2)x + (x^3-3x+2)}{\left(1-x + \frac{m^2}{Q^2}x \right)^2 r^2} \right\}.
\end{aligned} \tag{4.33}$$

Final Result:

The final result for the partonic form factor for a massive quark $\hat{W}_1^{(Q)}$ including the wave function counter terms for the external legs is

$$\begin{aligned}
\hat{W}_1^{(Q)}(x, Q^2, m^2, \mu^2) = & \frac{1}{2} \delta(1-x) + \frac{\alpha_s(\mu) C_F}{4\pi} \Theta(1-x) \left\{ -\frac{m^2}{Q^2} \delta'(1-x) \left[3 \operatorname{Log} \frac{\mu^2}{m^2} + 4 \right] \right. \\
& \delta(1-x) \left[-2 - 3 \frac{m^2}{Q^2} \left(4 + 3 \operatorname{Log} \frac{\mu^2}{m^2} \right) + 4 \operatorname{Log} \frac{m^2}{Q^2} - 3w \operatorname{Log} u \right. \\
& + \frac{1+w^2}{w} \left(-\operatorname{Li}_2 \left(\frac{w-1}{2w} \right) + \operatorname{Li}_2 \left(\frac{w+1}{2w} \right) + \operatorname{Li}_2(u^2) + \frac{\pi^2}{6} \right. \\
& + \operatorname{Log} u \left(\operatorname{Log} w^3 + \operatorname{Log} u - \frac{1}{2} \operatorname{Log} \frac{m^2}{Q^2} - 1 \right) \left. \right] \\
& - 2 \frac{1}{(1-x)_+} \left[2 + \frac{1+w^2}{w} \operatorname{Log} u \right] \\
& + \frac{1}{2r^2(1+x(\frac{m^2}{Q^2}-1))^2} \left((1-x)(9-6x-2x^2) + 2 \frac{m^2}{Q^2} (1-x)x(17+5x-10x^2) \right. \\
& + 4 \frac{m^4}{Q^4} x^2(10+3x-33x^2) + 16 \frac{m^6}{Q^6} x^3(1+x) \left. \right) \\
& + \frac{\operatorname{Log} \left(\frac{(r+1)(r+2x-1)}{(r-1)(r-2x+1)} \right)}{2r^3(1-x)x^2} \left(-1 + 4x(1-x+x^2) + r^2(2-4x+5x^2) \right. \\
& \left. \left. - 2x^3(2+w) + x^4 + r^4(-1+x^2) \right) - \frac{2}{1-x} \operatorname{Log} u \right\}. \tag{4.34}
\end{aligned}$$

All IR divergences have been regularized by the mass. The mass singularities in $\hat{W}_1^{(Q)}$ for $\frac{m^2}{Q^2} \rightarrow 0$ will be canceled by the SCET subtractions to yield the correct finite massless limit for $H_{1,V}^{(Q)}$ (see Sec. 4.3.5).

4.3.2 SCET Calculations

We have to calculate the diagrams in Fig. 10 again, this time with a massive quark. The mass does not enter the tree level calculation, so Fig. 10a is again just $\delta(1-\xi)$.

Diagram Fig. 10b:

$$\begin{aligned}
f_{Q/Q}^{(b)}(\xi) = & \int \frac{d^d k}{(2\pi)^d} \delta(p^- \xi - k^-) \frac{-i}{(p-k)^2 + i0} \\
& \times \frac{1}{2} \sum_s \bar{u}_n(p, s) V^{n,\mu,A}(p, k, m) F_n(k, m) \frac{\not{p}}{2} F_n(k, m) V_{n,\mu}^A(k, p, m) u_n(p, s), \tag{4.35}
\end{aligned}$$

with the massive propagator and vertex $F_n(k, m)$ and $V_{n,\mu}^A(k, p, m)$ from Sec. 2.3. This yields

$$\begin{aligned}
f_{Q/Q}^{(b)}(\xi) = & -8i\pi\alpha_s(\mu) C_F \tilde{\mu}^2 p^- \int \frac{d^d k}{(2\pi)^d} \delta(p^- \xi - k^-) \frac{1}{(k^2 - m^2 + i0)^2 ((p-k)^2 + i0)} \\
& \times \left(\frac{k^- m^2}{p^-} \left(2 - \frac{(1-\epsilon)(p^- - k^-)^2}{p^- k^-} \right) - (1-\epsilon) |k_\perp^2| \right). \tag{4.36}
\end{aligned}$$

With the change to light-cone coordinates and the further substitution to dimensionless integration variables $|k_\perp^2| = wp^+p^-$, $k^+ = yp^+$ and $k^- = zp^-$ and the on-shell condition $p^+p^- = m^2$ this simplifies

to

$$f_{Q/Q}^{(b)}(\xi) = \frac{-i\alpha_s(\mu)C_F}{4\pi^2\Gamma(1-\epsilon)} \left(\frac{\mu^2 e^{\gamma_E}}{m^2} \right)^\epsilon \int dy dz dw \delta(z-\xi) \frac{\Theta(w)w^{-\epsilon}}{(zy-w-1+i0)^2(y(z-1)-z+1-w+i0)} \\ \times \left[2z - (1-\epsilon)(1-z)^2 - (1-\epsilon)w \right]. \quad (4.37)$$

The z integration is trivial, the y integration can be solved by contour integration

$$\int_{-\infty}^{\infty} dy \frac{1}{(y\xi-w-1+i0)^2(y(\xi-1)-\xi-w+1+i0)} = \frac{-2\pi i(1-\xi)}{(w+(1-\xi)^2)^2} \Theta(\xi)\Theta(1-\xi) \quad (4.38)$$

and the remaining w integral is

$$\int_0^\infty dw \frac{w^{-\epsilon}(2\xi - (1-\epsilon)(1-\xi)^2 - (1-\epsilon)w)}{(w+(1-\xi)^2)^2} = -\Gamma(\epsilon)\Gamma(1-\epsilon) \left((1-\xi)^{-2\epsilon} - \epsilon(1+\xi^2)(1-\xi)^{-2-2\epsilon} \right). \quad (4.39)$$

Therefore the full expression reads

$$f_{Q/Q}^{(b)}(\xi) = \frac{\alpha_s(\mu)C_F}{2\pi} \Theta(\xi)\Theta(1-\xi) \left(\frac{\mu^2 e^{\gamma_E}}{m^2} \right)^\epsilon \Gamma(\epsilon) \left((1-\xi)^{1-2\epsilon} - \epsilon(1+\xi^2)(1-\xi)^{-1-2\epsilon} \right). \quad (4.40)$$

One can use Eq. (A.3) to expand the last term

$$\epsilon(1+\xi^2)(1-\xi)^{-1-2\epsilon} = -\frac{1}{2}(1+\xi^2)\delta(1-\xi) + \epsilon(1+\xi^2)\frac{1}{(1-\xi)_+} + \mathcal{O}(\epsilon^2) \\ = -\delta(1-\xi) + \epsilon \left(2\frac{1}{(1-\xi)_+} - 1 - \xi \right) + \mathcal{O}(\epsilon^2) \quad (4.41)$$

and so the final result is

$$f_{Q/Q}^{(b)}(\xi) = \frac{\alpha_s(\mu)C_F}{2\pi} \Theta(\xi)\Theta(1-\xi) \left(\left(\frac{1}{\epsilon} + \text{Log} \frac{\mu^2}{m^2} \right) (\delta(1-\xi) + 1 - \xi) - 2\frac{1}{(1-\xi)_+} \right. \\ \left. - 2(1-\xi)\text{Log}(1-\xi) + \xi + 1 \right). \quad (4.42)$$

Diagram Fig. 10c:

$$f_{Q/Q}^{(c)}(\xi) = \int \frac{d^d k}{(2\pi)^d} (\delta(p^-\xi - p^-) - \delta(p^-\xi - k^-)) \frac{-i}{((p-k)^2 + i0)} \frac{gT^A \tilde{\mu}^\epsilon \bar{n}^\mu}{(p^- - k^- - i0)} \\ \times \frac{1}{2} \sum_s \bar{u}_n(p, s) F_n(k, m) V_{n,\mu}^A(p, k, m) u_n(p, s). \quad (4.43)$$

All mass dependent terms in the vertex $V_\mu^A(p, k, m)$ do not survive the contraction with \bar{n}^μ in the n -coll. Wilson line and so the only contribution from the mass is in the propagator $F_n(k, m)$. With the same

substitutions as for the previous diagram we get

$$f_{Q/Q}^{(c)}(\xi) = \frac{i\alpha_s(\mu)C_F}{4\pi^2\Gamma(1-\epsilon)} \left(\frac{\mu^2 e^{\gamma_E}}{m^2} \right)^\epsilon \int dz dw (\delta(1-\xi) - \delta(z-\xi)) \frac{\Theta(w)w^{-\epsilon}z}{1-z} \times \underbrace{\int_{-\infty}^{\infty} dy \frac{1}{(y(z-1)+1-z-w+i0)(yz-1-w+i0)}}_{=2\pi i\Theta(z)\Theta(1-z)\frac{1}{w+(1-z)^2}} \quad (4.44)$$

$$= -\frac{\alpha_s(\mu)C_F}{2\pi\Gamma(1-\epsilon)} \left(\frac{\mu^2 e^{\gamma_E}}{m^2} \right)^\epsilon \int_0^1 dz (\delta(1-\xi) - \delta(z-\xi)) \frac{z}{1-z} \times \underbrace{\int_0^\infty dw \frac{w^{-\epsilon}}{w+(1-z)^2}}_{=\Gamma(\epsilon)\Gamma(1-\epsilon)(1-z)^{-2\epsilon}} \quad (4.45)$$

$$= \frac{\alpha_s(\mu)C_F}{2\pi} \left(\frac{\mu^2 e^{\gamma_E}}{m^2} \right)^\epsilon \Gamma(\epsilon) \times \left[\underbrace{\int_0^1 dz \delta(z-\xi)z(1-z)^{-1-2\epsilon}}_{=\Theta(\xi)\Theta(1-\xi)\xi(1-\xi)^{-1-2\epsilon}} - \delta(1-\xi) \underbrace{\int_0^1 dz z(1-z)^{-1-2\epsilon}}_{=B(2,-2\epsilon)=\frac{\Gamma(-2\epsilon)}{\Gamma(2-2\epsilon)}} \right] \quad (4.46)$$

$$= \frac{\alpha_s(\mu)C_F}{2\pi} \Theta(\xi)\Theta(1-\xi) \left(\frac{\mu^2 e^{\gamma_E}}{m^2} \right)^\epsilon \Gamma(\epsilon) \left(\xi(1-\xi)^{-1-2\epsilon} - \delta(1-\xi) \frac{\Gamma(-2\epsilon)}{\Gamma(2-2\epsilon)} \right). \quad (4.47)$$

The term $(1-\xi)^{-1-2\epsilon}$ can be expanded with Eq. (A.3) and the full result for $f_{Q/Q}^{(c)}$ is

$$f_{Q/Q}^{(c)}(\xi) = \frac{\alpha_s(\mu)C_F}{2\pi} \Theta(\xi)\Theta(1-\xi) \left(\left(\frac{1}{\epsilon} + \text{Log} \frac{\mu^2}{m^2} \right) \left(\delta(1-\xi) + \frac{1}{(1-\xi)_+} - 1 \right) - 2 \left(\frac{\text{Log}(1-\xi)}{1-\xi} \right)_+ + 2\delta(1-\xi) + 2\text{Log}(1-\xi) \right). \quad (4.48)$$

From the wave function counter term we get an additional term $\delta(1-\xi)\delta Z_\psi^{\text{OS}}$ and so the bare quark-quark PDF for a massive flavor is

$$f_{Q/Q}^0(\xi, m^2, \mu^2) = \delta(1-\xi) + \frac{\alpha_s(\mu)C_F}{2\pi} \Theta(\xi)\Theta(1-\xi) \left[\left(\frac{1}{\epsilon} + \text{Log} \frac{\mu^2}{m^2} \right) \frac{P_{qq}(\xi)}{C_F} + 2\delta(1-\xi) - 2 \frac{1}{(1-\xi)_+} - 4 \left(\frac{\text{Log}(1-\xi)}{1-\xi} \right)_+ + 2(1+\xi)\text{Log}(1-\xi) + \xi + 1 \right]. \quad (4.49)$$

The splitting function P_{qq} is given in Eq. (3.95). The UV divergences are not related to a low-energy scale like the mass and are therefore the same as for a massless quark, so in the $\overline{\text{MS}}$ renormalization scheme the new heavy quark PDF contributes to the DGLAP evolution just like an additional massless flavor.

Diagram Fig. 12:

To get $f_{Q/g}$ the diagram in Fig. 12 needs to be calculated with massive internal quarks

$$f_{Q/g}(\xi) = \int \frac{d^d k}{(2\pi)^d} \delta(p^+ - \xi - k^+) \frac{1}{2(1-\epsilon)} \sum_{\text{pol.}} \frac{1}{8} \sum_{\text{col.}} \epsilon_\mu^A(p) \epsilon_\nu^{*B}(p) \times (-1) \text{Tr} \left[V_n^{\mu,A}(k, k-p, m) F_n(k, m) \frac{\not{p}}{2} F_n(k, m) V_n^{\nu,B}(k-p, p, m) F_n(k-p, m) \right]. \quad (4.50)$$

Performing all sums and traces gives

$$\begin{aligned} & \frac{-i8\pi\alpha_s(\mu)T_f}{1-\epsilon} \tilde{\mu}^{2\epsilon} \int \frac{d^d k}{(2\pi)^d} \delta(p^-\xi - k^-) \frac{1}{(k^2 - m^2 + i0)^2 ((p-k)^2 - m^2 + i0)} \\ & \times \frac{|k_\perp^2| [(1-\epsilon)(p^-)^2 + 2k^-(k^- - p^-)] + m^2(1-\epsilon)(p^-)^2}{k^- - p^-} \end{aligned} \quad (4.51)$$

$$\begin{aligned} & = \frac{-i\alpha_s(\mu)T_f}{4\pi(1-\epsilon)\Gamma(1-\epsilon)} \left(\frac{\mu^2 e^{\gamma_E}}{m^2} \right)^\epsilon \int dy dz dw \delta(z-\xi) \frac{\Theta(w)w^{-\epsilon}}{(yz-w-1+i0)^2 (y(z-1)-w-1+i0)} \\ & \times \frac{w(2(1-z)z-1+\epsilon)-1+\epsilon}{1-z}. \end{aligned} \quad (4.52)$$

The z integration is again trivial and the for the y and w integrations one finds

$$\int_{-\infty}^{\infty} dy \frac{1}{(yz-w-1+i0)^2 (y(z-1)-w-1+i0)} = -\frac{2\pi i(1-\xi)}{(1+w)^2} \Theta(\xi)\Theta(1-\xi), \quad (4.53)$$

$$\int_0^{\infty} dw \frac{w^{-\epsilon} (w(2\xi(1-\xi)-1+\epsilon)-1+\epsilon)}{(1+w)^2} = -\Gamma(\epsilon)\Gamma(1-\epsilon)(1-\epsilon)(\xi^2 + (1-\xi)^2). \quad (4.54)$$

So the bare quark-gluon PDF for a heavy quark is

$$f_{Q/g}^0(\xi, m^2, \mu^2) = \frac{\alpha_s(\mu)T_f}{2\pi} \Theta(\xi)\Theta(1-\xi) \left(\frac{1}{\epsilon} + \text{Log} \frac{\mu^2}{m^2} \right) \frac{P_{qg}(\xi)}{T_f} \quad (4.55)$$

with the splitting function P_{qg} as in Eq. (3.108).

4.3.3 Matching at the Hard Scale

At the matching scale $\mu^2 \sim Q^2$ we have to match the effective theory operators onto the full theory results. The contributions from the massless flavors will be the same as in Sec. 3.3, so again we just write down the corrections due to the massive quark. The matching condition reads⁷

$$\hat{W}_{j,m}(x, \mu^2) = \left(H_{j,V}^{(Q)} \otimes f_Q \right) (\eta, \mu^2) + \left(H_{j,m,V}^{(g)} \otimes f_g \right) (\eta, \mu^2), \quad (4.56)$$

where η is defined as in Eq. (4.1) with the mass m of the initial state. Here the convolution on the right hand side of Eq. (4.56) is rescaled by using the variable η instead of x because for a massive initial the matching condition is changed compared to the massless case, see Sec. 4.1. If we have a massless particle in the initial state the rescaling variable η reduces to x . As initial states we can use a massive quark or a gluon (because there is no flavor changing at $\mathcal{O}(\alpha_s)$ a massless quark can not contribute to heavy flavor production) which yields

$$\hat{W}_j^{(Q)}(x, \mu^2) = \left(H_{j,V}^{(Q)} \otimes f_{Q/Q} \right) (\eta, \mu^2) + \left(H_{j,m,V}^{(g)} \otimes f_{g/Q} \right) (\eta, \mu^2), \quad (4.57)$$

$$\hat{W}_{j,m}^{(g)}(x, \mu^2) = \left(H_{j,V}^{(Q)} \otimes f_{Q/g} \right) (x, \mu^2) + \left(H_{j,m,V}^{(g)} \otimes f_{g/g} \right) (x, \mu^2). \quad (4.58)$$

Here we have used the rescaling variable η for the massive quark and x for the massless gluon. This gives the tree level matching coefficients

$$H_{1,V}^{(Q),(0)}(\eta) = \hat{W}_1^{(Q),(0)}(x) = \frac{1}{2} \delta(1-x) = \frac{w-1}{4w\frac{m^2}{Q^2}} \delta\left(\eta - \frac{w-1}{2\frac{m^2}{Q^2}}\right), \quad (4.59)$$

$$H_{1,m,V}^{(g),(0)}(x) = \hat{W}_{1,m}^{(g),(0)}(x) = 0, \quad (4.60)$$

where w was defined in Eq. (4.17). One could just use the result for $H_{1,V}^{(Q)}$ in this form but it would be more convenient to have the delta distribution in the form $\sim \delta(1-\eta)$ because this is the identity operator with respect to the convolution. So we define the new function \tilde{H} as

$$\tilde{H}_{j,V}^{(Q)}(\eta) := w H_{j,V}^{(Q)}\left(\frac{w-1}{2\frac{m^2}{Q^2}}\eta\right), \quad H_{j,V}^{(Q)}(\eta) = \frac{1}{w} \tilde{H}_{j,V}^{(Q)}(\chi(\eta)), \quad (4.61)$$

⁷Because we only work at $\mathcal{O}(\alpha_s)$ we do not see any flavor changing and therefore do not get any corrections to the light quark coefficients of the form $H_{j,m}^{(i)} \otimes f_i$

with the rescaling variable

$$\chi(\eta) = \frac{\eta(w+1)}{2}. \quad (4.62)$$

Then we can switch from $H_{1,V}^{(Q)}(\eta)$ to $\frac{1}{w}\tilde{H}_{1,V}^{(Q)}(\chi(\eta))$ in the convolution:

$$\left(H_{1,V}^{(Q)} \otimes f_Q\right)(\eta) = \frac{1}{w} \left(\tilde{H}_{1,V}^{(Q)} \otimes f_Q\right)(\chi(\eta)). \quad (4.63)$$

This additional rescaling from $H(\eta)$ to $\tilde{H}(\chi(\eta))$ does not change the result but it allows to write the leading order matching coefficient for the heavy quark as

$$\tilde{H}_{1,V}^{(Q),(0)}(\chi) = \frac{1}{2}\delta(1-\chi), \quad (4.64)$$

which has the delta distribution in the form we wanted to have it and looks the same as for the massless case. At order α_s the quark coefficient takes the form

$$\begin{aligned} \tilde{H}_{1,V}^{(Q),(1)}(\chi(\eta)) &= wW_1^{(Q),(1)}(x) - \frac{1}{2}f_{Q/Q}^{(1)}(\chi(\eta)) \\ \Rightarrow \tilde{H}_{1,V}^{(Q),(1)}(x) &= wW_1^{(Q),(1)}\left(\frac{2x}{1+w+x^2(1-w)}\right) - \frac{1}{2}f_{Q/Q}^{(1)}(x) \end{aligned} \quad (4.65)$$

and the gluon coefficient is

$$H_{1,m,V}^{(g),(1)}(x) = W_{1,m}^{(g),(1)}(x) - \frac{1}{2w}f_{Q/g}^{(1)}(\chi(x)). \quad (4.66)$$

The rescaling of the distributions with the function $g(x) = \frac{2x}{1+w+x^2(1-w)}$ gives

$$\frac{1}{(1-g(x))_+} = \frac{1}{w} \left(\frac{1}{(1-x)_+} + \delta(1-x) \text{Log } w + \frac{(w-1)(1+w+wx)}{1+w+x(w-1)} \right), \quad (4.67)$$

$$\delta(1-g(x)) = \frac{1}{w}\delta(1-x), \quad (4.68)$$

$$\delta'(1-g(x)) = \frac{1}{w^2} \left(\delta'(1-x) + \frac{1+w-2w^2}{w}\delta(1-x) \right). \quad (4.69)$$

The result for $H_{1,V}^{(Q)}(x)$ agrees with Ref. [22].

4.3.4 Matching at the Mass Scale

At the scale $\mu_m^2 \sim m^2$ we change from an effective theory with n_f flavors to one with $n_f + 1$ flavors. So at μ_m^2 we have to perform a matching between the two theories to find out how the PDFs in the n_f and $n_f + 1$ flavor theories are related. Also the running of the coupling $\alpha_s(\mu)$ has to be changed from n_f to $n_f + 1$ flavors at μ_m^2 . At the matching scale μ_m^2 the PDFs in the two theories have to be the same, so the matching condition is

$$f_a^{n_f+1}(x, \mu^2) = \sum_i (A_{ai} \otimes f_i^{n_f})(x, \mu^2) + (A_{ag} \otimes f_g^{n_f})(x, \mu^2). \quad (4.70)$$

The index a can stand for any light (anti-) quark i , a gluon g or a heavy (anti-) quark Q . The index i is just for light flavors. So $A(x, \mu^2)$ is a $(2(n_f + 1) + 1) \times (2n_f + 1)$ matrix of matching coefficients. As initial state for the matching we can use any light flavor j or a gluon. Because there is no flavor changing at order α_s the light quark PDFs do not get any contribution from the heavy flavor. The only other non zero coefficients are A_{Qg} and A_{gg} . These can be found from the matching conditions

$$f_{Q/g}^{n_f+1}(x, \mu^2) = (A_{Qg} \otimes f_{g/g}^{n_f})(x, \mu^2), \quad (4.71)$$

$$f_{g/g}^{n_f+1}(x, \mu^2) = (A_{gg} \otimes f_{g/g}^{n_f})(x, \mu^2). \quad (4.72)$$

We know from Sec. 3.4 that $f_{g/g}(x, \mu^2) = \delta(1-x) + \mathcal{O}(\alpha_s)$ and so the first condition yields

$$A_{Qg}(x, \mu^2) = f_{Q/g}^{n_f+1}(x, \mu^2) + \mathcal{O}(\alpha_s^2). \quad (4.73)$$

In the $n_f + 1$ theory there is one quark flavor more that contributes in the gluon wave function renormalization in $f_{g/g}^{n_f+1}$ compared to $f_{g/g}^{n_f}$, i.e.

$$f_{g/g}^{n_f+1}(x, \mu^2) = f_{g/g}^{n_f}(x, \mu^2) - \delta(1-x) \frac{\alpha_s(\mu) T_f}{3\pi} \text{Log} \frac{\mu^2}{m^2} + \mathcal{O}(\alpha_s^2). \quad (4.74)$$

Eventually we get

$$\begin{aligned} A_{ij}(x, m^2, \mu^2) &= \delta_{ij} \delta(1-x) + \mathcal{O}(\alpha_s^2), \\ A_{gi}(x, m^2, \mu^2) &= A_{ig}(x, \mu^2) = A_{Qi}(x, \mu^2) = 0 + \mathcal{O}(\alpha_s^2), \\ A_{gg}(x, m^2, \mu^2) &= \delta(1-x) \left(1 - \frac{\alpha_s^{n_f}(\mu) T_f}{3\pi} \text{Log} \frac{\mu^2}{m^2} \right) + \mathcal{O}(\alpha_s^2), \\ A_{Qg}(x, m^2, \mu^2) &= A_{\bar{Q}g}(x, \mu^2) = \frac{\alpha_s^{n_f}(\mu)}{2\pi} \text{Log} \frac{\mu^2}{m^2} P_{qg}^{(0)}(x) + \mathcal{O}(\alpha_s^2) \end{aligned} \quad (4.75)$$

for the matching coefficients and therefore

$$\begin{aligned} f_i^{n_f+1}(x, \mu^2) &= f_i^{n_f}(x, \mu^2) + \mathcal{O}(\alpha_s^2), \\ f_g^{n_f+1}(x, \mu^2) &= f_g^{n_f}(x, \mu^2) \left(1 - \frac{\alpha_s^{n_f}(\mu) T_f}{3\pi} \text{Log} \frac{\mu^2}{m^2} \right) + \mathcal{O}(\alpha_s^2), \\ f_Q^{n_f+1}(x, \mu^2) &= \bar{f}_Q^{n_f+1}(x, \mu^2) = \frac{\alpha_s^{n_f}(\mu)}{2\pi} \text{Log} \frac{\mu^2}{m^2} \left(P_{qg}^{(0)} \otimes f_g^{n_f} \right)(x, \mu^2) + \mathcal{O}(\alpha_s^2) \end{aligned} \quad (4.76)$$

for the PDFs. To avoid any large logarithms in the matching one should set $\mu_m^2 \sim m^2$. With $\mu_m^2 = m^2$ all PDFs are continuous at the matching scale at $\mathcal{O}(\alpha_s)$. This is no longer true at $\mathcal{O}(\alpha_s^2)$, when there is a discontinuity even if the matching scale is exactly at the mass scale. The matching coefficients to $\mathcal{O}(\alpha_s^2)$ can be found in Ref. [23].⁸

4.3.5 Massless Limit

For the gluon coefficient $H_{1,m,V}^{(g)}(x)$ it is straightforward to get the correct massless limit. Eq. (4.66) reduces to

$$\begin{aligned} H_{1,m,V}^{(g)}(x) &= H_{1,m,F}^{(g)}(x) - \frac{1}{2} f_{Q/g}(x) \\ &\xrightarrow{m^2 \rightarrow 0} -\frac{\alpha_s T_f}{4\pi} \Theta(1-x) \left[\frac{P_{qg}(x)}{T_f} \left(\text{Log} \frac{\mu^2}{Q^2} - \text{Log} \left(\frac{1-x}{x} \right) \right) + (1-2x)^2 \right]. \end{aligned} \quad (4.77)$$

The $\text{Log} \frac{\mu^2}{m^2}$ in $f_{Q/g}$ cancels the m^2 dependence in the $\text{Log} \frac{m^2}{Q^2}$ that we encountered in the massless limit in the FFN scheme. This gives the correct massless limit for the hard gluon coefficient (compare Eq.(3.109)). The large logs that arose in the limit $m^2 \ll Q^2$ disappeared from the matching coefficient, they are resummed in the evolution of the heavy quark PDF.

To find the massless limit for the quark coefficient $H_{1,V}^{(Q)}$ we have to work a little bit harder. Some of the terms that are non-distributive for finite m give rise to new distributions in x in the limit $\frac{m^2}{Q^2} \rightarrow 0$. We start from the QCD term $\hat{W}_1^{(Q)}$ and split it into terms with and without distributions

$$\hat{W}_1^{(Q)}(x) = \hat{W}_{1,\text{dist.}}^{(Q)}(x) + \hat{W}_{1,\text{non-dist.}}^{(Q)}(x). \quad (4.78)$$

For $\hat{W}_{1,\text{dist.}}^{(Q)}$ the limit $m^2 \rightarrow 0$ can be taken without any problems and yields

$$\begin{aligned} \hat{W}_{1,\text{dist.}}^{(Q)}(x) &\xrightarrow{m^2 \rightarrow 0} \frac{\alpha_s(\mu) C_F}{4\pi} \left[\delta(1-x) \left(-2 - \text{Log} \frac{m^2}{Q^2} + \text{Log}^2 \frac{m^2}{Q^2} \right) - \right. \\ &\quad \left. \frac{4}{(1-x)_+} \left(1 + \text{Log} \frac{m^2}{Q^2} \right) \right] + \mathcal{O} \left(\frac{m^2}{Q^2} \right). \end{aligned} \quad (4.79)$$

⁸Note that there is a typo in the Arxiv version of Ref. [23] in the coefficient A_{Hg} (A_{Qg} in our notation). It is fixed in the journal version.

The distributions that are hidden in $\hat{W}_{1,\text{non-dist.}}^{(Q)}$ in the limit $m^2 \rightarrow 0$ can be identified by integration over an infinitesimal interval around 1 as shown in Eqs. (A.13)-(A.16). The integration with the full integrand $\hat{W}_{1,\text{non-dist.}}^{(Q)}$ expanded for $m^2 \rightarrow 0$ is hard to perform, but because the integration is only in an infinitesimal interval around $x = 1$ one can expand for $(1-x) \sim \frac{m^2}{Q^2} \rightarrow 0$ instead of just $m^2 \rightarrow 0$ because only the singular parts give rise to distributions.⁹

$$\hat{W}_{1,\text{non-dist.}}^{(Q)}(x) \xrightarrow{(1-x) \sim \frac{m^2}{Q^2} \rightarrow 0} \hat{W}_{1,s}^{(Q)}(x) + \hat{W}_{1,ns}^{(Q)}(x), \quad (4.80)$$

$$\hat{W}_{1,s}^{(Q)}(x) = \frac{\alpha_s(\mu)C_F}{4\pi} \left[\frac{1-x}{2(1-x+\frac{m^2}{Q^2})^2} + \frac{2\text{Log}\left(\frac{\frac{m^2}{Q^2}}{1-x+\frac{m^2}{Q^2}}\right)}{1-x} \right], \quad (4.81)$$

$$\hat{W}_{1,ns}^{(Q)}(x) = \frac{\alpha_s(\mu)C_F}{4\pi} \left[4+x - \frac{1+x^2}{1-x} \text{Log } x + (1+x) \left(\text{Log}(1-x) + \text{Log} \frac{m^2}{Q^2} \right) \right] + \mathcal{O}\left(\frac{m^2}{Q^2}\right). \quad (4.82)$$

The singular part $\hat{W}_{1,s}^{(Q)}$ can now be integrated to get

$$\int_{1-\delta}^1 dx W_{1,s}^{(Q)}(x) = \frac{\alpha_s(\mu)C_F}{4\pi} \left[-\left(\frac{1}{2} + \frac{\pi^3}{3} + \frac{1}{2}\text{Log} \frac{m^2}{Q^2} + \text{Log}^2 \frac{m^2}{Q^2}\right) + \text{Log } \delta \left(\frac{1}{2} + 2\text{Log} \frac{m^2}{Q^2}\right) - \text{Log}^2 \delta \right] + \mathcal{O}(\delta) + \mathcal{O}\left(\frac{m^2}{Q^2}\right) \quad (4.83)$$

$$\Rightarrow [\text{new-dist.}](x) = \frac{\alpha_s(\mu)C_F}{4\pi} \left[-\delta(1-x) \left(\frac{1}{2} + \frac{\pi^3}{3} + \frac{1}{2}\text{Log} \frac{m^2}{Q^2} + \text{Log}^2 \frac{m^2}{Q^2}\right) + \frac{1}{(1-x)_+} \left(\frac{1}{2} + 2\text{Log} \frac{m^2}{Q^2}\right) - 2 \left(\frac{\text{Log}(1-x)}{1-x}\right)_+ \right]. \quad (4.84)$$

The full expression for the correct massless limit of $\hat{W}_1^{(Q)}$ is then the sum of Eqs. (4.79), (4.82) and (4.84)

$$\begin{aligned} \hat{W}_1^{(Q)}(x) &\xrightarrow[m^2 \rightarrow 0]{m^2 \rightarrow 0} \hat{W}_{1,\text{dist.}}^{(Q)}(x) + \hat{W}_{1,ns}^{(Q)}(x) + [\text{new-dist.}](x) \\ &= \frac{\alpha_s(\mu)C_F}{4\pi} \left[-2 \left(\frac{\text{Log}(1-x)}{1-x}\right)_+ - \frac{1}{(1-x)_+} \left(\frac{7}{2} + 2\text{Log} \frac{m^2}{Q^2}\right) \right. \\ &\quad - \delta(1-x) \left(\frac{5}{2} + \frac{\pi^2}{3} + \frac{3}{2}\text{Log} \frac{m^2}{Q^2}\right) + 4+x \\ &\quad \left. - \frac{1+x^2}{1-x} \text{Log } x + (1+x) \left(\text{Log}(1-x) + \text{Log} \frac{m^2}{Q^2}\right) \right] + \mathcal{O}\left(\frac{m^2}{Q^2}\right). \end{aligned} \quad (4.85)$$

After subtracting $\frac{1}{2}$ times the SCET result for $f_{Q/Q}$ Eq. (4.49) we get

$$\begin{aligned} H_{1,V}^{(Q)}(x) &\xrightarrow[m^2 \rightarrow 0]{m^2 \rightarrow 0} \frac{\alpha_s(\mu)C_F}{4\pi} \left[-\frac{P_{qq}(x)}{C_F} \text{Log} \frac{\mu^2}{Q^2} + 2 \left(\frac{\text{Log}(1-x)}{1-x}\right)_+ - \frac{3}{2} \frac{1}{(1-x)_+} \right. \\ &\quad \left. - \delta(1-x) \left(\frac{\pi^2}{3} + \frac{9}{2}\right) - (1+x) \text{Log}(1-x) - \frac{1+x^2}{1-x} \text{Log } x + 3 \right], \end{aligned} \quad (4.86)$$

which is just the massless result from Eq. (3.96). So again we do not have any problems with large logs of $\frac{m^2}{Q^2}$ in the matching coefficient in the VFN scheme and find the correct massless limit.

⁹This means we set $\frac{m^2}{Q^2} = a(1-x)$ with a dummy variable a , expand for $x \rightarrow 1$ and keep only the singular terms and then substitute back with $a = \frac{m^2}{Q^2(1-x)}$.

5 Deep Inelastic Scattering in the Endpoint Region

In the previous sections it was shown how a VFN scheme can be used to resum logs of the form $\text{Log} \frac{m^2}{Q^2}$. Another possible source of large logarithms are the ones of the form $\text{Log}(1-x)$ that appear in the limit $x \rightarrow 1$ in the hard matching coefficients. The origin of these logarithms can be understood if we take a look at the scales involved in the problem: so far we have considered the hard scale $\sim Q^2$, the scale of the PDFs $\sim \Lambda_{\text{QCD}}^2$ and the mass m^2 . Another scale is the invariant mass of the hadronic final state $P_X^2 = \frac{Q^2(1-x)}{x}$. If x is not too close to 1 this is of the same order as the hard scale, but in the kinematic endpoint region where $x \rightarrow 1$ all outgoing hadrons are collimated in one jet with small invariant mass that introduces the jet scale $\sim Q^2(1-x) \ll Q^2$. The logarithms containing the ratio of the hard scale over the jet scale are just these logs of the form $\text{Log}(1-x)$ that can spoil the perturbative expansion for large x . To resum these logarithms the factorization theorem has to be modified by introducing a new jet function that describes the outgoing jet and has the natural scale $\mu_J^2 \sim Q^2(1-x)$. This factorization theorem assumes a large hierarchy between the hard, jet and PDF scale, i.e. $Q^2 \gg Q^2(1-x) \gg \Lambda_{\text{QCD}}^2$ and it is easiest, but not necessary, to assume $(1-x) \sim \frac{\Lambda_{\text{QCD}}}{Q}$. This choice also defines when x should be considered as “large”. So the factorization theorem will consist of a hard function \mathcal{H} describing the hard interaction at the hard scale $\mu_H^2 \sim Q^2$, a jet function $J_{\bar{n}}$ for the outgoing \bar{n} -coll. hadronic jet at $\mu_J^2 \sim Q^2(1-x)$ and the PDF f at the scale $\mu_f^2 \sim Q^2(1-x)^2 \sim \Lambda_{\text{QCD}}^2$, Fig 15. As will be shown in Sec. 5.1.1, in this setup the PDF contains not only n -coll. but also soft physics. Since the collinear sector

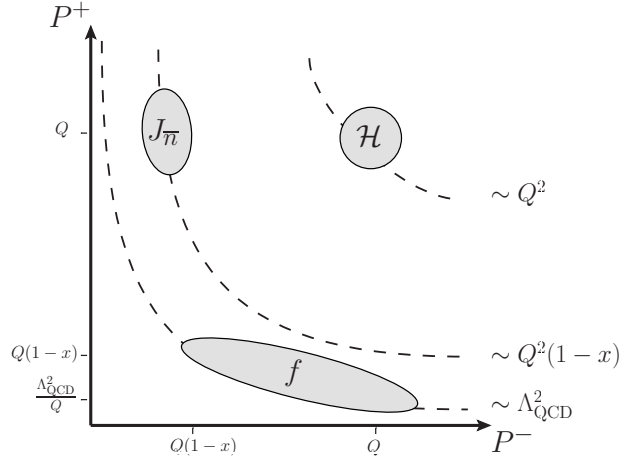


Figure 15: Scales of the PDF, hard and jet function for $x \rightarrow 1$. The hard and jet function are at the scales Q and $Q\sqrt{1-x}$ respectively. The natural scale for the PDF is again Λ_{QCD} , but the PDF is not purely n -coll. but also contains soft physics.

of the initial state is at the same invariant mass $\sim \Lambda_{\text{QCD}}$ as the soft one this is a typical SCET_{II} setup. In the derivation of the factorization theorem the two step matching procedure $\text{QCD} \rightarrow \text{SCET}_I \rightarrow \text{SCET}_{II}$, as briefly discussed in Sec. 2.1, will be applied.

5.1 Factorization Theorem

DIS in the endpoint region has been studied by using the SCET approach for massless quarks for example in Refs. [24–27]. We will rederive the factorization theorem for DIS for $x \rightarrow 1$ following the steps in Ref. [28] where it was derived for $e^+e^- \rightarrow 2$ Jets with the appropriate changes in the initial and final state to account for the differences between DIS and e^+e^- and the additional matching from SCET_{II} onto SCET_I, which will be just a renaming from usoft to soft fields. Here we will again consider only the contributions due to the massive quark to the total form factor.

We start from the definition of the hadronic tensor $W^{\mu\nu}$ as in Eq. (3.12)

$$W^{\mu\nu} = \frac{1}{4\pi} \sum_X \int d^4z e^{iqz} \langle P | J^{\mu\dagger}(z) | X \rangle \langle X | J^\nu(0) | P \rangle. \quad (5.1)$$

The electromagnetic current can be replaced by a current of SCET fields. We make the soft-collinear decoupling explicit by the field redefinitions shown in Sec. 2.4.2

$$J^\mu(x) \rightarrow C(\mu, Q) \bar{\chi}_{\bar{n}}(x) \gamma^\mu \chi_n(x), \quad (5.2)$$

$$\chi_n(x) \rightarrow Y_n(x) \chi_n^{(0)}(x), \quad (5.3)$$

$$\chi_{\bar{n}}(x) \rightarrow Y_{\bar{n}}(x) \chi_{\bar{n}}^{(0)}(x). \quad (5.4)$$

The hard Wilson coefficient $C(\mu, Q)$ can be determined from matching the SCET current onto QCD. If we write out the contractions over spin and color indices explicitly (letters i-l for spin and letters a-d for color), we get

$$\begin{aligned} W^{\mu\nu} &= \frac{|C(\mu, Q)|^2}{4\pi} \sum_X \int d^4z e^{iqz} \langle P | \bar{\chi}_n^{(0)}(z) Y_n^\dagger(z) \gamma^\mu Y_{\bar{n}}(z) \chi_{\bar{n}}^{(0)}(z) | X \rangle \langle X | \bar{\chi}_{\bar{n}}^{(0)}(0) Y_{\bar{n}}^\dagger(0) \gamma^\nu Y_n(0) \chi_n^{(0)}(0) | P \rangle \\ &= \frac{|C(\mu, Q)|^2}{4\pi} \sum_X \int d^4z e^{iqz} \langle P | \left(\bar{\chi}_n^{(0)}(z) Y_n^\dagger(z) \gamma^\mu \right)_i^a Y_{\bar{n}}^{ab}(z) \chi_{\bar{n},i}^{(0)b}(z) | X \rangle \\ &\quad \times \langle X | \bar{\chi}_{\bar{n},j}^{(0)c}(0) Y_{\bar{n}}^{\dagger cd}(0) \left(\gamma^\nu Y_n(0) \chi_n^{(0)}(0) \right)_j^d | P \rangle. \end{aligned} \quad (5.5)$$

The initial state contains only n -coll. particles, the final state only soft and \bar{n} -coll. particles. This can be seen if we split the final state momentum into light-cone components: $P_X^\mu = P^\mu + q^\mu = \frac{Q(1-x)}{x} \frac{n^\mu}{2} + Q \frac{\bar{n}^\mu}{2}$. In the endpoint region we have $(1-x) \sim \frac{\Lambda_{\text{QCD}}}{Q}$ and so the plus and minus components scale like $P_X^+ \sim Q$ and $P_X^- \sim \Lambda_{\text{QCD}}$, which allows for \bar{n} -coll. and soft but not for n -coll. modes. So the initial and final states can be factorized into these three sectors as

$$|X\rangle = |X_s\rangle |0_n\rangle |X_{\bar{n}}\rangle, \quad |P\rangle = |0_s\rangle |P_n\rangle |0_{\bar{n}}\rangle. \quad (5.6)$$

For our purposes it is not necessary to split the PDF in a collinear and a soft function, so we do not need distinguish between the n -coll. and soft states and define

$$|X_{n,s}\rangle := |X_s\rangle |0_n\rangle, \quad |P_{n,s}\rangle := |0_s\rangle |P_n\rangle. \quad (5.7)$$

$$\begin{aligned} W^{\mu\nu} &= \frac{|C(\mu, Q)|^2}{4\pi} \sum_X \int d^4z e^{iqz} \\ &\quad \times \langle P_{n,s} | \left(\bar{\chi}_n^{(0)}(z) Y_n^\dagger(z) \gamma^\mu \right)_i^a Y_{\bar{n}}^{ab}(z) | X_{n,s} \rangle \langle X_{n,s} | Y_{\bar{n}}^{\dagger cd}(0) \left(\gamma^\nu Y_n(0) \chi_n^{(0)}(0) \right)_j^d | P_{n,s} \rangle \\ &\quad \times \langle 0_{\bar{n}} | \chi_{\bar{n},k}^{(0)b}(z) | X_{\bar{n}} \rangle \langle X_{\bar{n}} | \bar{\chi}_{\bar{n},l}^{(0)c}(0) | 0_{\bar{n}} \rangle \delta_{ik} \delta_{jl}. \end{aligned} \quad (5.8)$$

Color conservation implies $\chi^b |X\rangle \langle X| \bar{\chi}^c = \frac{\delta_{bc}}{N_C} \chi^f |X\rangle \langle X| \bar{\chi}^f$ and applying the SCET version of the Fierz relation $\delta_{ik} \delta_{jl} = \frac{1}{2} \left(\frac{\not{n}}{2} \right)_{ij} \left(\frac{\not{n}}{2} \right)_{lk}$ yields

$$\begin{aligned} W^{\mu\nu} &= \frac{|C(\mu, Q)|^2}{8\pi} \int d^4z e^{iqz} \sum_{X_{n,s}} \text{Tr} \langle P_{n,s} | \bar{\chi}_n^{(0)}(z) Y_n^\dagger(z) \gamma^\mu \frac{\not{n}}{2} Y_{\bar{n}}(z) Y_{\bar{n}}^\dagger(0) \gamma^\nu Y_n(0) \chi_n^{(0)}(0) | P_{n,s} \rangle \\ &\quad \times \sum_{X_{\bar{n}}} \text{Tr} \langle 0_{\bar{n}} | \frac{\not{n}}{2N_C} \chi_{\bar{n}}^{(0)}(z) | X_{\bar{n}} \rangle \langle X_{\bar{n}} | \bar{\chi}_{\bar{n}}^{(0)}(0) | 0_{\bar{n}} \rangle, \end{aligned} \quad (5.9)$$

with the trace over color and spin. Here we have used the fact that the sum over all n -coll. and soft states gives a full set of states in the n -coll. and soft sector, i.e.

$$\sum_{X_{n,s}} |X_{n,s}\rangle \langle X_{n,s}| = \mathbf{1}_{n,s}. \quad (5.10)$$

To project the hadronic tensor onto W_1 we use the projector one can find from Eq. (3.29)

$$W_1 = \frac{1}{2-d} g_{\mu\nu}^\perp W^{\mu\nu}, \quad \frac{1}{2-d} g_{\mu\nu}^\perp \frac{\not{n}}{2} \gamma^\nu = \frac{\not{n}}{2}. \quad (5.11)$$

Acting with the longitudinal projector $P_L^{\mu\nu} \sim n^\mu n^\nu$ on $W^{\mu\nu}$ gives zero, so the longitudinal form factor W_L vanishes in the limit $x \rightarrow 1$. So we finally get

$$W_1 = \frac{|C(\mu, Q)|^2}{8\pi} \int d^4z e^{iqz} \text{Tr} \langle P_{n,s} | \bar{\chi}_n^{(0)}(z) Y_n^\dagger(z) Y_{\bar{n}}(z) \frac{\not{n}}{2} Y_{\bar{n}}^\dagger(0) Y_n(0) \chi_n^{(0)}(0) | P_{n,s} \rangle \\ \times \sum_{X_{\bar{n}}} \text{Tr} \langle 0_{\bar{n}} | \frac{\not{n}}{2N_C} \chi_{\bar{n}}^{(0)}(z) | X_{\bar{n}} \rangle \langle X_{\bar{n}} | \bar{\chi}_{\bar{n}}^{(0)}(0) | 0_{\bar{n}} \rangle, \quad (5.12)$$

$$W_L = 0. \quad (5.13)$$

With the jet function defined as in Ref. [28]

$$J_{\bar{n}}(Qr^- - m^2, m^2) = \frac{1}{2\pi Q N_C} \text{Im} \left[i \int d^4z e^{irz} \langle 0_{\bar{n}} | \text{Tr} \left[\frac{\not{n}}{2} T \{ \chi_{\bar{n}}^{(0)}(z) \bar{\chi}_{\bar{n}}^{(0)}(0) \} \right] | 0_{\bar{n}} \rangle \right], \quad (5.14)$$

with m the mass of the heavy quark, the \bar{n} -coll. matrix element can be expressed in terms of the jet function

$$\sum_{X_{\bar{n}}} \text{Tr} \langle 0_{\bar{n}} | \frac{\not{n}}{2N_C} \chi_{\bar{n}}^{(0)}(z) | X_{\bar{n}} \rangle \langle X_{\bar{n}} | \bar{\chi}_{\bar{n}}^{(0)}(0) | 0_{\bar{n}} \rangle = 2Q \delta(z^-) \delta^{(2)}(z_\perp) \int dr^- e^{-ir^- \frac{z^+}{2}} J_{\bar{n}}(Qr^- - m^2, m^2). \quad (5.15)$$

The remaining matrix element contains soft and collinear physics at the soft scale $Q(1-x)$ (see Fig. 15) and is therefore a SCET_{II} object. The matching from SCET_{II} onto SCET_I is trivial for DIS since every matrix element in SCET_I matches onto a corresponding matrix element in SCET_{II} with the replacement $Y_{\bar{n}} \rightarrow S_{\bar{n}}$, $Y_n \rightarrow S_n$ where S is a soft Wilson line containing soft gluons A_s^μ instead of usoft ones, i.e. no non-trivial matching coefficients have to be considered. So the only change in the matching is the renaming from usoft to soft Wilson lines and that the n -coll. operators are now defined with soft-bin subtractions instead of zero-bin subtractions. Soft-bin subtraction means that diagrams with a soft counting (instead of usoft for zero-bins) for the internal loop momenta are subtracted from the collinear diagrams to avoid double counting with the soft degrees of freedom. We write the n -coll./soft matrix element as

$$\langle P_{n,s} | \bar{\chi}_n^{(0)}(\frac{z^+}{2} \bar{n}) S_n^\dagger(\frac{z^+}{2} \bar{n}) S_{\bar{n}}(\frac{z^+}{2} \bar{n}) \frac{\not{n}}{2} S_{\bar{n}}^\dagger(0) S_n(0) \chi_n^{(0)}(0) | P_{n,s} \rangle = P^- \int d\xi e^{i\xi P^- \frac{z^+}{2}} f(\xi). \quad (5.16)$$

It will be shown in Sec. 5.1.1 that $f(\xi)$ corresponds to the PDF in the limit $x \rightarrow 1$. The hard function $\mathcal{H}(Q^2, \mu^2)$ is just the square of the current Wilson coefficient $|C(\mu, Q)|^2$. With these definitions the contribution from a massive quark to W_1 for a massless hadron has the form

$$W_1(x, Q^2, m^2) = \frac{1}{2} Q P^- \mathcal{H}(Q^2, \mu^2) \int d\xi J_{\bar{n}}(Q(q^- + \xi P^-) - m^2, m^2, \mu^2) f(\xi, \mu^2) \\ = \frac{Q^2}{2} \mathcal{H}(Q^2, \mu^2) \int \frac{d\xi}{\xi} \frac{\xi}{x} J_{\bar{n}}\left(Q^2\left(\frac{\xi}{x} - 1 - \frac{m^2}{Q^2}\right), m^2, \mu^2\right) f(\xi, \mu^2). \quad (5.17)$$

To get the convolution in a more convenient form one can define

$$\hat{g}(x) := g(1-x) \quad (5.18)$$

for any function with a hat. We can expand this for $x \rightarrow 1$. Because of kinematic restraints we also have $\frac{m^2}{Q^2} \leq \frac{1-x}{4x}$, so $\frac{m^2}{Q^2} \sim (1-x)$.¹⁰ After performing the expansion the factorized form of W_1 is

$$W_1(x, Q^2, m^2) = \frac{Q^2}{2} \mathcal{H}(Q^2, \mu^2) \int d\xi J_{\bar{n}}(Q^2((1-x) - \xi - \frac{m^2}{Q^2}), m^2, \mu^2) \hat{f}(\xi, \mu^2). \quad (5.19)$$

For a massless quark this reduces to

$$W_1(x, Q^2) = \frac{Q^2}{2} \mathcal{H}(Q^2, \mu^2) \int d\xi J_{\bar{n}}(Q^2((1-x) - \xi), \mu^2) \hat{f}(\xi, \mu^2), \quad (5.20)$$

where $J_{\bar{n}}(s, \mu^2)$ is the massless jet function. This agrees with Refs. [25, 27]. So in the case where the mass is above the jet scale the only difference between the massless and the massive case is a shift in the convolution and the change to the massive jet function.

¹⁰This is because at $\mathcal{O}(\alpha_s)$ there is only real radiation of massive quarks. At higher orders one would of course also have to consider virtual effects that are not restraint by kinematics so that different scenarios where the mass scale lies differently relative to the other scales could arise.

5.1.1 PDF / Soft Function

We have to check how the PDF in (3.47) looks like in terms of SCET fields in the case $\xi \rightarrow 1$. The Wilson line in the PDF is separated over a distance $t \sim \frac{1}{P^-(1-\xi)}$ and therefore only fluctuations over a length scale t , i.e. with momenta $\gtrsim \frac{1}{t} = (1-\xi)P^-$ can contribute in that Wilson line. In Sec 3.2, where we assumed ξ to be not too close to 1, only collinear gluon fields showed up but in the case $\xi \rightarrow 1$ also soft gluons contribute in that Wilson line. So when we change to SCET_I fields we have to write

$$\psi^{(i)}(x) \rightarrow \xi_n^{(i)}(x), \quad (5.21)$$

$$A^\mu(x) \rightarrow A_{us}^\mu(x) + A_n^\mu(x). \quad (5.22)$$

The Wilson line U^\dagger can be decomposed into two usoft and two collinear Wilson lines

$$U^\dagger(t\bar{n}, 0) \rightarrow W_n(t\bar{n})Y_{\bar{n}}(t\bar{n})Y_{\bar{n}}^\dagger(0)W_n^\dagger(0), \quad (5.23)$$

which leads to

$$f(\xi) = \frac{1}{2\pi} \int dt e^{-i\xi P^- t} \langle P_{n,s} | \bar{\chi}_n(t\bar{n})Y_{\bar{n}}(t\bar{n})\not{n}Y_{\bar{n}}^\dagger(0)\chi_n(0) | P_{n,s} \rangle. \quad (5.24)$$

After the soft-collinear decoupling in SCET_I and matching onto SCET_{II} the final SCET_{II} object that corresponds to the PDF in the endpoint region is

$$f(\xi) = \frac{1}{2\pi} \int dt e^{-i\xi P^- t} \langle P_{n,s} | \bar{\chi}_n^{(0)}(t\bar{n})S_n^\dagger(t\bar{n})S_{\bar{n}}(t\bar{n})\not{n}S_{\bar{n}}^\dagger(0)S_n(0)\chi_n^{(0)}(0) | P_{n,s} \rangle, \quad (5.25)$$

which results in the expression for the n -coll. matrix element we gave in Eq. (5.16). The PDF can also be split in a collinear part and a soft function by splitting the initial state into a n -coll. and a soft sector $|P_{n,s}\rangle = |P_n, 0_s\rangle$. When we pull out the labels from the jet fields ($W_n^\dagger \xi_n$) and use the fact of label conservation, i.e. $\delta(\omega - \mathcal{P}^+)\delta(\omega' - \mathcal{P}^-) = \delta(\omega' - \omega)\delta(\omega - \mathcal{P}^-)$, we get

$$f(\xi) = \frac{1}{2\pi} \int dt d\omega e^{-i(P^-\xi - \omega)t} \times \langle P_n, 0_s | (\bar{\xi}_{n,p} W_n S_n^\dagger S_{\bar{n}})(t\bar{n})\not{n} \left[\delta(\omega - \mathcal{P}^-) \left(S_{\bar{n}}^\dagger S_n W_n^\dagger \xi_{n,p'} \right)(0) \right] | P_n, 0_s \rangle. \quad (5.26)$$

To shift the residual fields from $t\bar{n}$ to 0 we can use the residual momentum operator K , since for any residual field $\phi_{n,p}(x)$ we have $\phi_{n,p}(x) = e^{iKx}\phi_{n,p}(0)e^{-iKx}$. The initial state is purely n -coll. and contains no residual momentum, so $\langle P_n, 0_s | e^{iK^- t} = \langle P_n, 0_s |$.

$$\begin{aligned} f(\xi) &= \frac{1}{2\pi} \int dt d\omega dk e^{-i(P^-\xi - \omega + k)t} \\ &\times \langle P_n, 0_s | (\bar{\xi}_{n,p} W_n S_n^\dagger S_{\bar{n}})(0)\not{n} \left[\delta(k - K^-)\delta(\omega - \mathcal{P}^-) \left(S_{\bar{n}}^\dagger S_n W_n^\dagger \xi_{n,p'} \right)(0) \right] | P_n, 0_s \rangle \\ &= \int dk \langle P_n, 0_s | (\bar{\xi}_{n,p} W_n S_n^\dagger S_{\bar{n}})(0)\not{n} \left[\delta(k - K^-)\delta(P^-\xi + k - \mathcal{P}^-) \left(S_{\bar{n}}^\dagger S_n W_n^\dagger \xi_{n,p'} \right)(0) \right] | P_n, 0_s \rangle. \end{aligned} \quad (5.27)$$

The residual momenta of the collinear fields scale like λ^2 while that in the soft Wilson lines are $\sim \lambda$, so we can neglect the action of the residual momentum operator on the collinear fields and split the whole matrix element in a collinear and a soft part

$$f(\xi) = \int dk S(k) \times \langle P_n | (\bar{\xi}_{n,p} W_n)(0)\not{n} \left[\delta(P^-\xi + k - \mathcal{P}^-) (W_n^\dagger \xi_{n,p'})(0) \right] | P_n \rangle, \quad (5.28)$$

where the soft function S is

$$S(k) = \langle 0_s | \left(S_{\bar{n}}^\dagger S_n \right)^\dagger(0) \left[\delta(k - K^-) \left(S_{\bar{n}}^\dagger S_n \right)(0) \right] | 0_s \rangle. \quad (5.29)$$

Now we have a look at the momenta that appear in the collinear matrix element. P^- and \mathcal{P} are both label momenta of order λ^0 while k is a soft momentum that scales as λ^1 . As a consistency check we first go back to the case where $1 - x \ll 1$. In this case we can drop k in the collinear part and get

$$\begin{aligned} f(\xi) &= \langle P_n | (\bar{\xi}_{n,p} W_n)(0)\not{n} \left[\delta(P^-\xi - \mathcal{P}^-) (W_n^\dagger \xi_{n,p'})(0) \right] | P_n \rangle \int dk S(k) \\ &= \langle P_n | (\bar{\xi}_{n,p} W_n)(0)\not{n} \left[\delta(P^-\xi - \mathcal{P}^-) (W_n^\dagger \xi_{n,p'})(0) \right] | P_n \rangle, \end{aligned} \quad (5.30)$$

which is indeed the form of the PDF we have already used in Sec. 3 and 4. But in the endpoint region this is not the correct expansion, because since $(P^-\xi - \mathcal{P}^-) \sim Q(1-x)$ this is no longer leading for $x \rightarrow 1$ where $(1-x) \sim \lambda$. In this case we can reorganize the terms in the delta distribution into labels and suppressed residual momenta and use the fact that these are separately conserved in SCET

$$\delta(P^-\xi + k - \mathcal{P}^-) = \delta(\underbrace{P^- - \mathcal{P}^-}_{\text{label}} + \underbrace{k - P^-(1-\xi)}_{\text{residual}}) \rightarrow \delta_{P^-, \mathcal{P}^-} \delta(k - P^-(1-\xi)). \quad (5.31)$$

Then the full PDF is split into a collinear PDF f_n and the soft function S

$$f(\xi) = f_n S(P^-(1-\xi)), \quad (5.32)$$

where the collinear PDF is just the local collinear matrix element

$$f_n = \langle P_n | (\bar{\xi}_{n,p} W_n)(0) \frac{\not{P}}{2} [\delta_{P^-, \mathcal{P}^-} (W_n^\dagger \xi_{n,p'})(0)] | P_n \rangle. \quad (5.33)$$

This form of splitting the PDF into a soft function and a collinear part agrees with reference Ref. [27], another form is given Ref. [26]. The factorization theorem then consists of four different functions: a hard, jet and soft function and the collinear PDF, Fig. 16.

$$W_1(x, m^2, Q^2) = \frac{Q}{2} \mathcal{H}(Q^2, \mu^2) f_n(\mu^2) \int dl J_{\bar{n}} \left(Q^2 \left((1-x) - \frac{l}{Q} - \frac{m^2}{Q^2} \right), m^2, \mu^2 \right) S(l, \mu^2). \quad (5.34)$$

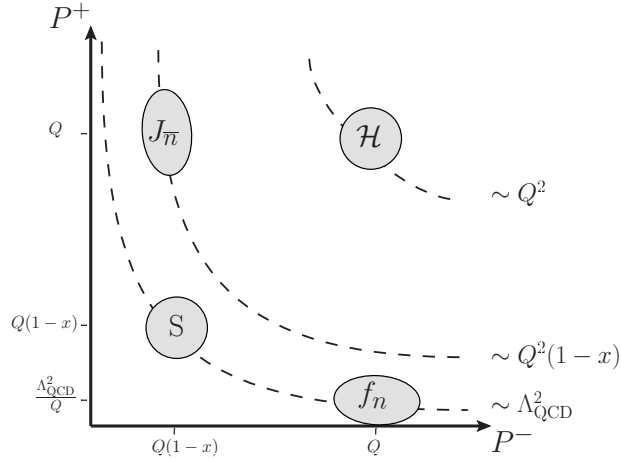


Figure 16: Scales of the collinear PDF, hard, jet and soft function. Here the PDF is split into a collinear part f_n and a soft function S , both at the scale Λ_{QCD} . f_n is purely n -coll. while S contains all the soft contributions.

The advantage of the form of the PDF in Eq. (5.32) over the one in Eq. (5.25) is that the separation of collinear and soft modes that are at the same scale allows for the resummation of rapidity logarithms that appear in the matching conditions for the PDFs as logs of $(1-x)$, see for example Ref. [27].

One import thing to notice about the PDFs in the limit $x \rightarrow 1$ is that all off-diagonal elements of the matrix of splitting functions P_{ij} are suppressed and only the flavor diagonal part P_{ii} is leading in the power counting for $x \rightarrow 1$. This can be understood from the SCET setup: we consider a particle with label P^- in the initial state that splits into a particle with longitudinal momentum fraction ξ that goes into the hard interaction and a second particle, Fig. 17. $x \rightarrow 1$ implies that the parton that enters the hard interaction was carrying almost all of the initial state's momentum, i.e. $\xi \rightarrow 1$. This implies that the second particle in the splitting with the light-cone component $(1-\xi)P^-$ has to be soft. In the SCET Lagrangian there is an interaction term between collinear quarks and usoft gluons at leading order in the power counting, allowing for the splitting in Fig. 17a, but interactions with soft quarks are suppressed and so we do not see the splitting of a collinear gluon in a collinear and a soft quark, Fig. 17b, at leading order in λ . This can be checked explicitly by expanding the splitting functions for $x \rightarrow 1$ and keeping only the leading singular terms. So there is no more mixing between the PDFs and every PDF evolves

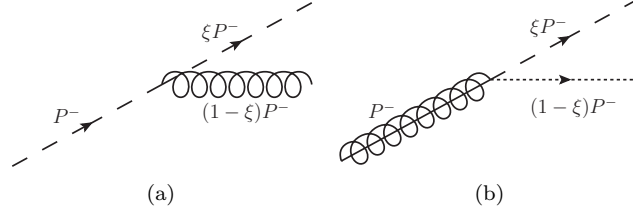


Figure 17: Splitting of a collinear particle into a collinear and a soft particle. The process on the right side is suppressed relatively to the process on the left side.

according to its own RGE with the corresponding anomalous dimension

$$\frac{d}{d\text{Log } \mu^2} \hat{f}(1-x, \mu^2) = (\gamma_f \hat{\otimes} \hat{f})(1-x, \mu^2). \quad (5.35)$$

Here the convolution with a hat $\hat{\otimes}$ is defined as

$$(g \hat{\otimes} h)(x, \mu^2) := \int d\xi g(x-\xi, \mu^2) h(\xi, \mu^2). \quad (5.36)$$

To see that the convolution \otimes of the form in Eq. (3.46) simplifies to the linear convolution $\hat{\otimes}$ in Eq. (5.36) in the limit $x \rightarrow 1$ we switch to the hatted functions $\hat{g}(x) := g(1-x)$ and substitute the integration variable $\xi \rightarrow 1-\hat{\xi}$:

$$\begin{aligned} (g \otimes h)(x) &= \int_x^1 \frac{d\xi}{\xi} g\left(\frac{x}{\xi}\right) h(\xi) \\ &= \int_x^1 \frac{d\xi}{\xi} \hat{g}\left(1-\frac{x}{\xi}\right) \hat{h}(1-\xi) \\ &= \int_0^{1-x} \frac{d\hat{\xi}}{1-\hat{\xi}} \hat{g}\left(\frac{(1-x)-\hat{\xi}}{1-\hat{\xi}}\right) \hat{h}(\hat{\xi}) \end{aligned} \quad (5.37)$$

When we expand for $x \rightarrow 1$ the integration limits tell us we can simultaneously expand for $\hat{\xi} \rightarrow 0$ which yields

$$(g \otimes h)(x) \sim \int_0^{1-x} d\hat{\xi} \hat{g}\left((1-x)-\hat{\xi}\right) \hat{h}(\hat{\xi}) = (\hat{g} \hat{\otimes} \hat{h})(1-x) \quad (5.38)$$

The anomalous dimension of the quark PDF $\gamma_f(x)$ is just the quark-quark splitting function $P_{qq}(1-x)$ in the limit $x \rightarrow 1$

$$\gamma_f(x, \mu^2) = \frac{\alpha_s(\mu) C_F}{4\pi} \left[4 \left(\frac{1}{x} \right)_+ + 3 \delta(x) \right]. \quad (5.39)$$

This also implies that if a PDF is zero at one scale, it remains zero at any scale. Since all matching coefficients A_{ij} between different partons are also subleading for $x \rightarrow 1$ (for the same reasons as the splitting functions), no heavy quark PDF is generated perturbatively in the matching or the evolution at leading order in the power counting.

5.1.2 Jet Function

As was argued in the previous section the heavy quark PDF is suppressed in the power counting, so no perturbatively generated heavy quark will enter the hard interaction and all contributions from heavy flavors are due to secondary effects. Nevertheless we will consider the jet function for a primary massive quark as was done in Ref. [29], which can be thought of as an intrinsic, non-perturbative constituent of the hadron.

To calculate the jet function $J_{\bar{n}}$ defined in Eq. (5.14) we define the function \mathcal{J}

$$\mathcal{J}(Qp^- - m^2, m^2) = \int d^4 z e^{ip^- z} \langle 0 | \text{Tr} \left[\frac{\not{n}}{2} T \{ \chi_{\bar{n}}^{(0)}(z) \bar{\chi}_{\bar{n}}^{(0)}(0) \} \right] | 0 \rangle, \quad (5.40)$$

so that the relation between $J_{\bar{n}}$ and \mathcal{J} is

$$J_{\bar{n}}(s, m^2) = \frac{1}{2\pi Q N_C} \text{Im} [i\mathcal{J}(s, m^2)], \quad (5.41)$$

The tree level contribution to \mathcal{J} is

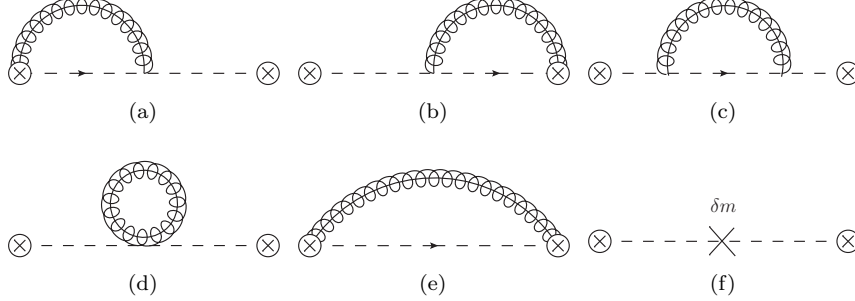


Figure 18: Diagrams for the jet function at $\mathcal{O}(\alpha_s)$

$$\begin{aligned} \mathcal{J}^{(\text{tree})}(Qp^- - m^2, m^2) &= \text{Tr} \left[\frac{\not{p}}{2} F_{\bar{n}}(p, m) \right] \\ &= i \frac{p^+}{p^2 - m^2 + i0} \text{Tr} \left[\frac{\not{p}}{2} \frac{\not{p}}{2} \right] \\ &= 2iN_C \frac{Q}{s}, \end{aligned} \quad (5.42)$$

with $p^+ = Q$ and $s := p^2 - m^2 + i0$. The relevant diagrams for \mathcal{J} at order α_s are shown in Fig. 18.

Diagram Fig. 18a:

$$\begin{aligned} \mathcal{J}^{(a)} &= \int \frac{d^d k}{(2\pi)^d} \frac{g\tilde{\mu}^\epsilon T^A n^\mu}{k^+ - p^+ + i0} \text{Tr} \left[\frac{\not{p}}{2} F_{\bar{n}}(p, m) V_{\bar{n}, \mu}^A(k, p, m) F_{\bar{n}}(k, m) \right] \frac{-i}{q^2 + i0} \\ &= -8\pi\alpha_s C_F \tilde{\mu}^{2\epsilon} \frac{p^+}{p^2 - m^2 + i0} \text{Tr} \left[\frac{\not{p}}{2} \frac{\not{p}}{2} \frac{\not{p}}{2} \frac{\not{p}}{2} \right] \int \frac{d^d k}{(2\pi)^d} \frac{k^+}{(k^2 - m^2 + i0)((k-p)^2 + i0)(k^+ - p^+ + i0)}. \end{aligned} \quad (5.43)$$

The trace over color and spin reduces to $\text{Tr} \left[\frac{\not{p}}{2} \frac{\not{p}}{2} \frac{\not{p}}{2} \frac{\not{p}}{2} \right] = 2N_C$ and after changing to light-cone variables the k^- integral can be solved by contour integration

$$\begin{aligned} &= -\frac{N_C \alpha_s C_F}{2\pi^2 \Gamma(1-\epsilon)} (\mu^2 e^{\gamma_E})^\epsilon \frac{p^+}{p^2 - m^2 + i0} \int dk^+ d|k_\perp^2| \frac{\Theta(|k_\perp^2|) k^+ |k_\perp^2|^{-\epsilon}}{k^+ - p^+ + i0} \\ &\quad \times \underbrace{\int dk^- \frac{1}{(k^+ k^- - |k_\perp^2| - m^2 + i0)((k^- - p^-)(^+ - p^+) - |k_\perp^2| + i0)}}_{= \frac{2\pi i \Theta(k^+) \Theta(p^+ - k^+)}{p^- k^+ (k^+ - p^+) + |k_\perp^2| p^+ - m^2 (k^+ - p^+)}}. \end{aligned} \quad (5.44)$$

Here the $i0$ is absorbed into p^- , i.e. $p^- \rightarrow p^- + i0$. The $|k_\perp^2|$ integral is

$$\int_0^\infty d|k_\perp^2| \frac{|k_\perp^2|^{-\epsilon}}{p^+ |k_\perp^2| + (k^+ - p^+)(p^- k^+ - m^2)} = (p^+)^{-1+\epsilon} \Gamma(\epsilon) \Gamma(1-\epsilon) (p^+ - k^+)^{-\epsilon} (m^2 - p^- k^+)^{-\epsilon}. \quad (5.45)$$

With the substitutions $p^+ = Q$, $z = \frac{k^+}{p^+}$ and $s = p^2 - m^2 + i0$ the remaining integral has the form

$$\begin{aligned} &\frac{iN_C \alpha_s C_F}{\pi} \frac{Q}{s} \Gamma(\epsilon) \left(\frac{\mu^2 e^{\gamma_E}}{-s} \right)^\epsilon \underbrace{\int_0^1 dz (1-z) z^{-1-\epsilon} \left(1 - \frac{s+m^2}{s} z \right)^{-\epsilon}}_{= \frac{\Gamma(-\epsilon)}{\Gamma(2-\epsilon)} {}_2F_1\left(\epsilon, -\epsilon, 2-\epsilon, \frac{s+m^2}{s}\right)}. \end{aligned} \quad (5.46)$$

${}_2F_1$ is the Gauss hypergeometric function. To expand the hypergeometric function the Mathematica package HypExp [30] was used, the full result expanded in ϵ is

$$\begin{aligned} \mathcal{J}^{(a)}(s) = -iN_C \frac{\alpha_s C_F}{\pi} \frac{Q}{s} & \left(\frac{1}{\epsilon^2} + \frac{1 + \text{Log} \frac{\mu^2}{-s}}{\epsilon} + 2 + \frac{\pi^2}{4} + \text{Log} \frac{m^2}{-s} \left(\text{Log} \frac{s+m^2}{-s} - \frac{1}{2} \text{Log} \frac{m^2}{-s} - \frac{m^2}{s+m^2} \right) \right. \\ & \left. + \frac{1}{2} \text{Log}^2 \frac{\mu^2}{-s} + \text{Log} \frac{\mu^2}{-s} - \text{Li}_2 \left(\frac{-s}{m^2} \right) \right). \end{aligned} \quad (5.47)$$

The diagram in Fig. 18b is the same as the one in Fig. 18a but with a different sign on the $i0$ in the Wilson line. Since this never enters the contour integration for the k^- integral the result is the same as in Eq. (5.47).

Diagram Fig. 18c:

$$\begin{aligned} \mathcal{J}^{(c)} &= \int \frac{d^d k}{(2\pi)^d} \frac{-i}{(p-k)^2 + i0} \text{Tr} \left[\frac{\not{k}}{2} F_{\bar{n}}(p, m) V_{\bar{n}}^{\mu A}(k, p, m) F_{\bar{n}}(k, m) V_{\bar{n}, \mu}^A(p, k, m) F_{\bar{n}}(p, m) \right] \\ &= \frac{-16\pi\alpha_s(\mu)C_F N_C \tilde{\mu}^{2\epsilon} Q^2}{s^2} \int \frac{d^d k}{(2\pi)^d} \frac{1}{((p-k)^2 + i0)(k^2 - m^2 + i0)} \\ &\quad \times \left[-\frac{2m^2(2-\epsilon)}{Q} + \frac{(1-\epsilon)}{k^+} \left(|k_{\perp}^2| + m^2 \left(1 - \frac{(k^+)^2}{Q^2} \right) \right) \right]. \end{aligned} \quad (5.48)$$

The term in brackets can be written in a more convenient form with the relation

$$|k_{\perp}^2| = \frac{2k^+}{Q} (p \cdot k) - k^2 - \frac{(k^+)^2}{Q^2} p^2 \quad (5.49)$$

and then reads

$$\frac{(1-\epsilon)}{Q} \left[-\frac{2m^2(2-\epsilon)}{1-\epsilon} + \left(2p_{\mu} - \frac{s}{Q} n_{\mu} \right) k^{\mu} - \frac{Q}{k^+} (k^2 - m^2) \right]. \quad (5.50)$$

With this the full diagram reduces to three different integrals

$$\mathcal{J}^{(c)} = \frac{-16\pi\alpha_s(\mu)C_F N_C Q(1-\epsilon)}{s^2} \left[-\frac{2m^2(2-\epsilon)}{(1-\epsilon)} I_1 + \left(2p_{\mu} - \frac{s}{Q} n_{\mu} \right) I_2^{\mu} - Q I_3 \right], \quad (5.51)$$

$$I_1 = \tilde{\mu}^{2\epsilon} \int \frac{d^d k}{(2\pi)^d} \frac{1}{((p-k)^2 + i0)(k^2 - m^2 + i0)}, \quad (5.52)$$

$$I_2^{\mu} = \tilde{\mu}^{2\epsilon} \int \frac{d^d k}{(2\pi)^d} \frac{k^{\mu}}{((p-k)^2 + i0)(k^2 - m^2 + i0)}, \quad (5.53)$$

$$I_3 = \tilde{\mu}^{2\epsilon} \int \frac{d^d k}{(2\pi)^d} \frac{1}{((p-k)^2 + i0)k^+}. \quad (5.54)$$

It is not necessary to calculate I_3 since this term will be canceled by the tadpole diagram Fig. 18d. I_1 and I_2^{μ} can be solved by using standard methods

$$\begin{aligned} I_1 &= \frac{i}{(4\pi)^2} \left(\frac{\mu^2 e^{\gamma_E}}{-s} \right)^{\epsilon} \Gamma(\epsilon) \frac{{}_2F_1 \left(1-\epsilon, \epsilon, 2-\epsilon, \frac{s+m^2}{s} \right)}{1-\epsilon} \\ &= \frac{i}{(4\pi)^2} \left[\frac{1}{\epsilon} + \text{Log} \frac{\mu^2}{-s} - \frac{m^2}{s+m^2} \text{Log} \frac{m^2}{-s} + 2 \right] + \mathcal{O}(\epsilon), \end{aligned} \quad (5.55)$$

$$\begin{aligned} I_2^{\mu} &= p^{\mu} \frac{i}{(4\pi)^2} \left(\frac{\mu^2 e^{\gamma_E}}{-s} \right)^{\epsilon} \Gamma(\epsilon) \left(\Gamma(1-\epsilon) {}_2F_1 \left(1-\epsilon, \epsilon, 2-\epsilon, \frac{s+m^2}{s} \right) - \frac{{}_2F_1 \left(2-\epsilon, \epsilon, 3-\epsilon, \frac{s+m^2}{s} \right)}{2-\epsilon} \right) \\ &= p^{\mu} \frac{i}{2(4\pi)^2} \left[\frac{1}{\epsilon} + \text{Log} \frac{\mu^2}{-s} - \frac{m^4}{(s+m^2)^2} \text{Log} \frac{m^2}{-s} + \frac{2s+3m^2}{s+m^2} \right] + \mathcal{O}(\epsilon). \end{aligned} \quad (5.56)$$

The final result for diagram Fig. 18c is

$$\begin{aligned} \mathcal{J}^{(c)} = & \frac{i\alpha_s(\mu)C_F N_C}{2\pi} \frac{Q}{s^2} \left[(6m^2 - s) \left(\frac{1}{\epsilon} + \text{Log} \frac{\mu^2}{-s} \right) + \frac{m^4}{s + m^2} \left(\frac{m^2}{s + m^2} - 7 \right) \text{Log} \frac{m^2}{-s} \right. \\ & \left. - \frac{m^4}{s + m^2} + 9m^2 - s \right] \\ & + \frac{16\pi\alpha_s(\mu)C_F N_C Q^2(1 - \epsilon)}{s^2} \times I_3. \end{aligned} \quad (5.57)$$

Diagram Fig. 18d:

The tadpole diagram is

$$\begin{aligned} \mathcal{J}^{(d)} = & \frac{1}{2} \int \frac{d^d k}{(2\pi)^d} \text{Tr} \left[\frac{\not{k}}{2} F_{\bar{n}}(p, m) V_{\bar{n}, \mu}^{\mu, AA}(p, p, k) F_{\bar{n}}(p, m) \right] \frac{-i}{k^2 + i0} \\ = & -\frac{8\pi\alpha_s(\mu)C_F N_C(1 - \epsilon)\tilde{\mu}^2 Q^2}{s^2} \int \frac{d^d k}{(2\pi)^d} \frac{1}{(k^2 + i0)} \left(\frac{1}{p^+ - k^+} + \frac{1}{p^+ + k^+} \right) \\ = & -\frac{16\pi\alpha_s(\mu)C_F N_C(1 - \epsilon)\tilde{\mu}^2 Q^2}{s^2} \int \frac{d^d k}{(2\pi)^d} \frac{1}{((p - k)^2 + i0)k^+} \\ = & -\frac{16\pi\alpha_s(\mu)C_F N_C Q^2(1 - \epsilon)}{s^2} \times I_3. \end{aligned} \quad (5.58)$$

This exactly cancels the corresponding term in the result for the self energy diagram Eq. (5.57).

Because $n \cdot n = 0$ diagram Fig. 18e is zero.

Diagram Fig. 18f:

The diagram with the mass counter term is

$$\begin{aligned} \mathcal{J}^{(f)} = & \text{Tr} \left[\frac{\not{k}}{2} F_{\bar{n}}(p, m) (-i \frac{\not{k}}{2} \frac{2m}{p^+} m \delta Z_m) F_{\bar{n}}(p, m) \right] \\ = & 4im^2 N_C \frac{Q}{s^2} \delta Z_m, \end{aligned} \quad (5.59)$$

where δZ_m is the mass counter term in the chosen renormalization scheme. Here we always use the $\overline{\text{MS}}$ scheme, $\delta Z_m^{\overline{\text{MS}}}$ is given in Eq. (4.16).

Final Result:

The final result for \mathcal{J} is the sum of all diagrams

$$\begin{aligned} \mathcal{J} = & \mathcal{J}^{(\text{tree})} + 2\mathcal{J}^{(a)} + \mathcal{J}^{(c)} + \mathcal{J}^{(d)} + \mathcal{J}^{(f)} \\ = & -i2\pi N_C Q \left\{ \frac{1}{\pi} \left[-\frac{1}{s} - \frac{2m^2 \delta m}{s^2} - \frac{\alpha_s(\mu)C_F}{4\pi} \frac{1}{s} \left(\frac{4}{\epsilon^2} + \frac{1}{\epsilon} \left(3 + 4 \text{Log} \frac{\mu^2}{-s} \right) + 2 \text{Log}^2 \frac{\mu^2}{-s} \right. \right. \right. \\ & + 3 \text{Log} \frac{\mu^2}{-s} + \text{Log} \frac{m^2}{-s} \left(-2 \text{Log} \frac{m^2}{-s} + 4 \text{Log} \frac{m^2 + s}{-s} + \frac{m^2(m^2 + 2s)}{(s + m^2)^2} \right) \\ & \left. \left. \left. - 4 \text{Li}_2 \frac{-s}{m^2} - \frac{s}{m^2 + s} + 8 + \pi^2 \right) \right] \right\}. \end{aligned} \quad (5.60)$$

Here δm is the difference between the on-shell mass counter term δZ_m^{OS} to whatever other mass renormalization scheme one might choose, i.e. $\delta m = \delta Z_m - \delta Z_m^{\text{OS}}$. When using the $\overline{\text{MS}}$ scheme we have

$$\delta_m^{\overline{\text{MS}}} = \frac{\alpha_s(\mu)C_F}{4\pi} \left(3 \text{Log} \frac{\mu^2}{m^2} + 4 \right) + \mathcal{O}(\alpha_s^2). \quad (5.61)$$

The bare one loop jet function $J_{\bar{n}}^0(s)$ is the imaginary part of the expression in curly brackets. The relations to take the imaginary part and rewrite the plus distributions are given in appendix A and B.

The result is

$$\begin{aligned}
J_n^0(s, m^2) = & \delta(s) - 2m^2 \delta m \delta'(s) + \frac{\alpha_s(\mu) C_F}{4\pi} \Theta(s) \left[\frac{8}{\mu^2} \left(\frac{\mu^2 \text{Log} \frac{s}{\mu^2}}{s} \right)_+ - \frac{4}{\mu^2} \left(\frac{\mu^2}{s} \right)_+ \left(\frac{1}{\epsilon} - \text{Log} \frac{\mu^2}{m^2} + 1 \right) \right. \\
& + \delta(s) \left(\frac{4}{\epsilon^2} + \frac{3}{\epsilon} + 2 \text{Log}^2 \frac{\mu^2}{m^2} - \text{Log} \frac{\mu^2}{m^2} + 8 - \frac{\pi^2}{3} \right) \\
& \left. + \frac{s}{(s+m^2)^2} - \frac{4}{s} \text{Log} \left(1 + \frac{s}{m^2} \right) \right]. \tag{5.62}
\end{aligned}$$

This agrees with Ref. [29]. To renormalize the jet function the divergences are absorbed into a counter term

$$J_n^0(s) = (Z_J \hat{\otimes} J_n)(s, \mu^2), \tag{5.63}$$

Since we only consider the contribution to heavy flavor production the jet scale is always above the mass scale so the heavy flavor is contributing to the RG evolution of the jet function. We use $\overline{\text{MS}}$ renormalization and absorb the the divergences into a counter term Z_J

$$Z_J(s, \mu^2) = \delta(s) + \frac{\alpha_s(\mu) C_F}{4\pi} \left[-\frac{4}{\epsilon} \frac{1}{\mu^2} \left(\frac{\mu^2}{s} \right)_+ + \delta(s) \left(\frac{4}{\epsilon^2} + \frac{3}{\epsilon} \right) \right]. \tag{5.64}$$

The anomalous dimension is

$$\begin{aligned}
\gamma_J(s, \mu^2) = & - \left(Z_J^{-1} \hat{\otimes} \frac{dZ_J}{d\text{Log} \mu^2} \right)(s, \mu^2) \\
= & \frac{\alpha_s(\mu) C_F}{4\pi} \left[-\frac{4}{\mu^2} \left(\frac{\mu^2}{s} \right)_+ + 3\delta(s) \right].
\end{aligned}$$

5.1.3 Hard Function

The hard function $\mathcal{H}(Q^2, \mu^2) = |C(\mu, Q)|^2$ is obtained from matching the QCD electromagnetic current $J^\mu = \bar{q}\gamma^\mu q$ onto the SCET current $C(\mu, Q)\bar{\chi}_n\gamma^\mu\chi_n$. Another way to get the hard function is to compare the hard coefficient $H_{1,V}^{(Q)}$, calculated in Sec. 4.3, and the jet function J_n in the limit $x \rightarrow 1$. At fixed order, i.e. without resummation of logs in the evolution of the jet function, the factorization theorem for $x \rightarrow 1$ and the factorization in the generic case have to agree in the limit $x \rightarrow 1$, i.e.

$$\begin{aligned}
W_1(x) = & \int \frac{d\xi}{\xi} H_{1,V}^{(Q)}(\xi, \mu^2) f_{Q/P} \left(\frac{\chi(x)}{\xi}, \mu^2 \right) \\
\stackrel{x \rightarrow 1}{=} & \int d\xi H_{1,V}^{(Q)}(\xi, \mu^2) f_{Q/P} \left(\frac{x(1 + \frac{m^2}{Q^2})}{\xi}, \mu^2 \right) \\
= & \int d\xi \hat{H}_{1,V}^{(Q)}(\xi, \mu^2) \hat{f}((1-x) - \frac{m^2}{Q^2} - \xi, \mu^2) \\
\stackrel{!}{=} & \frac{Q^2}{2} \mathcal{H}(Q^2, \mu^2) \int d\xi J_n(Q^2 \xi, \mu^2) \hat{f}((1-x) - \frac{m^2}{Q^2} - \xi, \mu^2). \tag{5.65}
\end{aligned}$$

The steps to get from the “DIS convolution” to the linear convolution are the same as displayed in Eq. (5.37). Note that in the third line we made the substitution $\xi \rightarrow 1 - \xi$, so here we have to consider the limit $\xi \rightarrow 0$ from now on. Here the hard and jet function and the hard coefficient $H_1^{(Q)}$ are all evaluated at the same scale. So the hard function can be determined from the relation

$$\hat{H}_{1,V}^{(Q)}(\xi, \mu^2) = \frac{Q^2}{2} \mathcal{H}(Q^2, \mu^2) J(Q^2 \xi, \mu^2) + \mathcal{O}(\lambda^0) \tag{5.66}$$

with the scaling $\xi \sim \frac{m^2}{Q^2} \sim (1-x) \sim \lambda$ in $\hat{H}_{1,V}^{(Q)}$ and $J_{\bar{n}}$. The leading order in λ is

$$\begin{aligned} \hat{H}_{1,V}^{(Q)}(\xi, \mu^2) = & \frac{1}{2}\delta(\xi) + \frac{\alpha_s(\mu)C_F}{4\pi} \left[\delta(\xi) \left(-4 - \frac{3}{2} \text{Log} \frac{\mu^2}{Q^2} + \text{Log}^2 \frac{m^2}{Q^2} + \frac{1}{2} \text{Log} \frac{m^2}{Q^2} \right) \right. \\ & - 2 \left(\frac{1}{\xi} \right)_+ \left(1 + \text{Log} \frac{\mu^2}{Q^2} + \text{Log} \frac{m^2}{Q^2} \right) + 4 \left(\frac{\text{Log} \xi}{\xi} \right)_+ \\ & \left. + \frac{\frac{\xi}{\xi + \frac{m^2}{Q^2}} - 4 \text{Log} \left(1 + \frac{Q^2 \xi}{m^2} \right)}{2\xi} \right] + \mathcal{O}(\lambda^0), \end{aligned} \quad (5.67)$$

$$\begin{aligned} \frac{Q^2}{2} J_{\bar{n}}(Q^2 \xi, \mu^2) = & \frac{1}{2}\delta(\xi) \\ & + \frac{\alpha_s(\mu)C_F}{4\pi} \left[\delta(\xi) \left(4 - \frac{\pi^2}{6} + \text{Log}^2 \frac{\mu^2}{Q^2} + \frac{3}{2} \text{Log} \frac{\mu^2}{Q^2} + \text{Log}^2 \frac{m^2}{Q^2} + \frac{1}{2} \text{Log} \frac{m^2}{Q^2} \right) \right. \\ & - 2 \left(\frac{1}{\xi} \right)_+ \left(1 + \text{Log} \frac{\mu^2}{Q^2} + \text{Log} \frac{m^2}{Q^2} \right) + 4 \left(\frac{\text{Log} \xi}{\xi} \right)_+ \\ & \left. + \frac{\frac{\xi}{\xi + \frac{m^2}{Q^2}} - 4 \text{Log} \left(1 + \frac{Q^2 \xi}{m^2} \right)}{2\xi} \right]. \end{aligned} \quad (5.68)$$

The only difference is in the term $\sim \frac{\alpha_s C_F}{4\pi} \delta(\xi)$ and so the hard function has to be

$$\mathcal{H}(Q^2, \mu^2) = 1 + \frac{\alpha_s(\mu)C_F}{4\pi} \left(-16 + \frac{\pi^2}{3} - 2 \text{Log}^2 \frac{\mu^2}{Q^2} - 6 \text{Log} \frac{\mu^2}{Q^2} \right). \quad (5.69)$$

This result agrees with Ref. [24], where the current matching for DIS was done explicitly and because of crossing symmetry with Ref. [29], where it was done for $e^+e^- \rightarrow \text{hadrons}$, with the replacement $Q^2 \rightarrow -Q^2$. The anomalous dimension can be derived from Eq. (5.69)

$$\gamma_H(Q^2, \mu^2) = \frac{\alpha_s(\mu)C_F}{4\pi} \left[-4 \text{Log} \frac{\mu^2}{Q^2} - 6 \right]. \quad (5.70)$$

5.2 Evolution Kernels

In the previous sections the anomalous dimensions for the hard and jet function and the PDF were derived. In this section it will be shown how the evolution kernels can be obtained from those. The anomalous dimensions of the jet function and PDF are of the form

$$\gamma(y, \mu^2) = \Gamma[\alpha_s] \frac{1}{\mu^d} \left(\frac{\mu^d}{y} \right)_+ + \gamma[\alpha_s] \delta(y), \quad (5.71)$$

where d is the dimension of the variable y , so we have $d = 2$ for the jet function and $d = 0$ for the PDFs. The cusp and non-cusp anomalous dimensions are series in α_s

$$\Gamma[\alpha_s] = \frac{\alpha_s(\mu)}{4\pi} \sum_{n=0} \left(\frac{\alpha_s(\mu)}{4\pi} \right)^n \Gamma^{(n)}, \quad \gamma[\alpha_s] = \frac{\alpha_s(\mu)}{4\pi} \sum_{n=0} \left(\frac{\alpha_s(\mu)}{4\pi} \right)^n \gamma^{(n)}. \quad (5.72)$$

We want to find the evolution kernel $U(y, \mu_1, \mu_0)$ for an arbitrary function g that fulfills the RGE

$$\frac{d g(y, \mu^2)}{d \text{Log} \mu^2} = (\gamma(\mu^2) \hat{\otimes} g(\mu^2))(y), \quad (5.73)$$

i.e. the function that evolves g from a scale μ_0 to the scale μ_1

$$g(y, \mu_1) = (U(\mu_1, \mu_0) \hat{\otimes} g(\mu_0^2))(y). \quad (5.74)$$

First we change to Fourier space, which disentangles the convolutions

$$\frac{d \tilde{g}(z, \mu^2)}{d \text{Log} \mu^2} = \tilde{\gamma}(z, \mu^2) \tilde{g}(z, \mu^2). \quad (5.75)$$

The Fourier transform of the plus distribution is given in appendix A. The anomalous dimension in Fourier space reads

$$\tilde{\gamma}(z, \mu^2) = -\Gamma[\alpha_s] \text{Log}(ize^{\gamma_E} \mu_0^d) - \frac{d}{2} \Gamma[\alpha_s] \text{Log} \frac{\mu^2}{\mu_0} + \gamma[\alpha_s]. \quad (5.76)$$

The evolution kernel can be obtained from the equation

$$\begin{aligned} \tilde{U}(z, \mu_1, \mu_0) &= \exp \left[\int_{\text{Log} \mu_0^2}^{\text{Log} \mu_1^2} d\text{Log} \mu^2 \tilde{\gamma}(z, \mu) \right] \\ &= (ize^{\gamma_E} \mu_0^d)^{\omega(\mu_1, \mu_0)} e^{K(\mu_1, \mu_0)}, \end{aligned} \quad (5.77)$$

with the functions ω and K defined as

$$\omega(\mu_1, \mu_0) = - \int_{\text{Log} \mu_0^2}^{\text{Log} \mu_1^2} d\text{Log} \mu^2 \Gamma[\alpha_s], \quad (5.78)$$

$$K(\mu_1, \mu_0) = \int_{\text{Log} \mu_0^2}^{\text{Log} \mu_1^2} d\text{Log} \mu^2 \left(-\frac{d}{2} \Gamma[\alpha_s] \text{Log} \frac{\mu^2}{\mu_0^2} + \gamma[\alpha_s] \right). \quad (5.79)$$

Performing the inverse Fourier transform yields

$$U(y, \mu_1, \mu_0) = \frac{e^{K(\mu_1, \mu_0)} (e^{\gamma_E})^{\omega(\mu_1, \mu_0)}}{\Gamma(-\omega(\mu_1, \mu_0))} \frac{1}{\mu_0^d} \left(\frac{\mu_0^{d(1+\omega(\mu_1, \mu_0))}}{y^{1+\omega(\mu_1, \mu_0)}} \right)_+. \quad (5.80)$$

To solve the integrals one can use the RGE for the coupling

$$\frac{d\alpha_s(\mu)}{d\text{Log} \mu^2} = \beta[\alpha_s] \quad \beta[\alpha_s] = -\frac{\alpha_s(\mu)^2}{4\pi} \sum_{n=0} \left(\frac{\alpha_s(\mu)}{4\pi} \right)^n \beta^{(n)} \quad (5.81)$$

to change the integration variable from $\text{Log} \mu^2$ to α_s

$$\int_{\text{Log} \mu_0^2}^{\text{Log} \mu_1^2} d\text{Log} \mu^2 \rightarrow \int_{\alpha_s(\mu_0)}^{\alpha_s(\mu_1)} d\alpha_s \frac{1}{\beta[\alpha_s]}. \quad (5.82)$$

With this substitution the integrals in ω and K take the form

$$\omega(\mu_1, \mu_0) = - \int_{\alpha_s(\mu_0)}^{\alpha_s(\mu_1)} d\alpha_s \frac{\Gamma[\alpha_s]}{\beta[\alpha_s]} \quad (5.83)$$

$$K(\mu_1, \mu_0) = \int_{\alpha_s(\mu_0)}^{\alpha_s(\mu_1)} d\alpha_s \frac{1}{\beta[\alpha_s]} \left(-\frac{d}{2} \Gamma[\alpha_s] \int_{\alpha_s(\mu_0)}^{\alpha_s} d\alpha'_s \frac{1}{\beta[\alpha'_s]} + \gamma[\alpha_s] \right). \quad (5.84)$$

The integrands can be expanded in α_s , the leading order gives the factors for leading log (LL) resummation:

$$\begin{aligned} \omega^{LL}(\mu_1, \mu_0) &= \frac{\Gamma^{(0)}}{\beta^{(0)}} \int_{\alpha_s(\mu_0)}^{\alpha_s(\mu_1)} d\alpha_s \frac{1}{\alpha_s} \\ &= \frac{\Gamma^{(0)}}{\beta^{(0)}} \text{Log} r(\mu_1, \mu_0), \end{aligned} \quad (5.85)$$

$$\begin{aligned} K^{LL}(\mu_1, \mu_0) &= -\frac{2d\pi\Gamma^{(0)}}{(\beta^{(0)})^2} \int_{\alpha_s(\mu_0)}^{\alpha_s(\mu_1)} d\alpha_s \frac{1}{\alpha_s} \int_{\alpha_s(\mu_0)}^{\alpha_s} d\alpha'_s \frac{1}{\alpha_s'^2} \\ &= \frac{2d\pi\Gamma^{(0)}}{(\beta^{(0)})^2 \alpha_s(\mu_1)} (-1 + r(\mu_1, \mu_0) - r(\mu_1, \mu_0) \text{Log} r(\mu_1, \mu_0)), \end{aligned} \quad (5.86)$$

where $r(\mu_1, \mu_0)$ is the ratio

$$r(\mu_1, \mu_0) = \frac{\alpha_s(\mu_1)}{\alpha_s(\mu_0)}. \quad (5.87)$$

The expanded form of ω and K up to N³LL can be found for example in the appendix of Ref. [31].¹¹ Since the hard function is local it is not necessary to go to Fourier space. Its anomalous dimension has the form

$$\gamma_H(Q^2, \mu^2) = \Gamma_H[\alpha_s] \text{Log} \frac{\mu^2}{Q^2} + \gamma_H[\alpha_s] \quad (5.88)$$

and calculations analogous to the ones above yield

$$U_H(Q, \mu_1, \mu_0) = e^{K_H(\mu_1, \mu_0)} \left(\frac{\mu_0^2}{Q^2} \right)^{\omega_H(\mu_1, \mu_0)}, \quad (5.89)$$

with

$$\omega_H(\mu_1, \mu_0) = \int_{\text{Log} \mu_0^2}^{\text{Log} \mu_1^2} d\text{Log} \mu^2 \Gamma_H[\alpha_s], \quad (5.90)$$

$$K_H(\mu_1, \mu_0) = \int_{\text{Log} \mu_0^2}^{\text{Log} \mu_1^2} d\text{Log} \mu^2 \left(\Gamma_H[\alpha_s] \text{Log} \frac{\mu^2}{\mu_0^2} + \gamma_H[\alpha_s] \right). \quad (5.91)$$

The solutions for ω_H and K_H can therefore be obtained from the solutions for ω and K in Eqs (5.85) and (5.86) with the replacement $\Gamma[\alpha_s] \rightarrow -\Gamma_H[\alpha_s]$ in ω and $\Gamma[\alpha_s] \rightarrow -\frac{2}{d}\Gamma_H[\alpha_s]$, $\gamma[\alpha_s] \rightarrow \gamma_H[\alpha_s]$ in K . The leading order coefficients for the cusp and non-cusp anomalous dimensions for the hard function, jet function and PDF, as calculated in the last sections, are summarized in Tab. 1.

	$\frac{\Gamma^{(0)}}{C_F}$	$\frac{\gamma^{(0)}}{C_F}$
hard	-4	-6
jet	-4	3
PDF	4	3

Table 1: Leading order anomalous dimensions for the hard function, jet function and PDF.

5.3 Consistency Relations

Because the physical form factor W_1 does not depend on the choice of the scale μ , the running of the hard and jet function and the PDF are not independent of each other and a consistency relation between the anomalous dimensions can be derived.

$$\begin{aligned} 0 &= \frac{d}{d\text{Log} \mu^2} W_1(x, Q^2) \\ &= \frac{Q^2}{2} \left(\gamma_H(Q^2, \mu^2) \mathcal{H}(Q^2, \mu^2) \int d\xi J(Q^2(x - \xi), \mu^2) \hat{f}(\xi, \mu^2) \right. \\ &\quad + \mathcal{H}(Q^2, \mu^2) \int d\xi d\xi' Q^2 \gamma_J(Q^2(x - \xi - \xi'), \mu^2) J(Q^2 \xi', \mu^2) \hat{f}(\xi, \mu^2) \\ &\quad \left. + \mathcal{H}(Q^2, \mu^2) \int d\xi d\xi' J(Q^2(x - \xi), \mu^2) \gamma_f(\xi - \xi'', \mu^2) \hat{f}(\xi'', \mu^2) \right) \\ &\Rightarrow \gamma_H(Q^2, \mu^2) \delta(x) + Q^2 \gamma_J(Q^2 x, \mu^2) + \gamma_f(x, \mu^2) = 0 \end{aligned} \quad (5.92)$$

With the anomalous dimensions derived in the previous sections

$$\gamma_f(x, \mu^2) = \frac{\alpha_s(\mu) C_F}{2\pi} \left[\frac{3}{2} \delta(x) + 2 \left(\frac{1}{x} \right)_+ \right], \quad (5.93)$$

$$\gamma_J(s, \mu^2) = \frac{\alpha_s(\mu) C_F}{2\pi} \frac{1}{\mu^2} \left[\frac{3}{2} \delta \left(\frac{s}{\mu^2} \right) - 2 \left(\frac{\mu^2}{s} \right)_+ \right], \quad (5.94)$$

$$\gamma_H(Q^2, \mu^2) = \frac{\alpha_s(\mu) C_F}{2\pi} \left[-3 - 2 \text{Log} \frac{\mu^2}{Q^2} \right], \quad (5.95)$$

¹¹Note that there are factors of 2 compared to our results due to different conventions in the definition of ω and K and the series expansion of the beta function.

it is easy to check that this consistency relation is indeed fulfilled at $\mathcal{O}(\alpha_s)$.

The consistency relation between the hard and jet function and the PDF can also be expressed in terms of the evolution kernels. The result must be the same whether all functions are evolved to the hard scale μ_H or all are evolved down to the scale of the PDFs μ_f , see Fig. 19.

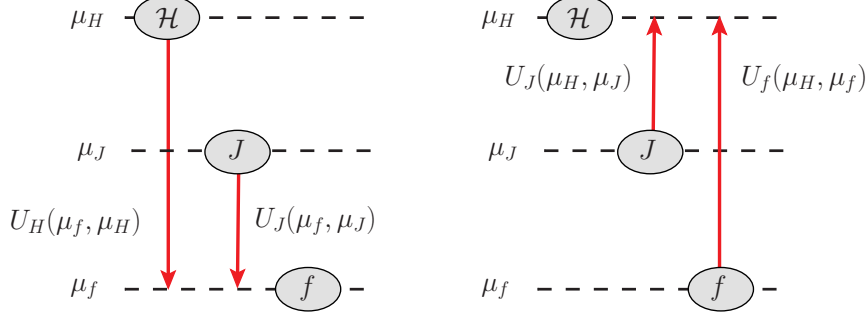


Figure 19: Consistency relation for the evolution kernels. The physical form factor can not depend on the choice of μ . It must be the same whether all functions are run from their natural scales to the soft scale μ_f (left) or all are run up to the hard scale μ_H (right).

$$\begin{aligned}
 W_1(x, Q^2) &= \frac{Q^2}{2} U_H(Q, \mu_f, \mu_H) \mathcal{H}(Q^2, \mu_H^2) \int d\xi d\xi' Q^2 U_J(Q^2(x - \xi - \xi'), \mu_f, \mu_J) J(Q^2\xi, \mu_J^2) \hat{f}(\xi', \mu_f^2) \\
 &= \frac{Q^2}{2} \mathcal{H}(Q^2, \mu_H^2) \int d\xi d\xi' d\xi'' Q^2 U_J(Q^2(x - \xi - \xi''), \mu_H, \mu_J) J(Q^2\xi, \mu_J^2) U_f(\xi' - \xi'', \mu_H, \mu_f) \hat{f}(\xi'', \mu_f^2)
 \end{aligned} \tag{5.96}$$

Obviously the first and the second line are the same if

$$U_H(Q, \mu_f, \mu_H) U_J(Q^2(x - \xi - \xi''), \mu_f, \mu_J) = \int d\xi' U_J(Q^2(x - \xi - \xi'), \mu_H, \mu_J) U_f(\xi' - \xi''). \tag{5.97}$$

Acting on both sides with $\int dx U_J(Q^2(y - x), \mu_J, \mu_H)$ and using that

$$\int d\xi U(y - \xi, \mu_0, \mu_1) U(\xi - x, \mu_1, \mu_2) = U(y - x, \mu_0, \mu_2) \quad U(x, \mu, \mu) = \delta(x) \tag{5.98}$$

results in the consistency relation for the evolution kernels in the form

$$U_f(x, \mu, \mu_0) = Q^2 U_H(Q, \mu_0, \mu) U_J(Q^2 x, \mu_0, \mu). \tag{5.99}$$

To check this explicitly we go back to Fourier space where the consistency relation reads

$$\tilde{U}_f(z, \mu, \mu_0) = U_H(Q, \mu_0, \mu) \tilde{U}_J\left(\frac{z}{Q^2}, \mu_0, \mu\right). \tag{5.100}$$

With $r := \frac{\alpha_s(\mu)}{\alpha_s(\mu_0)}$ and

$$\omega := \frac{4C_F}{\beta_0} \text{Log } r, \quad K := \frac{16\pi C_F}{\beta_0^2 \alpha_s(\mu)} (r - 1 - \text{Log } r) \tag{5.101}$$

Eqs. (5.77) and (5.89) give

$$\text{Log}\left(\tilde{U}_f(z, \mu, \mu_0)\right) = \omega \text{Log}\left(ize^{\gamma_E}\right), \tag{5.102}$$

$$\text{Log}\left(\tilde{U}_J\left(\frac{z}{Q^2}, \mu_0, \mu\right)\right) = \omega \text{Log}\left(ize^{\gamma_E} \frac{\mu^2}{Q^2}\right) + K, \tag{5.103}$$

$$\text{Log}\left(U_H(Q, \mu_0, \mu)\right) = -\omega \text{Log}\frac{\mu^2}{Q^2} - K, \tag{5.104}$$

so that one can easily see that the evolution kernels indeed fulfill the consistency relation.

6 Numerical Analysis

For the numerical analysis we follow the massless analysis in Ref. [25]. First we define a K -factor as

$$K^{(i)}(x, Q^2, m^2) = \frac{2F_1^{(i)}(x, Q^2, m^2)}{Q_i^2 f_i(x, Q^2)}, \quad (6.1)$$

where $F_1^{(i)}$ is just the contribution of a quark with flavor i to the total form factor F_1 and a dummy PDF f_i that has the form

$$f_i(x, Q^2) = (1 - x)^4 \quad (6.2)$$

for large x . The aim of this analysis is to study the effects of resummation for large x and to compare the results for the massless and massive short-distance coefficients. The K -factor in Eq. (6.1) is the ratio of the full result to the (massless) tree level result $F_1^{(i), \text{tree}}(x, Q^2) = Q_i^2 f_i(x, Q^2)$ and therefore shows the effects of higher order terms that are included in the resummed results. The dummy PDF in Eq. (6.2) is used as the PDF of a massive quark (for this analysis we do not care whether it is intrinsic or generated perturbatively). This PDF is used in the convolution with both the massless and the massive hard matching coefficients and jet functions to discuss the mass effects that arise solely from the perturbative calculations. The theoretical errors for the resummed results will be estimated by scale variation to check whether the effects of the mass in the short-distance coefficients can be neglected or not.

For the fixed order plots we used the results in Eq. (3.110) and Eq. (4.65) for the massless and massive case respectively. The log resummation in the large x limit was performed at NLL and NNLL. Here we used the factorization theorem as in Eq. (5.19) where only singular terms are included in the jet and the hard function. Whenever we speak about resummed results we refer to that, i.e. in contrast to the FO results there are no non-singular terms included. To which order the anomalous dimensions and matrix elements are needed for the different resummation schemes is shown in Tab. 2.

	NLL	NNLL
$\Gamma_{H,J}$	2-loop	3-loop
$\gamma_{H,J}$	1-loop	2-loop
matrix elements	tree level	1-loop

Table 2: NLL and NNLL resummation

The matrix elements up to 1-loop are given in Eq. (5.69) and Eq. (5.62), the 1-loop anomalous dimensions are shown in Tab. 1. The 2- and 3-loop results for the anomalous dimensions for the hard and jet function are summarized in the appendix of Ref. [25]¹². The matrix elements were expanded together to $\mathcal{O}(\alpha_s)$, i.e. the cross terms of order $\mathcal{O}(\alpha_s^2)$ were not included.

The running of α_s and the $\overline{\text{MS}}$ -masses was always performed at 4-loop level. We used the values $\alpha_s(m_Z) = 0.118$ with $m_Z = 91.187$ GeV for the coupling and $\overline{m}_b(\overline{m}_b) = 4.18$ GeV and $\overline{m}_c(\overline{m}_c) = 1.275$ GeV for the masses of the bottom and the charm quark respectively. For the hard and the jet scale we used $\mu_H = Q$ and $\mu_J = Q\sqrt{1-x}$. In the analysis at 30 GeV the charm quark was considered to be massless and the heavy flavor was a bottom quark with mass m_b , for the analysis at 5 GeV we used the charm quark as the heavy flavor and the bottom quark was decoupled at 5 GeV so that a 4-flavor running could be used over the whole range of the jet scale. The plotting range was chosen such that $\mu_J > 1$ GeV in the massless case and $\mu_J > m$ in the case with a heavy flavor with mass m . The hard and the jet function were run to the factorization scale Q^2 where the PDF is given as in Eq. (6.2).

¹²In Ref. [25] different conventions were used. To relate to our coefficients $\Gamma_{H,J}$ and $\gamma_{H,J}$ use:

$$\begin{aligned} \Gamma_H^{(n)} &= -\Gamma_n \\ \Gamma_J^{(n)} &= -\Gamma_n \\ \gamma_H^{(n)} &= \gamma_n^V \\ \gamma_J^{(n)} &= -\gamma_n^J \end{aligned}$$

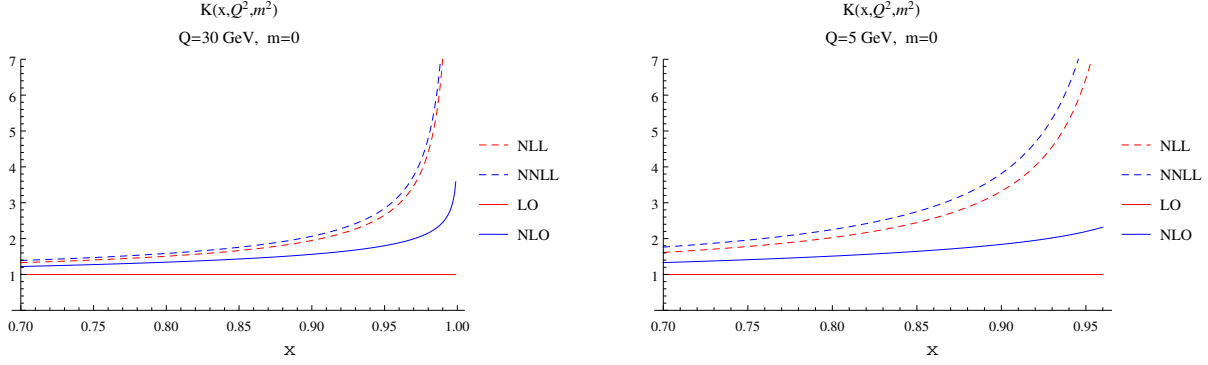


Figure 20: Comparison of fixed order and resummed results in the massless case at LO, NLO, NLL and NNLL for $Q=30$ GeV and $Q=5$ GeV.

Let us first analyse the effects of resummation in the massless case. In Fig. 20 the K-factor defined as in Eq. (6.1) is plotted for a massless quark. The FO results (LO, NLO) are plotted as solid lines, the results with log resummation (NLL, NNLL) as dashed lines. The LO result for the K-factor is just 1 because the LO result for the form factor is nothing but the PDF $f(x)$ itself. The difference between NLO and LO becomes large for $x \rightarrow 1$ which indicates that higher order terms become more and more important in that region. We see that the resummed results are much more stable for large x , i.e. there is only a very small shift from NLL to NNLL that is much smaller than the difference between LO and NLO. This indicates that the FO results are missing numerically important terms in the expansion whereas these contributions from large logs at higher orders in α_s are included in the NLL and NNLL results.

These results can be compared with the plots in Ref. [25] where the same analysis for massless quarks has been made¹³. We find small deviations from their plots which can be due to slightly different numerical values and different implementation of the factorization theorem¹⁴, but these deviations are much smaller than our theoretical uncertainties (see Fig. 24).

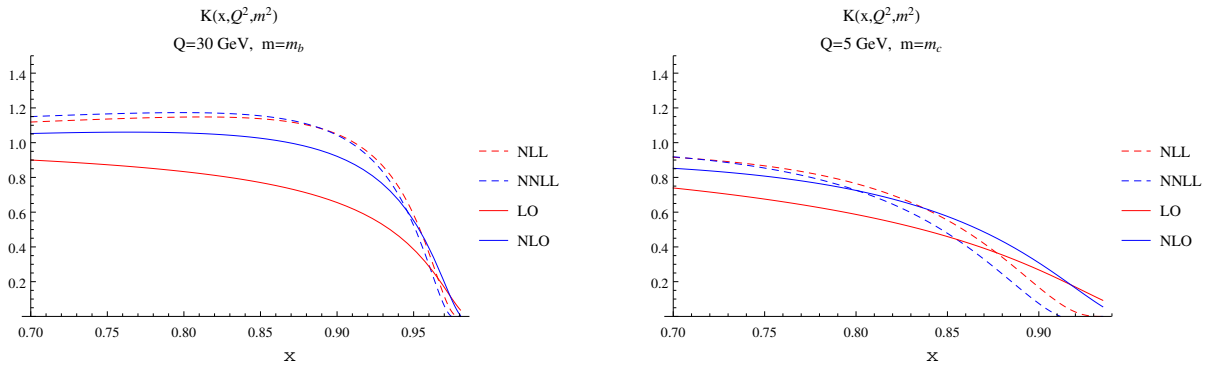


Figure 21: Comparison of fixed order and resummed results at LO, NLO, NLL and NNLL for different values of Q and m .

In Fig. 21 the results for massive short-distance coefficients are shown. Comparing this with the massless plots in Fig. 20 it becomes clear that the mass effects are mainly due to the shift in the convolution $f(x) \rightarrow f(x + \frac{m^2}{Q^2})$ (or, equivalently, the rescaling $f(x) \rightarrow f(\chi(x))$ in the FO calculation). This can be seen from the fact that already the LO and NLL results, where no matrix elements are included, show a similar behavior as the higher order plots. Even though the argument of the PDF is shifted only by

¹³Note that we defined the K-factor with the form factor F_1 while in Ref. [25] it was defined with F_2 . Since the longitudinal form factor is $F_L = 0$ in the limit $x \rightarrow 1$ this does not matter for the singular results, but it changes the K-factor for the FO results.

¹⁴One source of differences is a different choice for the jet scale and the argument in the convolution between jet function and PDF as $Q\sqrt{\frac{1-x}{x}}$ in contrast to the fully expanded form $Q\sqrt{1-x}$ that we are using in this work, other sources *might* be for example different values and running of α_s or cross terms of order α_s^2 in the product of the one-loop matrix elements that we have not included (both issues are not specified in their work).

$(\frac{m_c}{5 \text{ GeV}})^2 \sim 0.065$ and $(\frac{m_b}{30 \text{ GeV}})^2 \sim 0.02$ this small shift leads to a huge deviation in the region $(1-x) \ll 1$ because here the PDF falls off rapidly (as $\sim (1-x)^4$ in the case of our dummy PDF). Again the results with resummation are much more stable when we go to a higher order compared to the FO results, but here also the change from LO to NLO is not as large for $x \rightarrow 1$ as it was in the massless case, so the impact of resummation is smaller than for the massless case.

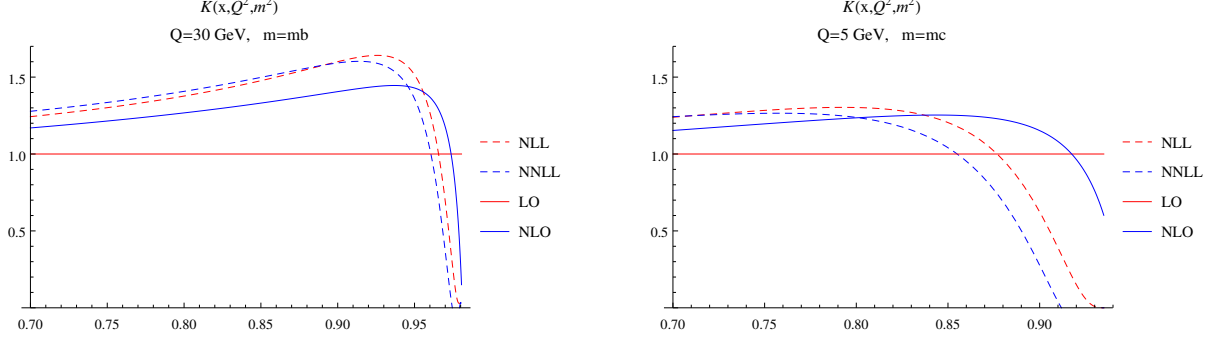


Figure 22: Comparison of fixed order and resummed results at LO, NLO, NLL and NNLL for different values of Q and m with rescaled K-factor $\tilde{K}(x, Q^2, m^2)$

In Fig. 22 the K-factor with a tilde was defined with a different normalization where the argument of the PDF is the rescaled variable $\chi(x) = \frac{x(1+\sqrt{1+4\frac{m^2}{Q^2}})}{2}$ as

$$\tilde{K}^{(i)}(x, Q^2, m^2) = \frac{2F_1^{(i)}(x, Q^2, m^2)}{Q_i^2 f_i(\chi(x), Q^2)}, \quad (6.3)$$

i.e. normalized to the massive FO tree level result for the form factor $\frac{Q_i^2}{2} f_i(\chi(x), Q^2)$. Here the effects of the shift/rescaling in the PDF are not as strong as before because they are already considered in the normalization, but still we get large deviations from the FO tree level result for large x . Again we see that higher order terms are important for large x and that resummation clearly improves the convergence when going to higher orders.

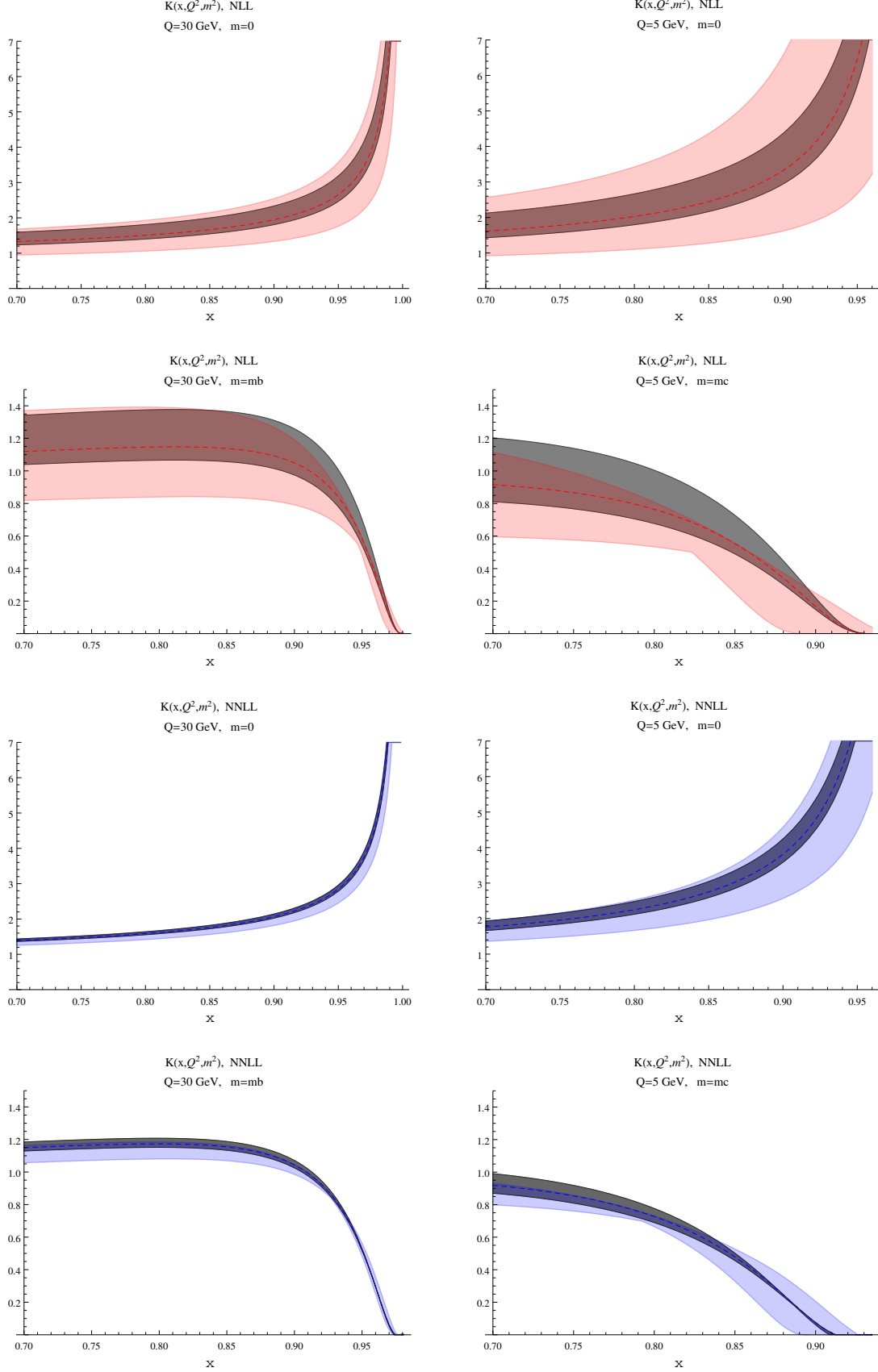


Figure 23: Comparison of the uncertainties estimated by variation of the jet scale (colored band) and hard scale (gray band) for different values of Q and m at NLL (red) and NNLL (blue). The bands are obtained by varying the jet scale between $\frac{1}{2}Q\sqrt{1-x} < \mu_J < 2Q\sqrt{1-x}$ and the hard scale between $\frac{1}{2}Q < \mu_H < 2Q$.

The theoretical uncertainties were estimated by varying the hard and the jet scale by a factor 2 about their canonical values $\mu_H = Q$ and $\mu_J = Q\sqrt{1-x}$. All variations for NLL and NNLL are shown separately in Fig. 23. The scale dependence is larger for $Q=5$ GeV because all scales are much lower and therefore the coupling α_s is larger. In the massless case the scale dependence introduced by the hard scale is much smaller than the one from the jet scale, but especially in the massive case it can not be neglected and so we used $\Delta_{\text{tot}} = \sqrt{\Delta_{\text{hard}}^2 + \Delta_{\text{jet}}^2}$ as an estimate for the total uncertainty, Fig. 24. The bands are much broader than one would expect from the very small shift from the NLL to the NNLL result that we already saw in Fig. 20 and Fig. 21, i.e. the scale variation for NNLL is larger by factor of 2-3 than the difference between the NLL and NNLL results for the canonical values of the scales (dashed lines), but the scale variation by a factor 2 yields a more conservative estimate for the theoretical uncertainty.

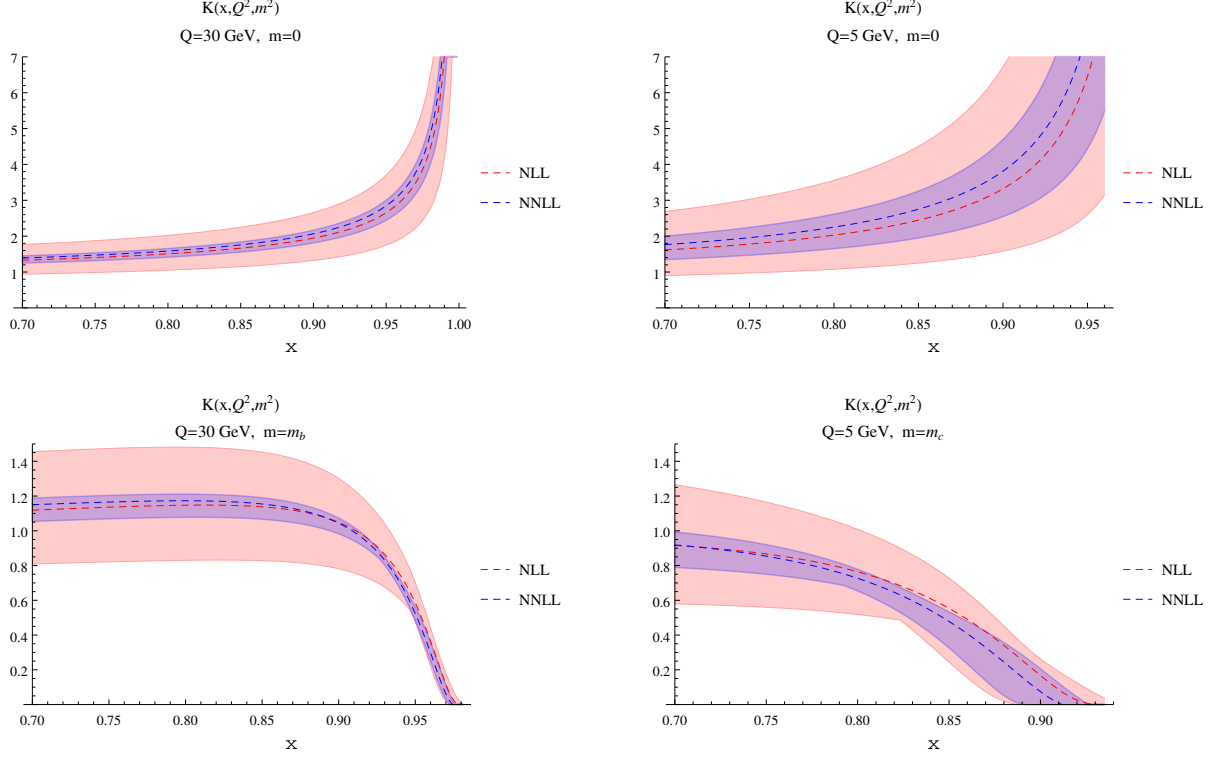


Figure 24: Convergence from NLL to NNLL for different values of Q and m . The bands are obtained by combining the uncertainties estimated from jet and hard scale variation in quadrature.

NNLL resummation reduces the scale dependence compared to NLL resummation by a factor 2-5 and we have good convergence from NLL to NNLL. The small deviations from the results in Ref. [25] that were mentioned above are also all clearly within these error bands.

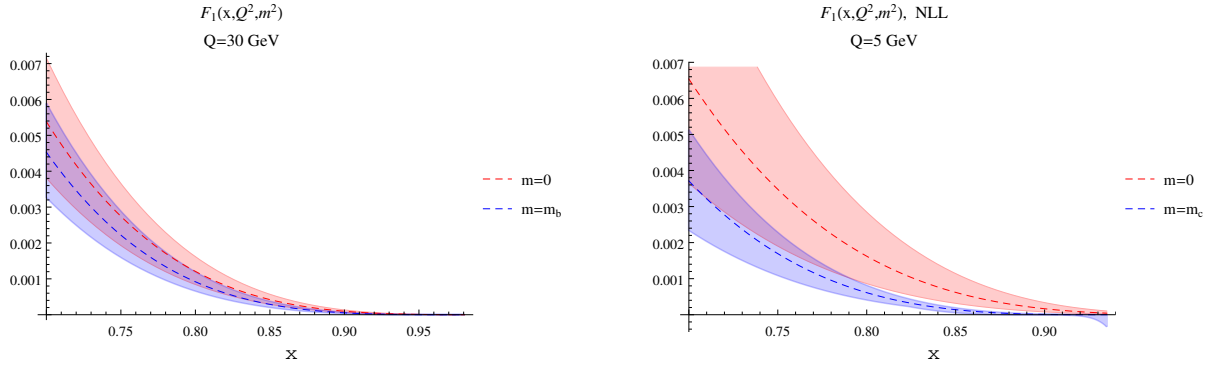


Figure 25: The massless and massive form factors $K(x, Q^2, m^2)f(x, Q^2)$ at NLL.

Besides considering the K-factor it is also interesting to display the effects for the physically measured form factor F_1 . Fig. 25 shows the the form factor F_1 for a quark with unit charge, i.e. $F_1(x) = K(x, Q^2, m^2)f(x, Q^2)$, with NLL resummation for $Q=5$ GeV and $Q=30$ GeV with massless (red) and massive (blue) quarks. We see that NLL resummation does not seem to be accurate enough to resolve the effects of a massive flavor compared to the massless calculations, especially for $Q=30$ GeV and the bottom quark as the heavy flavor the overlap between the massless and massive results is quite large.

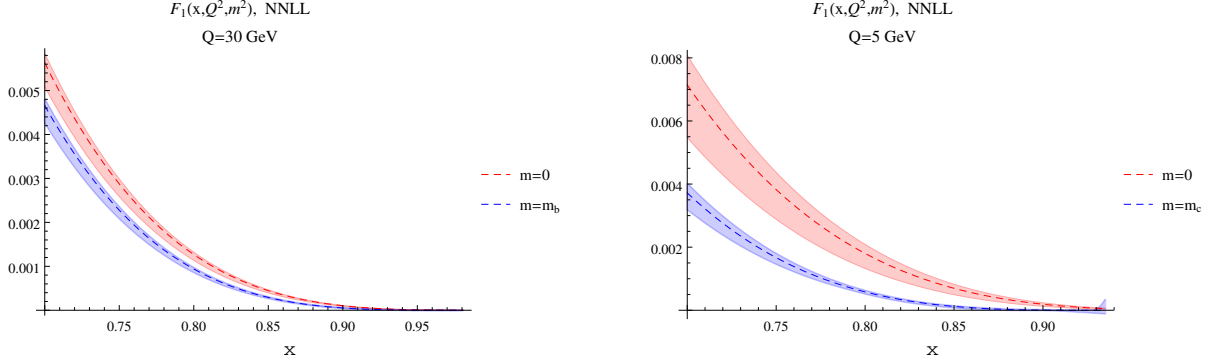


Figure 26: The massless and massive form factors $K(x, Q^2, m^2)f(x, Q^2)$ at NNLL.

In Fig. 26 the form factor F_1 is shown with NNLL resummation for massless (red) and massive (blue) quarks. NNLL resummation reduces the uncertainties such that the massive form factor can be clearly distinguished from the massless one. Although there is a huge factor between the massive and the massless result for the K-factor in the region $x \rightarrow 1$ (compare Fig. 20 and Fig. 21), this is strongly suppressed in the form factor because the PDF falls off rapidly for large x . This implies that it is unlikely to resolve the mass effects for extremely large x ($\gtrsim 0.95$) experimentally in the near future because they are simply too small, but for regions that are accessible to experiments (up to values of $x \sim 0.85$) the mass effects are clearly resolvable.

7 Conclusions

The goal of this work was to study the effects of heavy flavors in DIS using an effective field theory approach and to extend this approach from the classical OPE region to the endpoint region $x \rightarrow 1$.

The ACOT scheme for DIS was formulated systematically based on EFT methods and the QCD results at $\mathcal{O}(\alpha_s)$ were reproduced by using the SCET ansatz. These include the 1-loop splitting functions, the hard matching coefficients and the threshold corrections at the mass scale.

The already existing SCET factorization theorem for DIS in the endpoint region with massless quarks was extended to the massive case. The building blocks that appear in this factorization theorem like the hard or the jet function are universal and also appear in other SCET factorization theorems and were reproduced at $\mathcal{O}(\alpha_s)$.

The effects of the mass in the matching coefficients and of the resummation of large logs in the limit $x \rightarrow 1$ compared to the fixed order results were studied numerically. We found that the mass effects become important for large x and that the resummed results are much more stable when going to higher orders than the fixed order results. For the results with resummation we have very good convergence from NLL to NNLL resummation within the theoretical uncertainties estimated by scale variation. The theoretical uncertainties with NNLL resummation are small enough so that the mass should be resolvable, though experiments do not provide very precise data for measurements in the large x region so far.

This work was focused on heavy flavor production at $\mathcal{O}(\alpha_s)$. If one goes to $\mathcal{O}(\alpha_s^2)$ this leads to a more complicated structure because of mixing between different quark flavors in the evolution of the PDFs and the matching coefficients, but the general framework is the same. If one wants to include also the effects of secondary massive quarks this yields new threshold corrections in the different functions in the factorization theorem for $x \rightarrow 1$, depending on how the mass scales relatively to the other scales (hard, jet, soft/PDF) in the process, see Refs. [32, 33].

DIS is a good example for studying effects of heavy flavors because one has to deal with only one hadron in the initial state, but the concepts discussed in this work can also be applied to other processes like e.g. heavy flavor production in hadron colliders.

A Plus Distributions

Definition:

$$\left(\frac{\text{Log}^n(1-x)}{1-x} \right)_+ = \frac{\text{Log}^n(1-x)}{1-x} - \delta(1-x) \int_0^x dx' \frac{\text{Log}^n(1-x')}{1-x'} \quad (\text{A.1})$$

$$\int_{\Delta}^1 dx \left(\frac{\text{Log}^n(1-x)}{1-x} \right)_+ f(x) = \int_{\Delta}^1 dx \frac{\text{Log}^n(1-x)}{1-x} (f(x) - f(1)) + \frac{\text{Log}^{n+1}(1-\Delta)}{n+1} f(1) \quad (\text{A.2})$$

Expansion

$$\frac{\Theta(1-x)}{(1-x)^{1+a}} = -\frac{1}{a} \delta(1-x) + \Theta(1-x) \sum_{n=0}^{\infty} \frac{(-a)^n}{n!} \left(\frac{\text{Log}^n(1-x)}{1-x} \right)_+ \quad (\text{A.3})$$

Rescaling:

$$\kappa \left(\frac{\text{Log}^n(\kappa(1-x))}{\kappa(1-x)} \right)_+ = \frac{\text{Log}^{n+1}(\kappa)}{n+1} \delta(1-x) + \sum_{a=0}^n \frac{n!}{(n-a)!a!} \text{Log}^{n-a}(\kappa) \left(\frac{\text{Log}^a(1-x)}{1-x} \right)_+ \quad (\text{A.4})$$

Fourier Transform:

$$\mathcal{FT} [\delta(s)] = 1 \quad \mathcal{FT}^{-1} [1] = \delta(s) \quad (\text{A.5})$$

$$\mathcal{FT} \left[\frac{1}{\mu^2} \left(\frac{\mu^2}{s} \right) \right] = -\text{Log} (i\xi e^{\gamma_E} \mu^2) \quad \mathcal{FT}^{-1} [(i\xi \mu^2)^a] = \frac{1}{\Gamma(-a)} \frac{1}{\mu^2} \left(\frac{\mu^2}{s} \right)_+ \quad (\text{A.6})$$

some useful relations:

$$\frac{x}{(1-x)_+} = \frac{1}{(1-x)_+} - 1 \quad (\text{A.7})$$

$$\frac{x^2}{(1-x)_+} = \frac{1}{(1-x)_+} - 1 - x \quad (\text{A.8})$$

$$x \left(\frac{\text{Log}(1-x)}{1-x} \right)_+ = \left(\frac{\text{Log}(1-x)}{1-x} \right)_+ - \text{Log}(1-x) \quad (\text{A.9})$$

$$\left(\frac{1}{x} \right)_+ \text{Log}(x+c) = \left(\frac{1}{x} \right)_+ \text{Log} c + \frac{\text{Log} \left(1 + \frac{x}{c} \right)}{x} \quad (\text{A.10})$$

$$\left(\frac{1}{x} \right)_+ \frac{c(2x+c)}{(x+c)^2} = \left(\frac{1}{x} \right)_+ - \frac{x}{(x+c)^2} \quad (\text{A.11})$$

If $g(1) = 1$ and $g'(1)$ finite:

$$\frac{1}{(1-g(x))_+} = \frac{1}{|g'(1)|} \frac{1}{(1-x)_+} + \frac{\text{Log}(g'(1))}{|g'(1)|} \delta(1-x) + \frac{1}{1-g(x)} - \frac{1}{(1-x)|g'(1)|} \quad (\text{A.12})$$

Integrals:

$$\int_{1-\delta}^1 dx [\text{non-singular}](x) = \mathcal{O}(\delta) \quad (\text{A.13})$$

$$\int_{1-\delta}^1 dx \delta(1-x) = 1 \quad (\text{A.14})$$

$$\int_{1-\delta}^1 dx \frac{1}{(1-x)_+} = \text{Log} \delta \quad (\text{A.15})$$

$$\int_{1-\delta}^1 dx \left(\frac{\text{Log}(1-x)}{1-x} \right)_+ = \frac{\text{Log}^2 \delta}{2} \quad (\text{A.16})$$

B Imaginary Parts

$x \in \mathbb{R}$

$$\text{Im} [\text{Log}(-(1-x) \pm i0)] = \pm \pi \Theta(1-x) \quad (\text{B.1})$$

$$\text{Im} [\text{Log}^2(-(1-x) \pm i0)] = \pm 2\pi \Theta(1-x) \text{Log}(1-x) \quad (\text{B.2})$$

$$\text{Im} \left[\frac{1}{1-x \pm i0} \right] = \mp \pi \delta(1-x) \quad (\text{B.3})$$

$$\text{Im} \left[\frac{1}{(1-x \pm i0)^2} \right] = \pm \pi \delta'(1-x) \quad (\text{B.4})$$

$$\text{Im} \left[\frac{\text{Log}(-(1-x) - i0)}{1-x + i0} \right] = -\pi \Theta(1-x) \frac{1}{(1-x)_+} \quad (\text{B.5})$$

$$\text{Im} \left[\frac{\text{Log}^2(-(1-x) - i0)}{1-x + i0} \right] = \frac{\pi^3}{3} \delta(1-x) - 2\pi \Theta(1-x) \left(\frac{\text{Log}(1-x)}{1-x} \right)_+ \quad (\text{B.6})$$

$$\text{Im} [\text{Li}_s(x \pm i0)] = \pm \pi \Theta(x-1) \frac{\text{Log}^{s-1} x}{\Gamma(s)} \quad (\text{B.7})$$

$$\text{Im} [\tanh^{-1}(x \pm i0)] = \pm \frac{\pi}{2} \Theta(|x| - 1) \quad (\text{B.8})$$

$$\text{Im} [\tan^{-1}(x)] = 0 \quad (\text{B.9})$$

$$\text{Im} [\tan^{-1}(ix)] = \frac{1}{2} \text{Log} \left(\left| \frac{x+1}{x-1} \right| \right) \quad (\text{B.10})$$

real parts: $x, y \in \mathbb{R}$

$$\text{Re} [\tan^{-1}(i(x \pm i\epsilon))] = \mp \frac{\pi}{2} \Theta(|x| - 1) \quad (\text{B.11})$$

$$\text{Re} [\text{Log}(x + iy)] = \frac{1}{2} \text{Log}(x^2 + y^2) \quad (\text{B.12})$$

C n-point Functions

$$\begin{aligned} w &:= \sqrt{1 + \frac{4m^2}{Q^2}} & r &:= \sqrt{1 + \frac{4m^2 x^2}{Q^2}} \\ s &:= \sqrt{1 - \frac{4m^2 x}{Q^2(1-x)}} & t &:= \sqrt{1 + \frac{4m^2 x}{Q^2(1+x)}} \end{aligned}$$

divergent n-point functions:

The divergent n-point functions were taken from Ref. [34].

$$a_1 = A_0(m^2) = m^2 \left(\frac{1}{\epsilon} + \text{Log} \frac{\mu^2}{m^2} + 1 \right) \quad (\text{C.1})$$

$$b_1 = B_0(m^2, 0, m^2) = \frac{1}{\epsilon} + \text{Log} \frac{\mu^2}{m^2} + 2 \quad (\text{C.2})$$

$$b_2 = B_0(0, m^2, m^2) = \frac{1}{\epsilon} + \text{Log} \frac{\mu^2}{m^2} \quad (\text{C.3})$$

$$b_3 = B_0(-Q^2, m^2, m^2) = \frac{1}{\epsilon} + \text{Log} \frac{\mu^2}{m^2} + 2 + w \text{Log} \frac{w-1}{w+1} \quad (\text{C.4})$$

$$b_4 = B_0\left(\frac{Q^2(1-x)}{x}, m^2, m^2\right) = \frac{1}{\epsilon} + \text{Log} \frac{\mu^2}{m^2} + 2 + s \text{Log} \frac{s-1}{s+1} \quad (\text{C.5})$$

$$b_5 = B_0\left(-\frac{Q^2(1+x)}{x}, m^2, m^2\right) = \frac{1}{\epsilon} + \text{Log} \frac{\mu^2}{m^2} + 2 + t \text{Log} \frac{t-1}{t+1} \quad (\text{C.6})$$

$$b_6 = B_0\left(m^2 + \frac{Q^2(1-x)}{x}, 0, m^2\right) = \frac{1}{\epsilon} + \text{Log} \frac{\mu^2}{m^2} + 2 - \frac{1-x}{x \frac{m^2}{Q^2} + 1 - x} \left(\text{Log} \frac{-(1-x)}{x} - \text{Log} \frac{m^2}{Q^2} \right) \quad (\text{C.7})$$

$$c_1 = C_0(0, m^2, m^2, m^2, m^2, 0) = \frac{1}{2m^2} \left(\frac{1}{\epsilon} + \text{Log} \frac{\mu^2}{m^2} \right) \quad (\text{C.8})$$

$$d_1 = D_0\left(-Q^2, 0, m^2, m^2 + \frac{Q^2(1-x)}{x}, -Q^2, m^2, m^2, m^2, m^2, 0\right) = \frac{x}{2m^2 Q^2(1-x)} \left(\frac{1}{\epsilon} + \text{Log} \frac{\mu^2}{m^2} + 2 \text{Log} \frac{m^2}{Q^2} - 2 \text{Log} \frac{-(1-x)}{x} - \frac{1+w^2}{w} \text{Log} \frac{w-1}{w+1} \right) \quad (\text{C.9})$$

To get the correct imaginary part set $m^2 \rightarrow m^2 - i0$.

finite n-point functions:

The finite n-point functions were calculated by using Feynman parameters and following Ref. [35].

$$c_2 = C_0(0, 0, 0, m^2, m^2, m^2) = -\frac{1}{2m^2} \quad (\text{C.10})$$

$$c_3 = C_0(0, -Q^2, -Q^2, m^2, m^2, m^2) = \frac{-2 \tanh^{-1}\left(\frac{1}{w}\right)}{Q^2 w} \quad (\text{C.11})$$

$$\begin{aligned} c_4 = C_0(0, -Q^2, \frac{Q^2(1-x)}{x}, m^2, m^2, m^2) = \\ \frac{x}{Q^2} \left(\frac{1}{2} \text{Log}^2 \left(\frac{-(w-1)}{w+1} \right) - \text{Log} \left(\frac{-(w-1)}{w+1} \right) \text{Log} \left(\frac{w-1}{w+1} \right) \right. \\ \left. - \frac{1}{2} \text{Log}^2 \left(\frac{-(s-1)}{s+1} \right) + \text{Log} \left(\frac{-(s-1)}{s+1} \right) \text{Log} \left(\frac{s-1}{s+1} \right) \right) \end{aligned} \quad (\text{C.12})$$

$$\begin{aligned} c_5 = C_0(m^2, -Q^2, m^2 + \frac{Q^2(1-x)}{x}, 0, m^2, m^2) = \\ \frac{x}{Q^2 r} \left(-\text{Li}_2 \left(\frac{(r-1)(r-x+1)}{r^2 - wxr + x - 1} \right) + \text{Li}_2 \left(\frac{(r+1)(r+x-1)}{r^2 - wxr + x - 1} \right) \right. \\ - \text{Li}_2 \left(\frac{(r-1)(r-x+1)}{r^2 + wxr + x - 1} \right) + \text{Li}_2 \left(\frac{(r+1)(r+x-1)}{r^2 + wxr + x - 1} \right) - 2\text{Li}_2 \left(\frac{r+x-1}{x-1} \right) \\ + \text{Li}_2 \left(\frac{(r-1)(r-x+1)}{(r+1)(x-1)} \right) - \text{Li}_2 \left(\frac{(r+1)(r+2x-1)}{(r-1)(r-2x+1)} \right) \\ \left. + \text{Li}_2 \left(\frac{(r-x+1)(r+2x-1)}{(r-2x+1)(x-1)} \right) + \frac{\pi^2}{6} \right) \end{aligned} \quad (\text{C.13})$$

$$\begin{aligned} d_2 = D_0(0, 0, \frac{Q^2(1-x)}{x}, -Q^2, 0, -Q^2, m^2, m^2, m^2, m^2) = \\ \frac{x}{Q^2 m^2 w} \left(w + (1 + w^2(1-2x)) \tanh^{-1} \left(\frac{1}{w} \right) \right. \\ \left. + 2w(1-x) \sqrt{-s^2} \tan^{-1} \left(\frac{1}{\sqrt{-s^2}} \right) \right) \end{aligned} \quad (\text{C.14})$$

$$\begin{aligned} d_3 = D_0(0, \frac{Q^2(1-x)}{x}, 0, -\frac{Q^2(1+x)}{x}, -Q^2, -Q^2, m^2, m^2, m^2, m^2) \\ \text{Im}[d_3] = \pi \Theta \left(\frac{1}{w^2} - x \right) \frac{-2x^2}{Q^4} \text{Log} \left(\frac{1-s}{1+s} \right) \end{aligned} \quad (\text{C.15})$$

To get the correct imaginary part set $m^2 \rightarrow m^2 - i0$.

References

- [1] A. Martin, W. Stirling, R. Thorne, and G. Watt, “Parton distributions for the LHC,” *Eur.Phys.J.* **C63** (2009) 189–285, [arXiv:0901.0002 \[hep-ph\]](#).
- [2] H.-L. Lai, M. Guzzi, J. Huston, Z. Li, P. M. Nadolsky, *et al.*, “New parton distributions for collider physics,” *Phys.Rev.* **D82** (2010) 074024, [arXiv:1007.2241 \[hep-ph\]](#).
- [3] M. Aivazis, F. I. Olness, and W.-K. Tung, “Leptoproduction of heavy quarks. 1. General formalism and kinematics of charged current and neutral current production processes,” *Phys.Rev.* **D50** (1994) 3085–3101, [arXiv:hep-ph/9312318 \[hep-ph\]](#).
- [4] M. Aivazis, J. C. Collins, F. I. Olness, and W.-K. Tung, “Leptoproduction of heavy quarks. 2. A Unified QCD formulation of charged and neutral current processes from fixed target to collider energies,” *Phys.Rev.* **D50** (1994) 3102–3118, [arXiv:hep-ph/9312319 \[hep-ph\]](#).
- [5] F. Olness and I. Schienbein, “Heavy Quarks: Lessons Learned from HERA and Tevatron,” *Nucl.Phys.Proc.Suppl.* **191** (2009) 44–53, [arXiv:0812.3371 \[hep-ph\]](#).
- [6] C. W. Bauer, S. Fleming, and M. E. Luke, “Summing Sudakov logarithms in $B \rightarrow X_s \gamma$ in effective field theory,” *Phys.Rev.* **D63** (2000) 014006, [arXiv:hep-ph/0005275 \[hep-ph\]](#).
- [7] C. W. Bauer, S. Fleming, D. Pirjol, and I. W. Stewart, “An Effective field theory for collinear and soft gluons: Heavy to light decays,” *Phys.Rev.* **D63** (2001) 114020, [arXiv:hep-ph/0011336 \[hep-ph\]](#).
- [8] C. W. Bauer and I. W. Stewart, “Invariant operators in collinear effective theory,” *Phys.Lett.* **B516** (2001) 134–142, [arXiv:hep-ph/0107001 \[hep-ph\]](#).
- [9] C. W. Bauer, D. Pirjol, and I. W. Stewart, “Soft collinear factorization in effective field theory,” *Phys.Rev.* **D65** (2002) 054022, [arXiv:hep-ph/0109045 \[hep-ph\]](#).
- [10] C. W. Bauer, S. Fleming, D. Pirjol, I. Z. Rothstein, and I. W. Stewart, “Hard scattering factorization from effective field theory,” *Phys.Rev.* **D66** (2002) 014017, [arXiv:hep-ph/0202088 \[hep-ph\]](#).
- [11] J. C. Collins and D. E. Soper, “Parton Distribution and Decay Functions,” *Nucl.Phys.* **B194** (1982) 445.
- [12] G. Curci, W. Furmanski, and R. Petronzio, “Evolution of Parton Densities Beyond Leading Order: The Nonsinglet Case,” *Nucl.Phys.* **B175** (1980) 27.
- [13] C. W. Bauer, D. Pirjol, and I. W. Stewart, “Factorization and endpoint singularities in heavy to light decays,” *Phys.Rev.* **D67** (2003) 071502, [arXiv:hep-ph/0211069 \[hep-ph\]](#).
- [14] A. V. Manohar and I. W. Stewart, “The Zero-Bin and Mode Factorization in Quantum Field Theory,” *Phys.Rev.* **D76** (2007) 074002, [arXiv:hep-ph/0605001 \[hep-ph\]](#).
- [15] A. K. Leibovich, Z. Ligeti, and M. B. Wise, “Comment on quark masses in SCET,” *Phys.Lett.* **B564** (2003) 231–234, [arXiv:hep-ph/0303099 \[hep-ph\]](#).
- [16] I. W. Stewart, F. J. Tackmann, and W. J. Waalewijn, “The Quark Beam Function at NNLL,” *JHEP* **1009** (2010) 005, [arXiv:1002.2213 \[hep-ph\]](#).
- [17] C. Lee and G. F. Sterman, “Momentum Flow Correlations from Event Shapes: Factorized Soft Gluons and Soft-Collinear Effective Theory,” *Phys.Rev.* **D75** (2007) 014022, [arXiv:hep-ph/0611061 \[hep-ph\]](#).
- [18] J. Chay and C. Kim, “Proper factorization theorems in high-energy scattering near the endpoint,” *JHEP* **1309** (2013) 126, [arXiv:1303.1637 \[hep-ph\]](#).
- [19] W. van Neerven and A. Vogt, “NNLO evolution of deep inelastic structure functions: The Singlet case,” *Nucl.Phys.* **B588** (2000) 345–373, [arXiv:hep-ph/0006154 \[hep-ph\]](#).
- [20] W. van Neerven and A. Vogt, “NNLO evolution of deep inelastic structure functions: The Nonsinglet case,” *Nucl.Phys.* **B568** (2000) 263–286, [arXiv:hep-ph/9907472 \[hep-ph\]](#).

-
- [21] R. Mertig, M. Bohm, and A. Denner, “FEYN CALC: Computer algebraic calculation of Feynman amplitudes,” *Comput.Phys.Commun.* **64** (1991) 345–359.
 - [22] I. J. Schienbein, “Heavy quark production in CC and NC DIS and the structure of real and virtual photons in NLO QCD,” [arXiv:hep-ph/0110292](#) [[hep-ph](#)].
 - [23] M. Buza, Y. Matiounine, J. Smith, and W. van Neerven, “Charm electroproduction viewed in the variable flavor number scheme versus fixed order perturbation theory,” *Eur.Phys.J.* **C1** (1998) 301–320, [arXiv:hep-ph/9612398](#) [[hep-ph](#)].
 - [24] A. V. Manohar, “Deep inelastic scattering as $x \rightarrow 1$ using soft collinear effective theory,” *Phys.Rev.* **D68** (2003) 114019, [arXiv:hep-ph/0309176](#) [[hep-ph](#)].
 - [25] T. Becher, M. Neubert, and B. D. Pecjak, “Factorization and Momentum-Space Resummation in Deep-Inelastic Scattering,” *JHEP* **0701** (2007) 076, [arXiv:hep-ph/0607228](#) [[hep-ph](#)].
 - [26] J. Chay and C. Kim, “Deep inelastic scattering near the endpoint in soft-collinear effective theory,” *Phys.Rev.* **D75** (2007) 016003, [arXiv:hep-ph/0511066](#) [[hep-ph](#)].
 - [27] S. Fleming and O. Zhang, “Rapidity Divergences and Deep Inelastic Scattering in the Endpoint Region,” [arXiv:1210.1508](#) [[hep-ph](#)].
 - [28] S. Fleming, A. H. Hoang, S. Mantry, and I. W. Stewart, “Jets from massive unstable particles: Top-mass determination,” *Phys.Rev.* **D77** (2008) 074010, [arXiv:hep-ph/0703207](#) [[hep-ph](#)].
 - [29] S. Fleming, A. H. Hoang, S. Mantry, and I. W. Stewart, “Top Jets in the Peak Region: Factorization Analysis with NLL Resummation,” *Phys.Rev.* **D77** (2008) 114003, [arXiv:0711.2079](#) [[hep-ph](#)].
 - [30] T. Huber and D. Maitre, “HypExp: A Mathematica package for expanding hypergeometric functions around integer-valued parameters,” *Comput.Phys.Commun.* **175** (2006) 122–144, [arXiv:hep-ph/0507094](#) [[hep-ph](#)].
 - [31] R. Abbate, M. Fickinger, A. H. Hoang, V. Mateu, and I. W. Stewart, “Thrust at N³LL with Power Corrections and a Precision Global Fit for $\alpha_s(m_Z)$,” *Phys.Rev.* **D83** (2011) 074021, [arXiv:1006.3080](#) [[hep-ph](#)].
 - [32] S. Gritschacher, A. H. Hoang, I. Jemos, and P. Pietrulewicz, “Secondary Heavy Quark Production in Jets through Mass Modes,” *Phys.Rev.* **D88** (2013) 034021, [arXiv:1302.4743](#) [[hep-ph](#)].
 - [33] P. Pietrulewicz, “Variable Flavor Number Scheme for Final State Jets,” *PhD Thesis, University of Vienna* (2014) .
 - [34] R. K. Ellis and G. Zanderighi, “Scalar one-loop integrals for QCD,” *JHEP* **0802** (2008) 002, [arXiv:0712.1851](#) [[hep-ph](#)].
 - [35] G. ’t Hooft and M. Veltman, “Scalar one-loop integrals,” *Nucl.Phys.* **B153** (1979) 365–401.

Acknowledgements

First I would like to thank my supervisor Prof. André Hoang for giving me the opportunity to write this thesis and to join the particle physics group at the University of Vienna.

Special thanks go to Piotr Pietrlewicz who was a very competent and patient coworker during the whole project and without whose help this work would never have been completed.

I am very grateful to my family for their love and financial support during my studies, especially to my brother, not only for washing my clothes, but also for being a role model throughout my life.

Finally I would like to thank all my friends and colleagues who made the past five years in Vienna a wonderful time for me, at university as well as in personal life.

Thanks to all of you!

Curriculum Vitae

Personal Data

Name: Daniel Samitz
Date of birth: 16.11.1989 in Linz, Austria
Address: Lacknergasse 35
1170 Wien
Phone: (+43) 650 6932246
Mail: daniel.samitz@gmx.at

Education

since 2012: Master programme in Physics at University of Vienna

2012: Bachelor of Science (with distinction)
Bachelor Thesis: "Particle Oscillations, Entanglement and Decoherence"
Supervisor: ao. Univ.-Prof. i.R. Dr. Reinhold Bertlmann

2009-2012: Bachelor programme in Physics at University of Vienna

2008: Matura (A levels) in Linz (with distinction)

Languages German (native)
English (fluent)